DEVELOPMENT OF A HYDROGEL BASED PROSTATE TUMOR MODEL FOR CANCER CELL MIGRATION STUDIES

A THESIS SUBMITTED TO
THE GRADUATE SCHOOL OF NATURAL AND APPLIED SCIENCES
OF
MIDDLE EAST TECHNICAL UNIVERSITY

BY

DAMLA DEMİRKAYA

IN PARTIAL FULFILLMENT OF THE REQUIREMENTS
FOR
THE DEGREE OF MASTER OF SCIENCE
IN
MOLECULAR BIOLOGY AND GENETICS

JANUARY 2022

Approval of the thesis:

DEVELOPMENT OF A HYDROGEL BASED PROSTATE TUMOR MODEL FOR CANCER CELL MIGRATION STUDIES

submitted by **DAMLA DEMİRKAYA** in partial fulfillment of the requirements for the degree of **Master of Science** i**n Molecular Biology and Genetics, Middle East Technical University** by,

Prof. Dr. Halil Kalıpçılar
Dean, Graduate School of **Natural and Applied Sciences** _____

Prof. Dr. Ayşe Gül Gözen
Head of the Department, **Biological Sciences** _____

Prof. Dr. Ayşe Gül Gözen
Supervisor, **Biological Sciences, METU** _____

Dr. Ezgi Antmen Altunsoy
Co-Supervisor, **BIOMATEN, METU** _____

Examining Committee Members:

Prof. Dr. Sreeparna Banerjee
Biological Sciences, METU _____

Prof. Dr. Ayşe Gül Gözen
Biological Sciences, METU _____

Prof. Dr. Vasıf Hasırcı
Medical Engineering, Acıbadem University _____

Prof. Dr. Halime Kenar
Medical Engineering, Acıbadem University _____

Prof. Dr. Nülüfer Tülin Güray
Biological Sciences, METU _____

Date: 12.01.2022

I hereby declare that all information in this document has been obtained and presented in accordance with academic rules and ethical conduct. I also declare that, as required by these rules and conduct, I have fully cited and referenced all material and results that are not original to this work.

Name, Last name : Damla Demirkaya

Signature :

ABSTRACT

DEVELOPMENT OF A HYDROGEL BASED PROSTATE TUMOR MODEL FOR CANCER CELL MIGRATION STUDIES

Demirkaya, Damla
Master of Science, Molecular Biology and Genetics
Supervisor : Prof. Dr. Ayşe Gül Gözen
Co-Supervisor: Dr. Ezgi Antmen Altunsoy

January 2022, 83 pages

Prostate cancer is the second most diagnosed cancer in men and relapse due to the metastasis of cancer cells is the main reason of the high number of deaths in prostate cancer patients. Thus, there is a growing need for a tumor model to study the prostate cancer metastasis. In this study, a 3D model consisting of two natural polymer hydrogels (methacrylated collagen and methacrylated hyaluronic acid) with tunable mechanical and chemical properties carrying spheroids of two different prostate cancer cell lines (PC-3 and LNCAP) was developed to compare the effect of microenvironment on the migration. Fibroblast cells were incorporated in the hydrogel blend to increase the rate of migration of cancer cells. Migration of cancer cells in hydrogels with different compositions in the presence and absence of fibroblasts was studied with confocal laser scanning microscopy. The cancer cells in high collagen containing hydrogel were elongated, and the presence of fibroblasts in the microenvironment promoted the migration of prostate cancer cells by mimicking the microenvironment of prostate cancer more closely than other models. Epithelial-mesenchymal transition (EMT), a precondition for metastasis enhances

mobility by decreasing epithelial markers and increasing mesenchymal markers. The quantification of migration was achieved through determination of E-cadherin and vimentin expression, the EMT marker proteins, through their fluorescence intensities in the immunostained samples. It was shown that E-cadherin expression was downregulated while vimentin expression was upregulated in the presence of fibroblast cells in high collagen containing hydrogel model as an indicator of migration.

Keywords: Prostate cancer, migration, hydrogel, collagen, hyaluronic acid

ÖZ

KANSER HÜCRESİ GÖÇÜ ÇALIŞMALARI İÇİN HİDROJEL BAZLI PROSTAT TÜMÖR MODELİNİN GELİŞTİRİLMESİ

Demirkaya, Damla
Yüksek Lisans, Moleküler Biyoloji ve Genetik
Tez Yöneticisi: Prof. Dr. Ayşe Gül Gözen
Ortak Tez Yöneticisi: Dr. Ezgi Antmen Altunsoy

Ocak 2022, 83 sayfa

Prostat kanseri, erkeklerde en sık teşhis edilen ikinci kanserdir ve kanser hücrelerinin metastazına bağlı nüks, prostat kanseri hastalarında ölüm sayısının yüksek olmasının ana nedenidir. Bu nedenle, prostat kanseri metastazını incelemek için bir tümör modeline artan bir ihtiyaç vardır. Bu çalışmada, iki farklı prostat kanseri hücre hattının (PC-3 ve LNCAP) sferoidlerini taşıyan ayarlanabilir mekanik ve kimyasal özelliklere sahip iki doğal polimer hidrojelden (metakrilatlanmış kollajen ve metakrilatlanmış hyaluronik asit) oluşan bir 3B model mikroçevrenin hücre göçü üzerindeki etkisini karşılaştırmak üzere geliştirilmiştir. Fibroblast hücreleri, kanser hücrelerinin göç hızını artırmak için hidrojel karışımına dahil edildi. Fibroblastların varlığında ve yokluğunda farklı bileşimlere sahip hidrojellerde kanser hücrelerinin göçü, konfokal lazer tarama mikroskobu ile incelenmiştir. Mikroçevredeki fibroblastların varlığı, prostat kanserinin mikroçevresini diğer modellere göre daha yakından taklit ederek prostat kanseri hücrelerinin göçünü teşvik etmiş ve yüksek kolajen içeren hidrojelde kanser hücrelerinde uzama gözlemlenmiştir. Metastaz için bir ön koşul olan epitelyal-mezenkimal geçiş (EMT), epitel markerlerini azaltarak

ve mezenkimal markerleri artırarak mobiliteyi artırır. Hücre göçünün nicelleştirilmesi, EMT marker proteinler olan E-cadherin ve vimentin ifadelerinin, immüno boyanmış numunelerdeki flüoresans yoğunluklarından hesaplanarak sağlanmıştır. Migrasyon göstergesi olarak, yüksek kolajen içeren hidrojel modelinde fibroblast hücrelerinin varlığında vimentin ifadesinin artarken, E-cadherin ifadesinin azaldığı gösterilmiştir.

Anahtar Kelimeler: Prostat kanseri, hücre göçü, hidrojel, kolajen, hyalüronik asit

Dedicated to all my beloved ones

ACKNOWLEDGMENTS

I would like to express my special endless thanks and gratitude to my supervisor, Prof. Dr. Ayşe Gül Gözen for her support and encouragement.

I also thank to my co-supervisor Dr. Ezgi Antmen Altunsoy for her continuous guidance, advice, support, encouragement and insight throughout the research.

I am especially grateful to Prof. Dr. Vasıf Hasırcı for his advice, criticism comments and continuous support in this study and also giving me opportunity to work in this field.

I present my endless thanks to my thesis examining committee members, especially the chair of the committee Prof. Dr. Sreeparna Banerjee, for their time and valuable contributions.

I would like to thank to all members of BIOMATEN especially Dr. Menekşe Ermiş Şen, Dr. Senem Büyüksungur, Dr. Damla Arslantunalı, Dilara Tamay for their support in this study. Also, I am very grateful to my labmates especially Ceren Gedik, for her contribution by spending hours in tissue culture, and Mahsa Moniri for her help in mechanical tests.

I give my deepest love and thanks to my lovely family. I would like to thank my beloved and supportive sister, Özge Demirkaya, for her unending moral and material support during my study and writing my thesis. I thank my dear father, Adnan Demirkaya, and my mother, Aysel Demirkaya, for their endless love, guidance, support and trust during my whole life. Also, I am grateful for having the world's best brother, Samet Demirkaya. He always encourage me, when I doubt throughout my life. I am so lucky to have you all.

I am also deeply grateful to my lovely friends especially Bilge Durgut, Kübra Doğan, Kübra Atalık and Hüseyin Karabürk for their presence in my life.

TABLE OF CONTENTS

LIST OF TABLES

TABLES

LIST OF FIGURES

FIGURES

LIST OF ABBREVIATIONS

ABBREVIATIONS	
2D	Two-Dimensional
3D	Three-Dimensional
ADT	Androgen Deprivation Theraphy
BNP	Benign Prostatic Hyperplasia
BSA	Bovine Serum Albumin
CLSM	Confocal Laser Scanning Microscopy
CO_2	Carbon Dioxide
ColMA	Methacrylated Collagen
CRPC	Castration Resistant Prostate Cancer
CSC	Cancer Stem Cell cm^{-1}
CTCs	Circulating Tumour Cells
D_2O	Deuterium Oxide
DAPI	4', 6-Diamidino-2-phenylindole
DM	Degree of Methacrylation
DMEM	Dulbecco's Modified Eagle Medium
DMF	Dimetilformamid
DMSO	Dimethyl Sulfoxide
DR	Dynamic eciprocity
E	Young's modulus
ECM	Extracellular Matrix

EDTA	Ethylenediamine tetraacetic Acid
EMT	Epithelial-Mesenchymal Transition
FBS	Fetal Bovine Serum
FGF	Fibroblast Growth Factor
FTIR	Fourier-Transform Infrared Spectroscopy
GAG	Glycosaminoglycan
HA	Hyaluronic Acid
HAMA	Methacrylated Hyaluronic Acid
HDFa	Human Dermal Fibroblast, adult
Irgacure	2-Hydroxy-4′-(2-hydroxyethoxy)-2-methylpropiophenone
mCRPC	Metastatic Castration Resistant Prostate Cancer
NMR	Nuclear Magnetic Resonance
PAA	Polyacrylic acid
PAM	Polyacrylamide
PBS	Phosphate Buffer Saline
PCL	Poly(ε-caprolactone)
PDMS	Poly(dimethylsiloxane)
PEG	Polyethylene glycol
PIA	Proliferative Inflammatory Antrophy
PIN	Prostatetic intraepithelial neolasia
PVA	Polyvinyl Alcohol
RHAMM	Receptor for Hyaluronan Mediated Motility

RP	Radical Prostatectomy
RPMI	Roswell Park Memorial Institute
SNP	Single-Nucleotide Polymorphism
T	Transmittance
TCPS	Tissue Culture Polystyrene
VEGF	Vascular Endothelial Growth Factor

CHAPTER 1

INTRODUCTION

Cancer is a major group of diseases of higher multicellular organisms. At the simplest level, cancer cells are the cells that have lost the ability to follow the normal control that the body exerts on all cells. In the human body, there are billions of cells with different functions. It is very complicated process under incredibly phenomenal control. In the cells' natural division process, the accumulation of replication errors leads to the loss of normal control, and particular cells continue to grow and they may spread. The abnormal proliferation of cells is called cancer, and those cells together form a tumor. Cancer is a malignant tumor; since, it can not only invade the adjacent organs but spread to the other tissues and become life-threatening. (Hassanpour & Dehghani, 2017) Cancer can occur anywhere in the body; since, the cells are found everywhere in the body. Lung cancer is the most common cancer in both women and men. In women, one of the most common cancers is breast cancer, and in men, it is prostate cancer. It is important that cancer which occurs in one individual is very different than the cancer that occurs in another, the cancer is not homogenous. The heterogeneity of cancers leads to complexity in cancer treatment. The development of 3D cancer tumor models are important for the revolution of cancer therapy studies (Meacham & Morrison, 2013).

In this study, it was aimed to develop a hydrogel-based prostate cancer tumor model for migration studies and further applications. Prostate cancer is one of the most diagnosed cancer. Due to its heterogeneity, the development of prostate cancer treatments is a necessity. This 3D hydrogel-based model aims to mimic the tumor microenvironment and provides a better *in vitro* tool for prostate cancer studies.

1.1 Hallmarks of Prostate Cancer

Prostate cancer is the second most prevalent cancer that causes a large number of deaths in men (Bray et al., 2018, Villers and Grosclaude, 2008). According to Global Cancer Observatory, GLOBOCAN estimates for 2020, there were almost 1.4 million new cases of prostate cancer and 375,000 prostate cancer-associated deaths worldwide in 2020 (Sung et al., 2021). Due to its high incidence and mortality rate (Figure 1), prostate cancer studies have a growing interest. Also, the number of cases and deaths in 2040 is expected to be 2.3 million and 738,000, respectively (Ferlay et al., 2020). Prostate cancer is the most commonly diagnosed cancer among men in 112 of 185 countries in the world in 2020 (Sung et al., 2021). Risk factors for prostate cancer are generally analyzed in five aspects; aging, inheritance, race, hormones and environmental factors (Abate-Shen & Shen, 2000). Early detection of prostate cancer is crucial for preventing the high mortality rate and the local symptoms like urinary tract obstruction and bleeding (Barry, 2001). Prostate specific antigen (PSA) testing is highly recommended for early diagnosis. The elevated level of PSA is an indicator of prostate cancer; however; it can also occur due to non-cancerous enlargement or inflammation of prostate gland. Thus, the biopsy is the second stage for diagnosing prostate cancer (Tikkinen et al., 2018). Prostate cancer can be treated in its early stages. Whole prostate radiation therapy or radical prostatectomy (RP), surgical removal of the prostate gland, is the most common treatment for localized prostate cancer (Michaelson et al., 2008). However, once a significant number of tumor cells metastasizes, a new tumor is formed at a distant site in the body, leading to later relapse. It is known that the high mortality rate in prostate cancer patients is associated with the metastatic spread of the cancer cells, especially to bones, lungs and liver (Sartor and de Bono, 2018). In advanced stages of prostate cancer, medical theraphy is used for treatment, the most common one is androgen deprivation therapy (ADT) (Litwin & Tan, 2017).

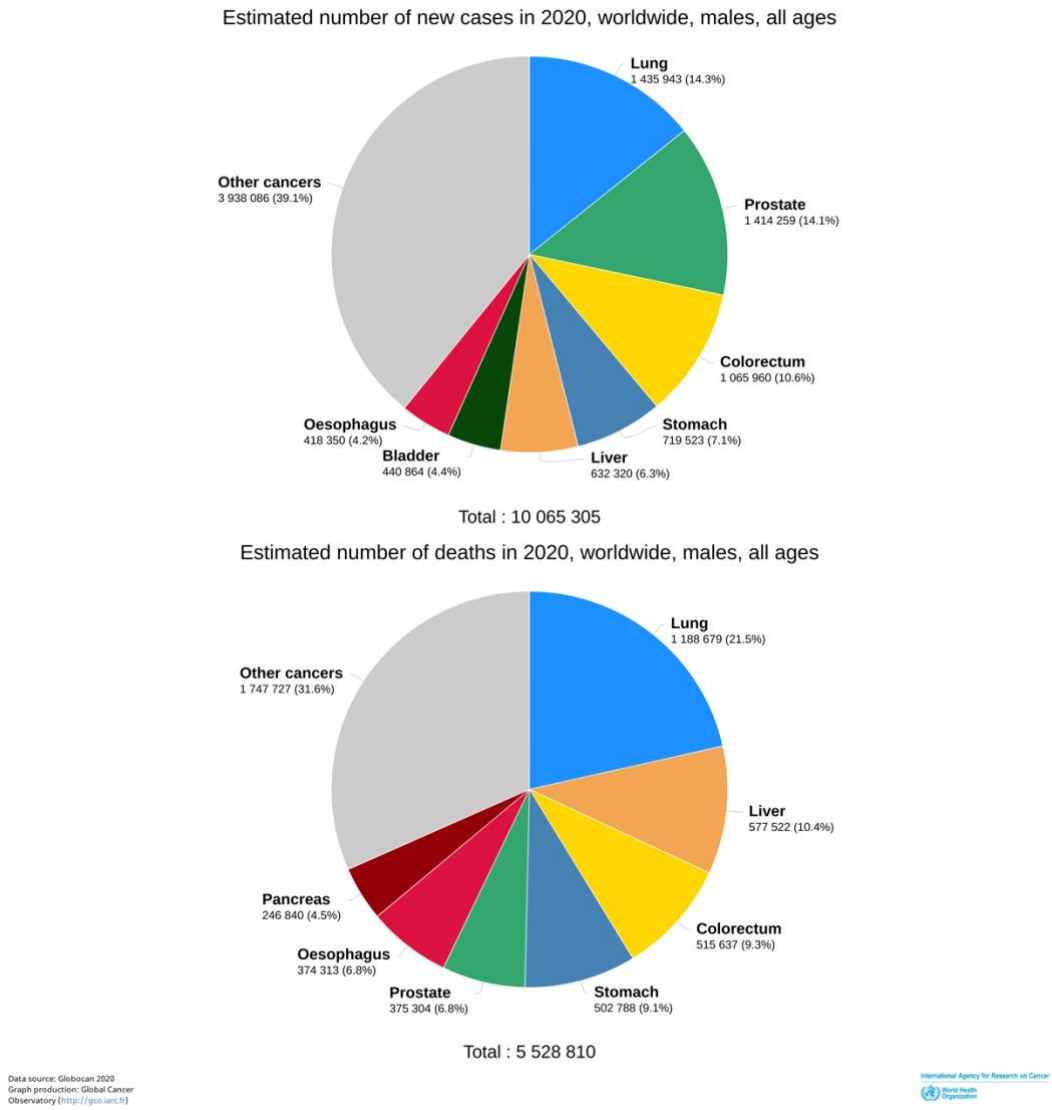

Figure 1.1. Incidence and mortality rates of prostate cancer among the other most common cancer types (Globocan, 2021)

1.1.1 Biology of Prostate Cancer

The prostate is a walnut-size exocrine gland found in the male's reproductive system. It is located at the bladder base and wraps around the urethra. It serves two purposes in men; it contributes to the semen by secreting fluid which is protective for sperm cells and more importantly, the urine tube known as the urethra passes from the bladder through the prostate gland to the exterior, so it carries urine as well (Coakley & Hricak, 2000).

The normal adult prostate is composed of different cell types; glandular epithelial and fibromuscular stroma network, endothelial vasculature, diverse immune cells and autonomic nerve fibers (Packer & Maitland, 2016; Barron & Rowley, 2012). All these cell populations maintain a circulation with stable cell proliferation and death levels. The circular section of the prostate gland has three different zones; central zone, peripheral zone, transition zone and fibromuscular zone. The center zone surrounds the ejaculatory ducts, forms almost 20% of the gland. In the middle of the prostate gland, there is the prostatic urethra, which is surrounded by the transition zone (Scardino & Kelman, 2010). The transition zone is small and insignificant in young men; however, it may develop progressive hyperplastic alterations with age. Benign Prostatic Hyperplasia (BNP) arises in this zone of prostate cancer (Coakley & Hricak, 2000). The peripheral zone of the prostate is found at the posterior side of the gland, close to the rectal wall and, forms almost 70% of the gland. It surrounds the central zone posteroanteriorly, and a large portion of the transition zone as a capsule. Most Prostatetic Intraepithelial Neoplasia (PIN) and cancer occur in the peripheral zone of the prostate gland (Wang, Zhao, Spring & DePinho, 2018).

Two main hypotheses clarify cancer's origin and heterogeneity: cancer stem cell (CSC) model and stochastic model. CSC model proposes that a system of hierarchy leads to the formation of tumors, CSCs are cancer cells that show the characteristics of normal stem cells and can be found in tumors. These cells can differentiate into all cell types, therefore, compared to other cancer cells, CSCs are more tumorigenic, more prone to form tumors. This CSC pool lies at the base of an aberrant

differentiation lineage, leading to the cellular variance of prostate and many other major human tumors (Packer & Maitland, 2016).

On the other hand, stochastic model hypothesizes that a mutation in a tumor-suppressing gene may form a cancerous cell. The cancerous features of the cell do not undergo changes due to mitosis; each new cell continues to carry the same tumourogenic potential (Rich, 2016). These hypothesis are not mutually exclusive. Prostate cancer is an heterogenic disease, which means that each patient's genomic and phenotypic alterations are unique. This situation leads to difficulties in treating prostate cancer (Haffner et al., 2020).

According to twin studies, it is observed that the prostate cancer is one of the most inheritable cancers (Lichtenstein et al., 2000). Moreover, epidemiological studies have shown that a potential risk dramatically increases with a family background with prostate cancer (Lange, 2010). Several prostate cancer susceptibility loci are specified by genome-wide association studies. For instance, it is shown that risk associates single-nucleotide polymorphism (SNP) rs339331 enhance the binding of prostate cancer susceptibility gene HOXB13 to enhancer, which leads over-expression of RFX6 cancer-promoting gene (Huang et al., 2014).

In 1941, Huggins and Hodges discovered the hormone responsiveness of prostate cancer based on tumor regression in prostate cancer patients due to castration. This discovery was awarded the 1966 Nobel Prize for Physiology or Medicine. Normal prostate cells are androgen-dependent for growth, proliferation and function. Most androgens are produced by the testicles, but some androgens are also produced in the adrenal glands. The main androgens in male's body are testosterone and dihydrotestosterone, which is formed by reducing testosterone with 5α-reductase enzyme (Banerjee et al., 2018). Although testosterone is non-tumorigenic by itself, it is also vital for the growth and proliferation of prostate carcinoma cells (Campbell, Wein & Kavoussi, 2007). Androgen deprivation therapy (ADT), which was developed on a thesis that androgen stimulation is necessary for the growth and proliferation of malignant prostate cells, became one of the standard care for prostate

cancer. Reducing androgen levels or preventing them from being used by prostate cancer cells often causes prostate cancers to shrink or slow their growth for a while; however, hormone therapy alone does not entirely cure prostate cancer. Cancer cells may develop resistance to ADT, and primary castration resistant prostate cancer (CRPC) or metastatic castration resistant prostate cancer (mCRPC) may arise. (Wang et.al., 2018)

The malignant transformation of prostate cancer is a multistep phenomenon, as is shown in Figure 1.2. The epithelia are organised into a contiguous basal layer containing 3 major cell sub-types; stem, transit-amplifying (TA) and committed basal (CB) cells. A driver mutation in normal human prostate epithelial cells leads to a transformation into cancerous stem cells, oxidative stress, and inflammation. This inflammation results in proliferative inflammatory antrophy (PIA), hyperproliferation of luminal cells, which secrete PSA, an indicator of prostate cancer at high level, and androgen receptor, DNA-binding transcription factor. Subsequently, PIA originates prostatetic intraepithelial neoplasia (PIN), the main precancerous legion for the prostate, most generally in the peripheral zone. PIN turns over into advanced prostate adenocarcinoma by invading local zone. Cancer is characterised by luminal hyperproliferation, loss of the basal layer and stromal reactivity. Finally, metastic prostate cancer emerges due to epithelial-mesenchymal transition (EMT). EMT is a mechanism in which cells lose their epitelial characteristics, and gain mesenchymal characteristics (Packer & Maitland, 2016).

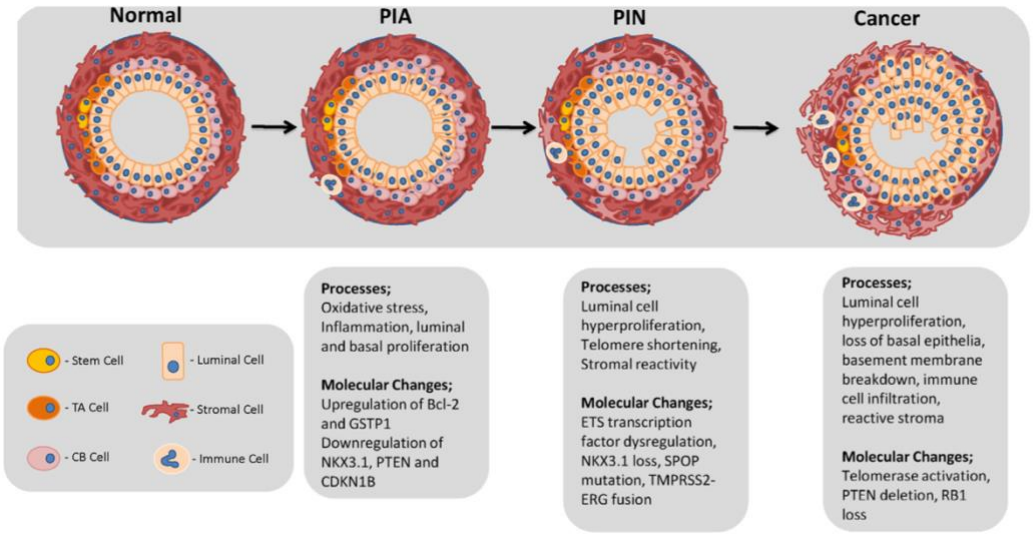

Figure 1.2 Malignant transformation of prostate cancer. (Packer & Maitland, 2016)

1.1.2 Metastasis of Prostate Cancer

Metastasis is the major source of prostate cancer-associated deaths. Through EMT, epithelial cells become mesenchymal stem cells by losing their polarity and adhesion ability. In this way, cancer cells gain the ability to migrate and invade. They can spread in the circulation as circulating tumor cells (CTCs). The first possible regions for metastatic prostate cancer are generally adjacent lymph nodes; besides, CTCs may metastase to bone, lungs and liver (Sleeman & Thiele, 2009).

In prostate cancer tissues, stromal cells represent a composite population, able to support cancer cells' survival, growth, and motility. The cell population is classified into four cell groups; immune cells, fibroblasts, endothelial cells, and progenitor cells. Immune cells, such as lymphocytes and macrophages, counteract the tumor progression after being activated by tumor-released cytokines. Also, cancer-associated fibroblasts and myofibroblasts, which influence the stiffness by ECM composition, produce useful metabolites to promote cancer progression and cytokines for invasiveness. Endothelial cells participate in the remodeling of ECM

and formation of sprouting vessels. And lastly, bone marrow–derived stem/progenitor cells are recruited to the tumor site and contribute to an increase in the reservoir of other stromal cells (Chiarugi, Paoli & Cirri, 2014). In the prostate gland, the proliferation of luminal cells are directly related to ECM composition and stromal cells. Among the stromal cells, cancer-associated fibroblasts (CAFs) play an important role in behaviour and malignancy of prostate cancer by activating ECM. It has been reported that CAFs activate EMT of prostate cancer cells by inducing a transcriptional program to lose their cell-cell adhesions and gain motility. Therefore, prostate cancer cells can go out primary malignant side and spread. CAFs also enhance anchorage-independent growth and repopulating ability of cancer cells by boosting their stem-like traits such as CD44, which is a cell surface protein that is highly expressed in cancer cells and can intreact with hyaluronic acid and collagen to enchance metastasis (Senbanjo & Chellaiah, 2017; Giannoni et al., 2010). It was shown that CD44 expression increases the tumor initiation potential of prostate cancer cells (Patrawala et al., 2006).

1.1.3 Prostate Cancer Cell Lines

Due to prostate cancer's high incidence and death rate, it has been a subject of various studies for decades. Prostate cancer cell lines have been used very widely to understand the disease's mechanism and develop different treatment strategies. The requirement for an ideal *in vitro* models of prostate cancer in different stage has led to the establishment of various cells lines from human prostate cancer cells (van Bokhoven et al., 2003). The human prostate cancer cell lines vary depending on their sources e.g. bone metastasis, lymph node metastasis, lumbar metastasis; requirements, and characteristics e.g. androgen sensitivity (Russell & Kingsley, 2003).

Among the most popular human prostate cancer cell lines (e.g. DU-145, DuCap, 22Rv1, etc.), PC-3 and LNCaP (Lymph Node Carcinoma of the Prostate) are widely-used for prostate cancer research. The PC-3 cell line was established from a 62-year-

old Caucasian man's prostatic adenocarcinoma cells which are metastatic to bone in 1979 (Kaighn et al, 1979). LNCaP cell line was established from a 50-year-old Caucasian man's prostatic adenocarnoma cells which are metastatic to the supraclavicular lymph node in 1977 (Horoszewicz, 1983; Reiter et al., 2013).

The main difference between PC-3 and LNCap is androgen sensitivity; LNCaP is the first established androgen-sensitive prostate cancer cell line, while PC-3 is androgen-independent (Russell & Kingsley, 2003). Over the decades, these two prostate cancer cell lines have been studied by researchers to mimic vairous aspects of prostate cancer with PC-3 as an aggressive form of prostate cancer due to refractory characteristic to androgen and LNCaP as a less-aggressive form of prostate cancer. LNCaP is less aggressive than PC-3, they still represent tumorigenic and metastatic phenotypes (Pogoda et al., 2021). Moreover, PC-3 has been studied to mimic castration-resistant tumours whereas LNCaP has been used to mimic androgen-dependent tumors (Morgan, Saba & Gower, 2000). As an indicator of EMT, the mesenchymal marker N-cadherin increases and epithelial marker E-cadherin, one of the most important epithelial markers lost in EMT, decreases in both cells lines (Brett, Pandey & Fraizer, 2013). Studies shows that E-cahderin's reduction or absence provides cancer cell lines metastatic and invasive potential (Isaacs et al., 1994; Thakuri, Liu, Luker & Tavana, 2017). Also, the gain of vimentin, an intermediate filament protein, indicates the development of metastases in prostate cancer tumor biology (Singh et al., 2003). A study states that the drug resposivenesses of these two prostate cancer cell lines are very similar (Rae & Mairs, 2016). In the light of this information, LNCaP and PC-3 prostate cancer cell lines were used to represent the essensial behaviours of the prostate cancer in this particular study.

1.2 Tumor Models in Cancer Research

Not only the prostate cancer, but cancer has also become one of the most leading concerns of the world as a severe disease with extremely high death rates for decades.

GLOBOCAN 2020 statistics show that almost 20 million new cancer cases and 10 million cancer-associated deaths were recorded in 2020 worldwide. Therefore, cancer studies have gained a very significant role for the human race. The disease mechanisms and cure strategies are widely studied to overcome the cancer-dependent loss. Proper tumor models that can mimic carcinoma are badly needed to carry out cancer pathogenesis, metastasis, treatment, and cancer therapy studies *in vitro*. However, a wide range of tumor models has been developed and used for these studies, they have both advantages and disadvantages against each other (Stock et al., 2016).

Due to the high incidince of prostate cancer, it has become the most diagnosed cancer among men, but its etiology still remains relatively unknown. For this reason, many different *in vitro* and *in vivo* models have been developed to study the initiation, progression and metastasis of prostate cancer. Dogs and primates also have prostate cancer and have been used as animal models in prostate cancer studies. However, these models are not economical and their physiology is significantly different from human beings. Human-derived models, such as primary cells or tissue slice grafts implanted to immunodeficient mice (Zhao et al., 2010; Song et al., 2014) and xenografting of cancer tissue to mice (Lawrence et al., 2013) have the same limitations as the animal models. They do not imply the exact mechanism of prostate cancer in the human body. Thus, *in vitro* models are used rather than animal models as they are more relevant and less expensive. However, there are still challenges in their suitability of *in vitro* models. *In vitro* tumor models can be discussed in two groups; two-dimensional (2D) and three-dimensional (3D) tumor models. Each group still contains various models generated and designed with different methodology, approaches, and purposes. Figure 1.3 represents *in vitro* tumor models; 2D models are the monolayer culture of cancer cells, 2.5D models are coculture of cancer cells on biomatrices, 3D models are the spheroids aggregates of cancer cells, and bioengineered complex *ex vivo* models retains the original tissue morphology and heterogenity with 3D scaffold. *In vitro* models for cancer tissues have differences in the structure of the model and the organization of cells.

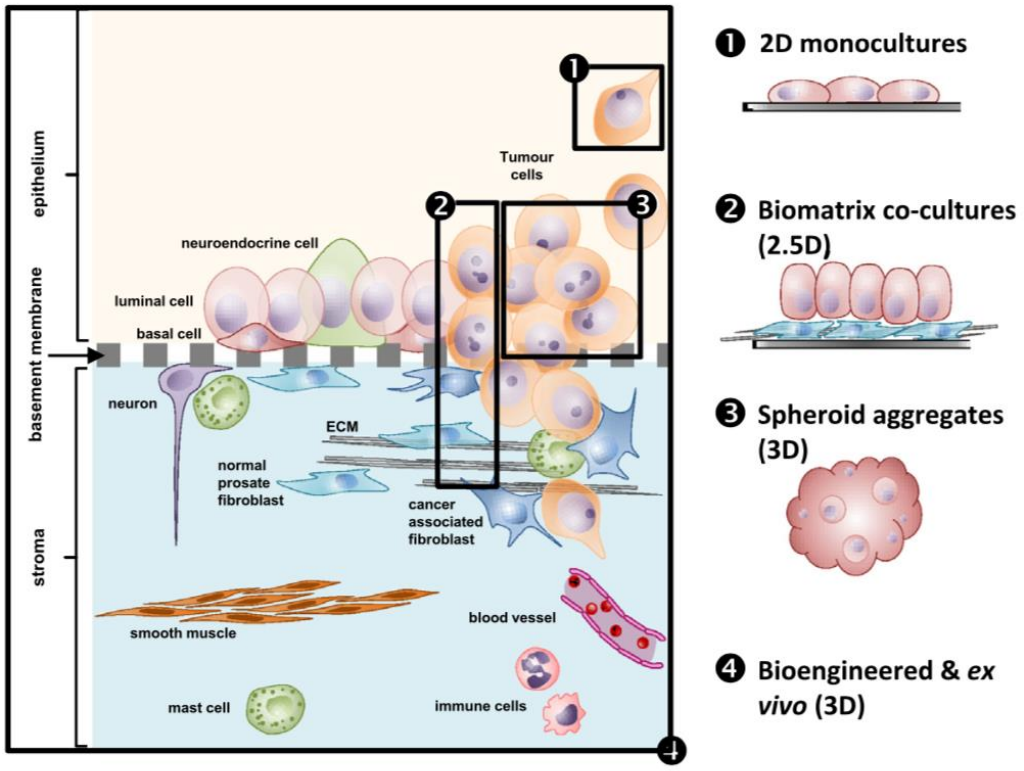

Figure 1.3. *In vitro* modelling systems of prostate cancer (Ellem et al., 2014)

1.2.1 2D Prostate Tumor Models

Two-dimensional (2D) tumor models are widely used to study cancer cell behavior. They are basicly monolayer culture of carcinogenic cell lines in a culture flask or Petri dishes. 2D monocultures are mainly dependent on immortalized cells. 2D cell culture is a widely used *in vitro* technique for providing an opportunity to research cell biology, tissue morphology, and mechanisms of diseases, protein expression, drug action, and the development of tissue engineering. Most studuies about cancer biology are based on experiments using 2D cell cultures *in vitro* due to their simplicity and low-cost maintenance (Kapałczyńska et al., 2016). Besides, they are highly preferred *in vitro* tool for cancer studies. They cannot recapitulate the three-dimensional (3D) architecture and complexity of human tumors due to the

limitations of 2D cell cultures. These limitations arise because single layers of cells cannot present the same cell morphology and proliferation rate with the cells within the tumor tissue (Blanco-Fernandez, Gaspar, Engel & Mano, 2021; Stock et al., 2016). Thus, 2D models do not sufficiently mimic the microenvironment of cancer cells or present the *in vivo* tumor characteristics (Hutmacher et al., 2010). Furthermore, the 2D monolayer culture systems tend to fail to recapitulate the complex nature of *in vivo* tumors due to limitations such as lack of mimicking natural 3D microenvironment and morphology of cancer cells due to loss of cell polarity, the structural integrity of the extracellular matrix (ECM), and tertiary structure of ECM proteins (Ellem et al., 2014).

Despite all the disadvantages of 2D monolayer models, they are still used for cancer studies. These models cells are commonly cultured in typical flat cell culture dishes at body temperature, with a corresponding medium which generally contains antibiotics, serum, and some growth factors to improve the cell growth. The major advantage of the 2D models is that they are easy to handle with simple cell culture methods. Also, they are very accessible and reproducible, allowing them to work with these models in any laboratory. As mentioned before, the most used 2D models for prostate cancer are PC-3, LNCaP, and DU-145 cell lines in prostate cancer cell lines.

2D cell culture systems are currently used to research genetic and biological prostate cancer. Different prostate cancer cell lines are subjected to study molecular alterations associated with drug response (Jia et al., 2019), the effect of mechanical stimulation on the development of prostate cancer (Han et al., 2019), determination of the potential benefit of the combination of radiation treatment with cytotoxic drugs (Rae & Mairs, 2021), androgen response (Horning et al., 2017), molecular biosensors and probes (Varnosfaderani, Emamzadeh, Nazari & Zarean, 2019), mechanism of osteoblastic bone metastasis (Elshafae et al., 2020), and anti-tumor effects of zinc (Xue et al., 2019), estramustine phosphate (Wei et al., 2018), and 3′,4′,5′-trimethoxyflavonol (Hill et al., 2015).

1.2.2 3D Prostate Tumor Models

Due to these challenges that 2D models are faced with, there is an increasing demand for the development of 3D models which mimic the actual cancerous tissues. As shown in Figure 1.3., 3D models can be generated either by aggregation of cells as spheroids or in a more complex manner as bioengineered *ex vivo* 3D models, which are developed to support cells with more native-like tissue properties and study the characteristics of the tumor tissue within a three-dimensional ECM like microenvironment with cells entrapped in appropriate scaffolds (Katt, Placone, Wong, Xu & Searson, 2016). Most frequently used 3D models are generated in spheroids which can be seen as multicellular 3D systems. Spheroids are more likely to mimic the tumor tissue properties rather than 2D monolayer cultures, and cells behave more similarly to *in vivo* in terms of cellular topology, gene expression, metabolism, and signaling. 3D morphology of the spheroids mimics avascular tumors in the sense of cell-cell adhesion. These physical interactions and intercellular signaling between cancer cells in spheroids regulate the tumor growth, invasion, and drug response (Thakuri, Liu, Luker & Tavana, 2017). Low oxygen level in the core of the spheroids results in hypoxic and dormant cells and an acidic extracellular environment. This hypoxic tumor environment promotes the evolution of cancer stem cells that can repopulate a tumor mass and resist drug treatments. Low pH in the environment reduces uptake of weakly alkaline drugs (Benien & Swami, 2014). However, the spheroids are still typically homogenous and cannot mimic the tumor microenvironment exactly. Biomaterial-based 3D scaffolds have been developed to improve the 3D spheroid models (Ellem et al., 2014). These engineered 3D tumor models provide cells a complex tissue matrix and a functional *in vivo* tissue environment with various cell adhesion sites offered by the chemical structure of the biomaterials.

It is known that in 3D tissue-mimicking models, there are significant changes in cell morphology, rates of proliferation, and expression of biomarkers (Windus et al., 2012). Thus, there is a need to develop a reliable 3D tumor microenvironment for

prostate cancer studies. 3D *in vitro* models can overcome the limitations in 2D models and mimic the appropriate environment for tumor development and migration which makes it possible to mimic prostate cancer metastasis and to test anticancer drugs. Also, 3D *in vitro* models are unique to replace animals in cancer metastasis research.

Studies show that spheroids as 3D tumor models are more reliable than 2D in terms of studying pre-clinical tests for the screening of therapies (Boucherit, Gorvel & Olive, 2020), anti-cancer drug discovery (Zanoni, Pignatta, Arienti, Bonafè & Tesei, 2019), drug sensitivity (Muguruma et al., 2020; Mosaad, Chambers, Futrega, Clements & Doran, 2018), tumor targetted drug delivery systems (Huang & Gao, 2018), treatment strategies (Sioud, Juzenas, Zhang, Kleinauskas & Peng, 2021) and tumor-stroma interaction (Shao et al., 2020). Previous studies have extended the usage of 3D prostate cancer models in drug discovery (Fontana et al., 2020), clinical decision making (Van Hemelryk & van Weerden, 2020), tumor growth and progression (Neuwirt et al., 2020) and metastasis (Ahangar et al., 2018; Molla, Katti & Katti, 2017; Qiao & Tang, 2018)

1.3 Biomaterials Used in the Design of 3D models

In situ, cancerous cells are found in a 3D tumor microenvironment which affects their development and responses to external stimuli. Dynamic reciprocity (DR) is a phenomenan that refers the interaction between cells and their microenvironment, espeacially the ECM. It is demonstrated that the changes in the ECM directly influences the expression of genes through the cell adhesion sites (Bissell, Hall & Parry, 1982). This natural microenvironment of tumors can be mimicked by developing a scaffold with biomaterials which provide 3D structural environment by supplying physiologically relevant functional and structural 3D support to cell *in vitro* as *in vivo*.

Biomaterials are substances designed to interact with biological systems for diagnostic or therapeutic purposes. They are divided into 4 groups; metals, ceramics, polymers, and composites. A specific subgroup of polymeric biomaterials that is used as a scaffold material for 3D tumor models is hydrogels. Hydrogels are complex networks that are produced by cross-linkage of hydrophilic polymers. In the design of 3D models, natural, synthetic, or hybrid biomaterials can be used to produce the hydrogel scaffold, as shown in Figure 1.4 (Kundu et al., 2019). Figure 1.4 presents the engineered tumor microenvironments created by natural and synthetic hydrogels. These hydrogel materials are fabricated through numerous physical and/or chemical crosslinking reactions. Physical and biological properties of these hydrogel scaffolds, such as stiffness, 3D topography, cell adhesion ligands, can be controlled; thus, an advanced 3D tumor model can be designed to better understand cancer biology. Hydrogel scaffolds serve as the carrier biomaterial since they can mimic the microenvironment of the natural ECM and tumor tissue and represent a more relevant microenvironment than the other 3D tumor models.

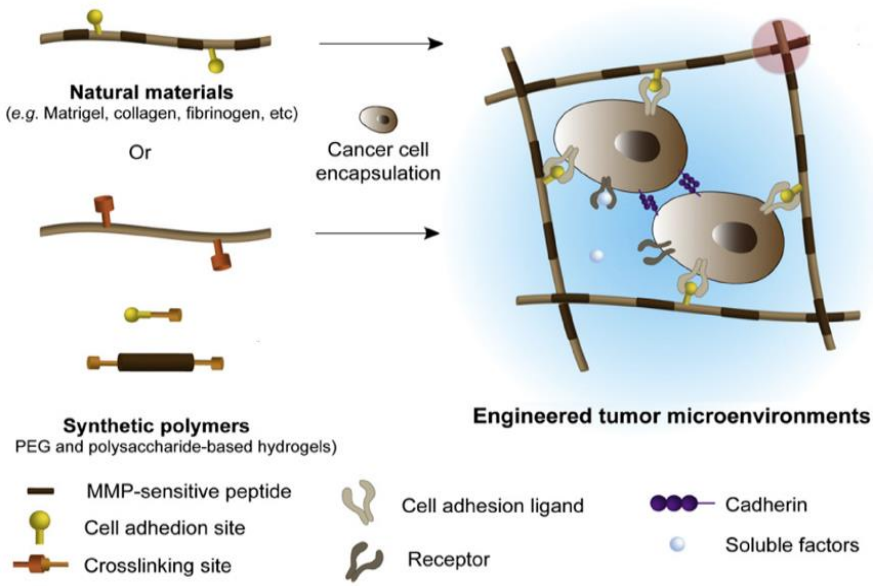

Figure 1.4. A schematic representation of engineered tumor microenvironment created by using natural/synthetic hydrogels for *in vitro* tumor models (Song et al., 2014).

1.3.1 Hydrogel Based Tumor Models in Cancer Metastasis

Hydrogels, hydrophilic polymers, are commonly used as biomaterials of choice for tissue models. Their excellent properties provide support as cell carriers and ECM-like environment for mimicking the cancer tissue and enable more control on the generated microenvironment by their tunable shape, mechanical, and chemical properties. Thus, they can be adapted according to desired mechanical properties of tissue of interest (Song et al., 2014). Hydrogels are highly water absorbent thanks to their hydrophilic nature, which provides a desirable ECM for the exchanges of cellular metabolites (Caballero, Reis & Kundu, 2020).

The tumor model can be developed either synthetic or natural hydrogels or hybrid, composed of two or more hydrogels. Synthetic hydrogels commonly used for 3D models are polyethylene glycol (PEG), polyvinyl alcohol (PVA), polyacrylamide (PAM), polyacrylic acid (PAA), poly(ε-caprolactone) (PCL), and their derivatives (Madduma-Bandarage & Madihally, 2020). They generally possess better mechanical properties than natural hydrogels since they are easy to synthesize and control mechanical and chemical properties. Despite these advantages of synthetic hydrogels, they do not provide natural cell adhesion sites, a critical ECM feature. They have to be functionalized with cell adhesion ligands (Caballero, Reis & Kundu, 2020).

Natural hydrogels commonly used for 3D models are collagen, fibrin, gelatin, polysaccharides such as chitosan, alginate hyaluronic acid (HA) (Kundu, Reis & Kundu, 2020). Natural hydrogels are mostly made of native ECM proteins and components; this feature makes them highly biocompatible and suitable for 3D modeling applications. Cells interact better with these hydrogels due to cell adhesion sites that synthetic hydrogels lack. (Catoira, Fusaro, Di Francesco, Ramella & Boccafoschi, 2019). On the other hand, natural hydrogels also have disadvantages, such as complex molecular structure, biodegradability, or batch-to-batch variability.

Collagen is the most abundant protein found in the ECM; this makes it one of the best choices for tumor modeling. Collagen is widely used for the 3D tumor models. It provides an excellent scaffold for tumor microenvironments since it is a natural ECM protein. It is known that tumor cells bind collagen through the tripeptide RGD (Arg-Gly-Asp), an integrin-binding site (Saltzman, 2004). Integrins are important regulators for communication between cells and their microenvironment. These integrins play a major role in cancer progression and metastasis (Nieberler et al., 2017). Even though collagen is the perfect material for tissue modeling, it also has limitations in its degradability and low cross-linking. Gelatin, denatured collagen, is also used in place of collagen and has similar properties with collagen. Gelatin can be used as sacrificial micromolding material due to its thermoresponsive gelation below 30–35 °C through the establishment of noncovalent interactions (Blanco-Fernandez, Gaspar, Engel & Mano, 2021).

Hyaluronic acid (HA) is the simplest glycosaminoglycan (GAG) found in ECM, which is also known to accumulate in tumors tissues (Thakuri, Liu, Luker & Tavana, 2017). The interaction between HA and cells is provided through the cell surface receptors such as receptor for hyaluronan mediated motility (RHAMM) and CD44, which are cell surface adhesion receptors that are highly expressed cancer cells and regulate metastasis via their interaction with extracellular matrix ligands (Turley, Noble & Bourguignon, 2002; Wang et al., 2016; Senbanjo & Chellaiah, 2017). HA is a desired polymer for tissue engineering studies since it is inherently biocompatible, bioactive, biodegradable, and non-immunogenic like collagen (Balazs & Laurent, 1998). HA does not have the tripeptide RGD; thus, it cannot provide integrin-mediated cell engagement.

Recently, in the literature, various natural and synthetic hydrogels have been used for manufacturing 3D tumor models for different studies. Hybrid alginate, gelatin, and decellularized ECM hydrogel bioink model for immortalized human squamous cell carcinoma was developed (Kort-Mascort et al., 2021). GelMA and Matrigel-based hydrogel tumor model of osteosarcoma is designed to study drug response

(Monteiro, Gaspar, Ferreira & Mano, 2020). The hybrid of collagen and alginate hydrogels was used for the human breast cancer cells model to study cell migration (Liu, Lewin Mejia, Chiang, Luker & Luker, 2018). Methacrylated hyaluronic acid (HAMA) and methacrylated gelatin (GelMA) hydrogels-based breast cancer cell model was generated to study EMT and migration (Wang et al., 2018). Also, commercially available dextran-CD hydrogels were used for invasion and migration studies of glioblastoma (Huang et al., 2017). PEG-based hydrogel models for lung cancer were used to analyze the natural killer cell suppression in cancerous tissues (Temples, Adjei, Nimocks, Djeu & Sharma, 2020). Mesenchymal stem cells and PC-3 seeded PCL-based tumor model was used to repopulate the bone microenvironment for prostate cancer metastasis (Molla et al., 2019). Among hydrogel-based tumor model studies, collagen-based models exist (Redmond, McCarthy, Buchanan, Levingstone & Dunne, 2021). However, methacrylated collagen is not widely used for tumor models.

1.4 Aim, Approach and Novelty of the Study

The physical and cellular microenvironment influences cancer proliferation, progression, and metastasis. 2D monolayer culture systems are still used in cancer studies; however, these systems lack the cell-cell and cell-ECM interactions, which play an important role in cancer biology through biochemical and mechanical signals. Hydrogel-based 3D *in vitro* scaffold models enable to recapitulate 3D structure and signaling in tumors by mimicking the ECM.

There are studies based on natural or synthetic polymer hydrogels for prostate tumor tissues in the literature. Hyaluronic acid-alginate (Tang et al., 2017), chitosan-alginate (Xu et al., 2019), HAMA, and GelMA (Antunes et al., 2019) hydrogels were used for the generation of prostate tumor cancer models. In a recent study, HAMA and GelMA were used to generate 3D spheroid microgels. The interaction of PC-3 cells with osteoblasts was studied for the drug screening process. The different ratios (by 2.5% HAMA-5% GelMA and 5% HAMA-5% GelMA) of hydrogels were used

to form microhydrogels to examine the viability of osteoblasts and matrix mineralization (calcium deposition) by these cells entrapped in the gels to mimic the prostate stroma. They showed that the interaction between prostate cancer cells and osteoblast activated the bone-forming cells. The microgels composed of 2.5% HAMA - 5% GelMA resulted in higher drug resistance in cells. However, the study mainly focused on using superhydrophobic surfaces to produce a spheroidal 3D disease model of prostate cancer and the interaction between PC-3 and osteoblasts to promote the bioactivity of bone-forming cells. However, it did not present any data on the prostate cell migration and metastasis, which still generates a need for a model tumor tissue for cell metastasis studies.

We developed a hybrid hydrogel system composed of methacrylated collagen (ColMA) and methacrylated hyaluronic acid (HAMA) to mimic tumor microenvironments in prostate cancer for migration studies. As the material choice, collagen and hyaluronic acid were used in the study to produce hydrogels since they are the most abundant components of natural tissues. The prostate stroma and collagen are chemically similar to native tissues ECM (Antunes et al., 2019). Also, it is known that the presence of the collagen affects the cells to undergo epithelial-mesenchymal transition (EMT). (Shintani, Maeda, Chaika, Johnson & Wheelock, 2008) Microgels were developed in 96-well plates with different compositions. Tumor vascularization is required for the invasion of tumor cells. Vascular endothelial growth factor (VEGF) is the most important factor for vascularization. It was shown that the fibroblasts around the metastatic prostate cancer cells secrete VEGF and increase metastases (Kaminski et al., 2006).

In the literature, the existing models do not consider the effect of both collagen and fibroblasts on the metastatic behavior of cancer cells. A healthy prostate stroma is mainly composed of smooth muscle cells. However, it is shown that there is a significant decrease in smooth muscle cells. At the same time, myofibroblast and fibroblast contents increase in prostate cancer tissue. In the present study, the tumor model was developed to mimic the metastasis of prostate cells in the proposed hydrogel model. Fibroblasts were included in the gel microenvironment because they

have a significant effect on the metastatic behavior of the cells. Besides, the prostate tumor microenvironment involves many fibroblast and myofibroblast cells, which significantly affect tissue stiffness. The stiffness of cancerous prostate tissue is almost 2.4 times greater than normal prostate tissue (Hoyt et al., 2008). The alterations in cell content affect the mechanical properties of the cancerous tissue by increasing the ECM protein expression such as collagen type I (Tuxhorn et al., 2002). Thus, it is important to include fibroblast cells in a tumor mimicking hydrogel to obtain a reliable model. Moreover, metastatic prostate cells have an epithelial-mesenchymal transition (EMT) mechanism, which is an indication of metastasis, and this is an important marker to track the stage of prostate cancer (Khan et al., 2015), so the EMT markers, E-cadherin and vimentin, were used to detect the migration of prostate cells in this study.

It was expected that the mechanical and chemical properties of different compositions of hydrogels and the presence of fibroblast cells would highly improve the similarity of the prostate tumor microenvironment to that in metastatic cancer cells. As a result of this study, it was shown that the presence of high ColMA concentration and fibroblast in the 3D hydrogel scaffold promotes the migration of prostate cancer cells through EMT. The expression levels of E-cadherin, which is an epithelial marker, and vimentin, which is a mesenchymal marker, were calculated from the fluorescence intensities in the immunostained samples. It was shown that E-cadherin expression was downregulated. In contrast, vimentin expression was upregulated in the presence of fibroblast cells in the hydrogel model as an indicator of migration.

There is a need for rapid, repeatable, high throughput platforms to study cell-material interactions and the effects of drugs on the metastatic process. Thus this project aims to meet the shortcomings of the existing methods. The model can be used as a screening platform for drugs, cell migration studies, and cell-material interactions and in patient-specific testing and screening in future studies. Due to its tunable nature, different compositions of gels can be designed for specific purposes.

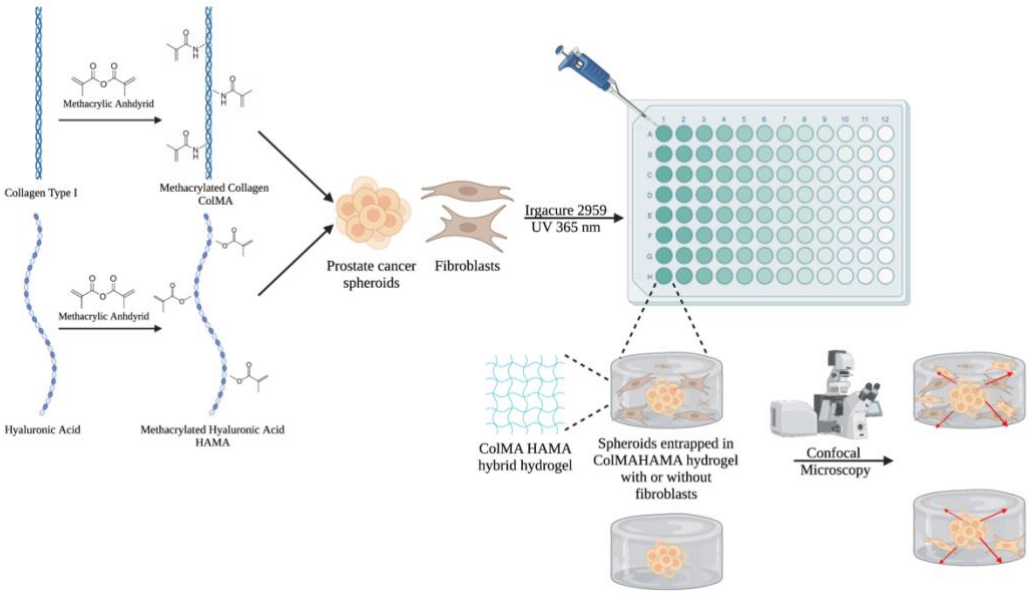

Figure 1.5. A schematic representation of the project methodology.

CHAPTER 2

MATERIALS AND METHODS

2.1 Materials

Triethylamine, glycidyl methacrylate, hyaluronic acid (HA), methacrylic anhydride, deuterium oxide (D_2O), 2-hydroxy-4′-(2-hydroxyethoxy)-2-methylpropiophenone (Irgacure 2959 photo initiator), hydrocortisone, insulin, ascorbic acid, penicillin and bovine serum albumin (BSA) were purchased from Sigma (USA).

Roswell Park Memorial Institute (RPMI) 1640 medium, fetal bovine serum (FBS), sodium pyruvate, Dulbecco's Modified Eagle Medium (DMEM) High Glucose medium, 0.25%(w/v) Trypsin-EDTA (Ethylenediaminetetraacetic acid) and 0.05%(w/v) Trypsin-EDTA were bought from Sartarius (Israel).

Live/Dead™ Viability/Cytotoxicity Kit, Qtracker™ 655 Cell Labeling Kit, CellTracker™ Green CMFDA Dye, Alexa Fluor 488® labeled Phalloidin solution, 4',6-Diamidino-2-Phenylindole, Dihydrochloride (DAPI), Alexa Fluor 647® labeled Phalloidin, Goat anti-Mouse IgG Alexa Fluor ™ Plus 647 and Goat anti-Rabbit IgG Alexa Fluor ™ Plus 555 were bought from Invitrogen (USA).

Dimethyl sulfoxide (DMSO) and 4% paraformaldehyde were purchased from CruzChem (USA). Acetic acid, Tween-20 and dimetilformamide (DMF) were purchased from Merck (Germany).

Anti E-cadherin antibody [HECD-1] mouse monoclonal and Anti-Vimentin antibody [EPR3776] – rabbit monoclonal were bought from Abcam (UK).

Dialysis tubes (10,000 MWCO, SnakeSkin® Dialysis Tubing) was bought from Thermo Scientific (USA).

Fibroblast growth factor (FGF) was bought from Cell Signaling Technology (USA).

1% Triton-X 100 solution was purchased from Acros Organics (Germany).

2.2 Methods

2.2.1 Preparation of Hydrogel Microtumor Mimics

2.2.1.1 Synthesis of Methacrylated Collagen (ColMA)

Collagen (1 g) was dissolved in 5% acetic acid (200 mL) (Merck, Germany) at room temperature for 3-5 days and filtered by V50 vacuum filter. The solution was neutralized (to pH 7.4) with 5N NaOH. Triethylamine (5 mL) (Sigma, USA) and tween-20 (1.8 mL) (Merck, Germany) were added to solution before a dropwise addition of glycidyl methacrylate (3.3 mL) (Sigma, USA). The solution was stirred at 4°C overnight. Then, pure ethanol (2-volume excess of solution) was added to precipitate the ColMA. The ColMA precipitate was recovered by centrifugation (12,000 rpm, for 5 min) (Sigma, USA) and lyophilized by freeze drier (Labconco, USA).

2.2.1.1.1 Isolation of Collagen

Type I collagen was isolated from male Sprague Dawley rat tails. Tendons from rats' tails were removed and placed in 0.5 M acetic acid for a few days at 4 °C to dissolve. The solution was filtered and dialyzed in dialysis buffer (5 L, 12.5 mM sodium phosphate sibasic, 11.5 mM sodium phosphate monobasic, pH: 7.2). Then, it was centrifuged and the pellet will be dissolved in 500 mL of 0.15 M acetic acid at 4 °C overnight and dialyzed for 5 days. Obtained collagen was centrifuged and dissolved in 70% EtOH for 48 h and the pellet was lyophilized for 12 h..

2.2.1.2 Synthesis of Methacrylated Hyaluronic Acid (HAMA)

0.5% hyaluronic acid (HA) (Sigma, USA) was dissolved at room temperature overnight. Dimetilformamide (DMF) (Merck, Germany) was added to the solution after the complete dissolution of HA (DMF: H_2O, 2:3). The solution was cooled at 4°C for at least 1 hour and placed on an ice bed on a magnetic stirrer at 4°C. 2 mL of Methacrylic anhydride (Sigma, USA) was added to the solution and pH was adjusted to 8-9 by adding 5N NaOH. Methacrylic anhydride (1 mL) was added dropwise to the solution and pH was adjusted to 8-9 by adding 5N NaOH. This step was repeated until about 10 mL methacrylic anhydride was added in total. The solution was stirred at 4 °C overnight and dialyzed against dH_2O in dialysis tubes (10,000 MWCO, SnakeSkin® Dialysis Tubing, Thermo Scientific, USA) at 4 °C for 4-7 days. After dialysis, solution was filtrated to remove any particles. The filtrate will be poured into poly(dimethylsiloxane) (PDMS) coated petri dishes and frozen at -80 °C. The samples are lyophilized by freeze drying until completely dry.

2.2.1.3 Characterization of ColMA & HAMA Hydrogels

2.2.1.3.1 Nuclear Magnetic Resonance (NMR) Analysis

Hydrogels were characterized with NMR spectra. Hydrogels (collagen, ColMA, HA and HAMA) were dissolved in deuterium oxide (D_2O) (5 mg/mL) (Sigma, USA) at 4°C, ^{1}H-NMR spectra of solution were generated at 400 MHz via Bruker DPX 400 spectrometer (Bruker, USA).

2.2.1.3.2 Fourier-Transform Infrared Spectroscopy (FTIR) Analysis

Hydrogels were characterized with FTIR analysis. FTIR spectra of dry samples of collagen, ColMA, HA and HAMA were analysed in the range of 4000 to 400 cm^{-1},

at a resolution of 1 cm^{-1} via Frontier FTIR spectrophotometer (Perkin Elmer, USA), and spectra were generated.

2.2.2 Preparation & Crosslinking of ColMA/HAMA Hydrogel

HAMA and ColMA were dissolved in PBS containing the Irgacure 2959 photo initiator (0.5% w/v) (Sigma, USA). HAMA and ColMA solutions were combined in different ratios (Table 2.1). Col/HA hydrogels were formed by UV cross-linking via OmniCure® S2000 UV lamp (Lumen Dynamics, Canada) (365 nm, 1 W/cm^2 from 3 cm distance for 5 sec) for further analysis in gel form. Cell loaded hydrogels were obtained by mixing the cells with or placing the spheroids in the solution before UV cross-linking to obtain the cell loaded hydrogel.

Table 2.1 ColMA and HAMA contents of different designs of ColHA hydrogels.

	ColMA (% w/v)	:	HAMA (% w/v)
ColMA:HAMA 1:1	0.05	:	0.05
ColMA:HAMA 1:1.5	0.05	:	0.075
ColMA:HAMA 1:2	0.05	:	0.1
ColMA:HAMA 1:5	0.05	:	0.25
ColMA:HAMA 1:10	0.05	:	0.5
ColMA:HAMA 1:1-High	0.5		0.5

2.2.2.1 Characterization of ColMA/HAMA hydrogels

2.2.2.1.1 Mechanical Testing of Hydrogels

Five replicates of different ratios of COL-HA hydrogels were prepared for mechanical testing. Mechanical tests were done using a mechanical tester with a 50 N load cell Shimadzu AGS-X 5 kN, (Shimadzu Scientific Instruments, Japan).

2.2.2.1.2 *In situ* Degradation

For the degradation test of COL-HA hydrogels, three samples from each hydrogel ratio were lyophilized and their dry weights were recorded. Lyophilized hydrogels were incubated in PBS (10 mM, pH 7.4) on a rotary shaker at 50 rpm and 37°C (New Brunswick Scientific, USA). At 3 time points (1, 4 and 7 days), samples were taken from PBS, washed with distilled water 3 times and lyophilized. Lyophilized samples were weighed in order to determine weight loss.

2.2.2.1.3 Swelling Testing of Hydrogels

Water retention of different ratios of COL-HA hydrogels were obtained by swelling test. The dry weights of three samples for each hydrogel compositions were determined. These samples were incubated in PBS (10 mM, pH 7.4) for 48 h. The samples were removed from PBS at 30 min, 1, 2, 4, 6, 24 and 48 h. The wet weight of each sample was determined after the excess PBS was removed with tissue paper. The following equation was used to calculate the Water Content .

$$WC\ (\%) = \frac{W_w - W_d}{W_w} x100$$

where WC (%): Water Content (%, w/w)

W_d: Dry weight of the samples (mg)

W_W: Wet weight of the samples (mg)

2.2.3 *In Vitro* Studies

2.2.3.1 Culture of Prostate Cancer Cell Lines: PC-3 & LNCaP

PC-3 and LNCaP prostate cell lines were used. They were cultured in RPMI 1640 medium supplemented with 10% fetal bovine serum (FBS), 2 mM L-glutamine, 100 units/mL penicillin, and only LNCaP cells 1mM sodium pyruvate, were all purchased from Sartorius, Israel. Cells were incubated in tissue culture polystyrene (TCPS) flasks placed in CO_2 incubators arranged in culture conditions at 37 °C with a 5% CO_2 humidified atmosphere by renewing media every 2-3 days. Cells were subcultured by removing the cell from TCPs flask by 0.25%(w/v) Trypsin-EDTA (Sartorius, Israel). Cells were stored frozen in their complete growth medium containing 5% DMSO (v/v) (CruzChem, USA) at -196°C in liquid nitrogen.

2.2.3.2 Culture of Human Dermal Fibroblast

Human Dermal Fibroblast, adult (HDFa) cell line was cultured in DMEM high glucose medium (Sartorius, Israel) supplemented with 2% fetal bovine serum (FBS), 1 µg/mL hydrocortisone (Sigma, USA), 4 mM L-glutamine, 5 µg/mL insulin (Sigma, USA), 5 ng/mL FGF (Cell Signaling Technology, USA), 50 µg/mL ascorbic acid (Sigma, USA) and 100 U/mL penicillin (Sigma, USA). Cells were incubated in the same conditions with prostate cancer cell lines. Cells were subcultured by removing the cells from TCPs flask by 0.05%(w/v) Trypsin-EDTA (Sartorius, Israel). Cells were stored frozen in their complete growth medium containing 5% DMSO (v/v), at -196°C in liquid nitrogen.

2.2.3.3 Formation of Prostate Cancer Spheroids

When cells reached approximately 80% confluency in the T75 TCPs flask, the medium was discarded. The cell layer was rinsed with PBS (5 mL). After adding 0.25%(w/v) trypsin-EDTA (3 mL), flask was incubated 37 °C for 5 min. A complete growth medium (6 mL) was added to inhibit trypsin when the dispersion of the cell layer was observed. The cell suspension was collected and centrifuged at 3,000 rpm for 5 min (Rotofix 32A, Hettich, Germany). The supernatant was discarded without disrupting the cell pellet. Pellet was dissolved in a complete growth medium (~10 mL), and cells were counted by Nucleocounter (Biolab, Turkey). The concentration of cell suspension was adjusted to 1 x 10^6 cells/mL. The lid of a 60 mm tissue culture dish was removed, and the dish chamber was filled with PBS (5 mL). 50 µL of cell suspension droplets with 1 x 10^6 cells/mL cell concentration were put onto the lid with a sufficient distance between them to prevent touch. Approximately 15-20 droplets were placed onto the lid per dish. The lid was inverted on the bottom of dishes filled with PBS. Tissue culture dishes were incubated at 37 °C in a 5% CO_2 incubator. They were checked daily until the cell spheroids formed, which took almost 5-7 days.

2.2.3.4 Preparation of Spheroid Loaded Hydrogels

After the formation of cell spheroids, each spheroid was placed into a hybrid hydrogel solution (50 µL), prepared corresponding growth medium of cell of interest in a 96 well plate whose bottom was covered with PDMS and were UV crosslinked with the same conditions mentioned above. Cell-loaded hydrogels were incubated in the same medium. They were prepared in a 24 well plate at the same culturing conditions mentioned above.

2.2.3.5 Co-culture of Prostate Cancer Spheroids & Fibroblasts in Microtumor Model

Microtumor models were prepared by placing a prostate cancer spheroid into a hybrid hydrogel solution (50 μL) containing HDFa cells (1 x 10^6 cells/mL) and UV crosslinking. Co-culture of HDFa and prostate cancer spheroids are cultured at the same conditions with the spheroid-loaded hydrogels by mixing their respective media (HDFa and corresponding prostate cancer cell line) by the ratio of 1:1.

2.2.3.6 Characterization of microtumor models

2.2.3.6.1 Live-Dead Assay

Hydrogels loaded with cells were tested for the viability of the cells via Live/Dead™ Viability/Cytotoxicity Kit (Invitrogen, USA). After the medium was discarded, samples were washed with and stained with calcein and ethidium homodimer-1 for 30 min. After washing with PBS, samples were examined by Confocal Laser Scanning Microscope (CLSM) under 488 nm and 561 lasers (Zeiss LSM800, Germany).

2.2.4 Microscopy Studies

2.2.4.1 Staining of Spheroids

Spheroids were stained with live-cell tracker dyes before microtumor models were prepared to distinguish prostate cancer cells from HDFa cells. Qtracker™ 655 Cell Labeling Kit (Invitrogen, USA) or CellTracker™ Green CMFDA Dye (Invitrogen, USA) used for spheroid staining according to manufacturer's directions.

2.2.4.2 Cell and Nucleus Staining

The cell-loaded hydrogels were washed twice with PBS. The samples were fixed in 4% paraformaldehyde (CruzChem, USA) for 30 min at room temperature and washed with PBS. They were permeabilized with 1% Triton-X 100 solution (Acros Organics, Germany) for 15 min at room temperature. After washing with PBS twice, they were incubated in BSA blocking solution (1%, w/v, in PBS) (Sigma, USA) at 37 °C for 60 min to prevent nonspecific binding. Then they were incubated in Alexa Fluor 488® labeled Phalloidin (Invitrogen, USA) or in Alexa Fluor 647® labeled Phalloidin (Invitrogen, USA) solution (1:100 dilution in 0.1% BSA in PBS) for 1.5 h at 37 °C for staining of the actin cytoskeleton. After washing with PBS twice, they were counterstained with DAPI (Invitrogen, USA) for 30 min at room temperature for the staining of nucleic acids. They were washed twice with PBS and stored in well plates in PBS solution at 4 °C. Plates containing stained samples were covered with aluminum foil for light protection until analysis.

2.2.4.3 Immunocytochemistry

Microtumor samples were fixed, permeabilized, and blocked, as mentioned above. For E-cadherin and vimentin imaging, Anti-Vimentin (ab92547) and anti-E-cadherin (ab1416) antibodies (Abcam, UK) which are specific to these proteins, were applied according to the manufacturer's directions. Then, antibodies were tagged with incubation in anti-Mouse IgG Alexa Fluor ™ Plus 647 (Invitrogen, USA) and anti-Rabbit IgG Alexa Fluor ™ Plus 555 (Invitrogen, USA) solution (1:1000 dilution in 0.1% BSA in PBS) for confocal analysis.

2.2.4.4 Monitoring Cell Migration

Micrographs of the cells will be obtained using an inverted Confocal Laser Scanning Microscope under 350 nm, 488 nm, 550 nm, or 630 nm laser sources and appropriate filter sets (Zeiss LSM 800, Germany).

2.2.5 Quantification of Cell Migration via Image Analysis Software

ImageJ (NIH) and cell profiler image analysis software will be used to analyze the micrographs of cell migration assay.

Confocal micrographs of the samples stained with antibodies specific to E-cadherin and vimentin were analyzed using Fiji's image analysis software. Images were processed to obtain gray scale 8-bit images. Then, Fiji's “Lookup table” menu, “HiLo” was selected. Background subtraction was done by adjusting the rolling ball radius to 100 pixels. From the “set measurements” panel, “mean gray value” was chosen. Finally, the intensity of the antibody-specific stain was measured, and a mean gray value (sum of the gray values of all the pixels in the selection divided by the number of pixels) was obtained for each micrograph.

2.2.6 Statistical Analysis

All quantitative data in this study were expressed as mean ± standard deviations with $n \geq 3$ unless otherwise stated. Statistical analysis was performed by one-way ANOVA (analysis of variance) and two-way ANOVA test followed by Tukey’s test for normally distributed data and Kruskal-Wallis test for non-normally distributed data. P-values less than 0.05 were considered statistically significant.

CHAPTER 3

RESULTS AND DISCUSSION

3.1 Characterization of ColMA & HAMA Hydrogels

In this study, hybrid hydrogel containing methacrylated collagen (ColMA) and hyaluronic acid (HAMA) was used in order to develop a prostate cancer tumor model. The naturally occurring extracellular matrix protein (collagen) and glycosaminoglycan (HA) were modified in order to obtain photo-crosslinkable hydrogels with higher long-term stability and mechanical stiffness and with minimal decrease in cytocompatibility (Burdick, Chung, Jia, Randolph & Langer, 2004). Methacrylation provides hydrogels to be designed, as scaffolds can be directly photo-crosslinked with UV to fixate their shape (Billiet, Gevaert, De Schryver, Cornelissen & Dubruel, 2014). Methacrylation modifications of these ECM macromolecules were analysed via NMR and FTIR.

3.1.1 Nuclear Magnetic Resonance (NMR) Analysis

The proton NMR spectra of collagen and ColMA hydrogels were generated at 400 MHz via Bruker DPX 400 spectrometer to determine the incorporation of methacrylate groups into collagen and the degree of methacrylation (DM). Figure 3.1 displays the difference between collagen and ColMA, methacrylation occurs through lysine residues in collagen and results in the formation of olefin (carbon-carbon double bond). ^{1}H NMR spectra (Figure 3.2) display the signals between δ 6.9 and 7.5 ppm (A) from the aromatic group of both samples. The integrated intensity of the aromatic group peaks was used as a comparison reference for the calculation DM of ColMA (Brinkman, Nagapudi, Thomas & Chaikof, 2003). ^{1}H NMR spectrum of ColMA displays signals of olefinic protons of methacrylate between δ 5.30 and

5.56 ppm(B) and the methyl signal of methacrylate at δ 1.8 ppm (D), where collagen spectrum does not display any signal, as an indicator of the methacrylation (Figure 3.2). Signals between δ 2.8 and 2.95 ppm (C) correspond to the methylene group of the lysine, it is known that the functionalization of collagen generally occurs through the lysine. The amine group on the lysine residue undergoes nucleophilic substitution with methacrylate in our methacrylation procedure. Signals of lysine methylene were used as a reference to calculate the degree of methacrylation. (Ravichandran et al., 2016)

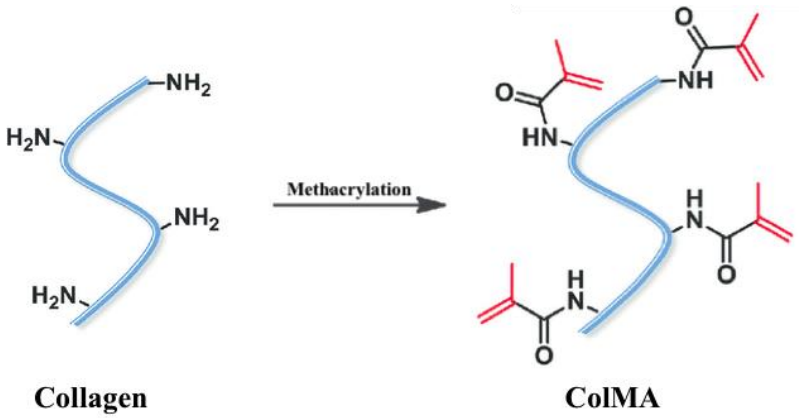

Figure 3.1. Methacrylation of collagen, adapted from (Ravichandran et al., 2016)

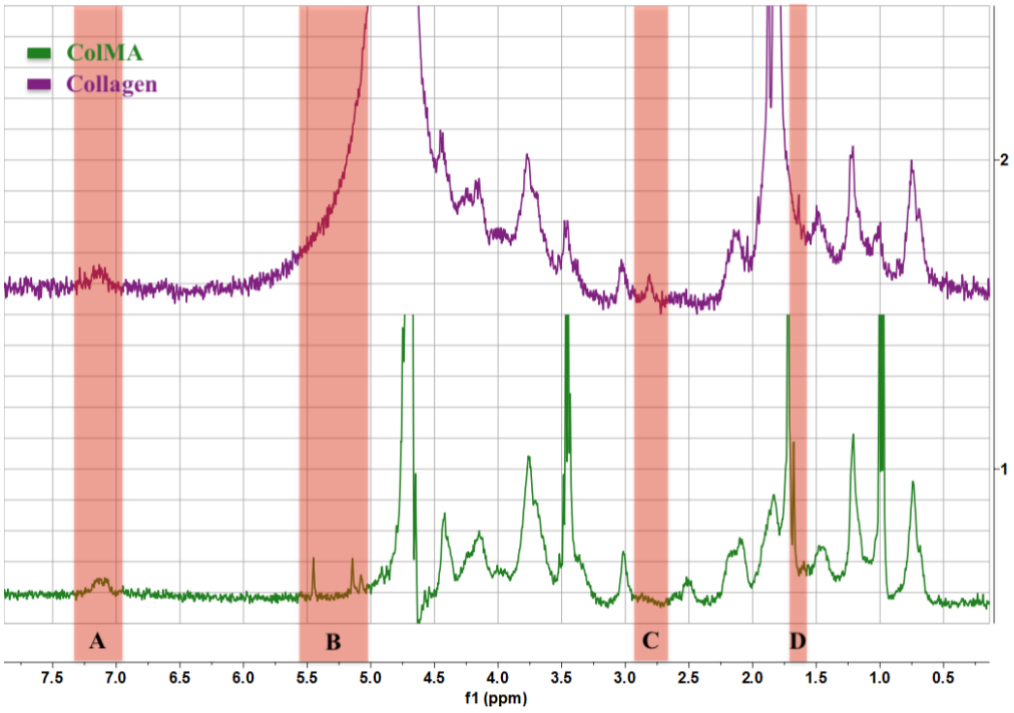

Figure 3.2. ^{1}H NMR spectra of collagen and ColMA. Signal peaks correspond to aromatic region (A) (6.9-7.5 ppm), olefinic protons from methacrylate (B) (5.56-5.30 ppm), lysine methylene (C) (2.8-2.95 ppm) and the methyl signal of methacrylate (D).

In this analysis, the signals of aromatic region were used to superimpose the collagen and ColMA ^{1}H NMR spectra via MestreNova NMR analysis software (v6.0.2, Mestrelabs Research, Spain). For calibration, the integrals of aromatic region of both spectra were defined as 1 to calculate the degree of methacrylation (DM). The integrals of the lysine methylene region of collagen and ColMA were calculated as 10.11 and 3.25 respectively. The degree of methacrylation (DM) of ColMA sample was calculated as 67% with the equation below.

$$DM = \left(1 - \frac{A_{ColMA}}{A_{collagen}}\right) x\ 100$$

A_{ColMA}: Integral of signal of lysine methylene region of ColMA spectrum

$A_{Collagen}$: Integral of signal of lysine methylene region of Collagen spectrum

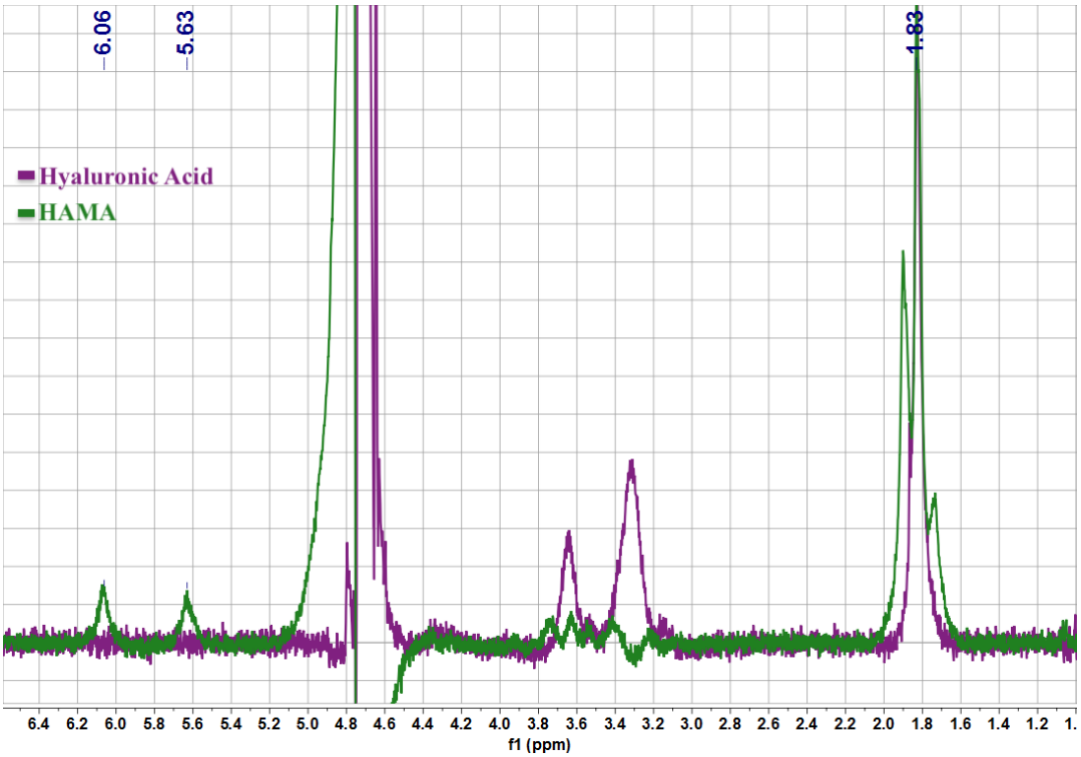

Figure 3.3.^{1}H NMR spectra of hyaluronic acid and HAMA. Signal peaks correspond to methyl signal at δ 1.83 ppm and olefinic protons from methacrylate at δ 5.6 and 6 ppm.

The proton NMR spectra of hyaluronic acid and HAMA hydrogels were generated to determine the incorporation of methacrylate groups into hyaluronic acid (Figure 3.3). Both spectra have a peak corresponding to the methyl group of hyaluronic acid at δ 1.83 ppm, also HAMA has a higher peak due to the methyl signal of methacrylate. The spectra were examined via MestreNova NMR analysis software (v6.0.2, Mestrelabs Research, Spain). The spectra were superimposed by a reference point as a signal of methyl protons at 1.9 ppm of HA and HAMA spectra. As the indicator of methacrylation, signals of methacrylate olefinic protons were detected in the HAMA spectrum at 5.6 and 6 ppm (Chandrasekharan et al., 2018). However, the degree of methacrylation (DM) could not be quantified since the signals coming from the methyl groups of both HAMA and HA overlapped at 1.8 ppm. This

overlapping is the same with the data presented in the literature (Oudshoorn et al., 2007)

3.1.2 Fourier Transform Infrared Spectroscopy (FTIR) Analysis

Another characterization of collagen, hyaluronic acid, ColMA and HAMA hydrogels was FTIR analysis. FTIR transmittance (T) spectra of hydrogels were generated in the range of 4000 to 400 cm^{-1}, at a resolution of 1 cm^{-1}, and collagen-ColMA and hyaluronic acid-HAMA spectrums were respectively superimposed to display the same and different peaks which methacrylation leads.

FTIR spectrum of collagen has specific amide bands as an indicator of its structural organization (Li et al., 2015). It is expected that the collagen and ColMA spectra display the same amide bands since the methacrylation process should not disrupt the structure of the collagen. These specific characteristic amide bands of collagen were shown in the spectra (Figure 3.4). The amide A and B bands, which are corresponding to N-H groups, are found at 3300 cm^{-1} and 3082 cm^{-1}, respectively. The amide I band, at 1625 cm^{-1} is a sensitive indicator of the secondary structure of proteins, corresponds to C=O stretching vibration in the peptide groups (Prystupa & Donald, 1996). The amide II band, at 1550 cm^{-1}, corresponds to N-H bonds and C-N stretching vibrations (J. nior et al., 2015). The amide III band, at 1240 cm^{-1}, corresponds to N–H bending and C–N stretching vibrations (Yang et al., 2017). FTIR spectra of collagen and ColMA were superimposed, and these characteristic bands of collagen spectrum were preserved in ColMA spectrum meaning that the structural organization of collagen was mainly preserved after methacrylation.

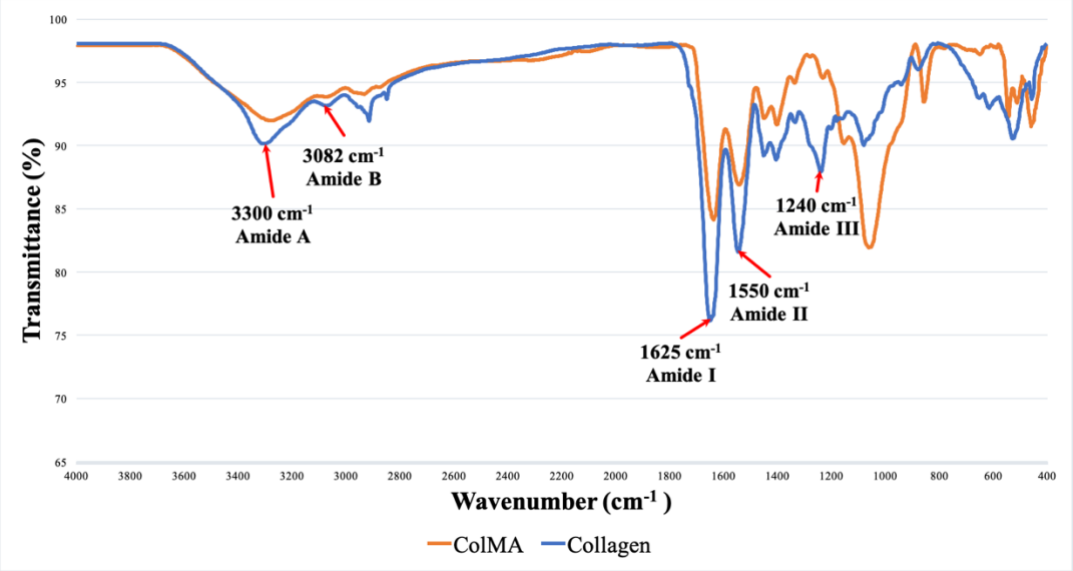

Figure 3.4. FTIR transmittance spectra of collagen and ColMA. Featured specific amide bands of collagen are displayed in the collagen spectrum.

FTIR spectra of hyaluronic acid and HAMA were superimposed as shown in Figure 3.5. A strong band at 3300 cm^{-1}, corresponding OH and NH stretching vibrations, and the band at 2900 cm^{-1} corresponding CH symmetrical and CH_2 asymmetrical stretching are the characteristic bands of hyaluronic acid. Also, the bands at 1155 cm^{-1}, 1050 cm^{-1} and 944.61 cm^{-1} are the typical bands for carbohydrates (Chen, Qin & Hu, 2019). These bands are common for two spectra, showing that after methacrylation, hyaluronic acid preserves its structure. On the other hand, at 1730 cm-1, a new peak, corresponding C=O groups, was observed in HAMA spectrum as an indicator of methacrylation. (Xia et al., 2016)

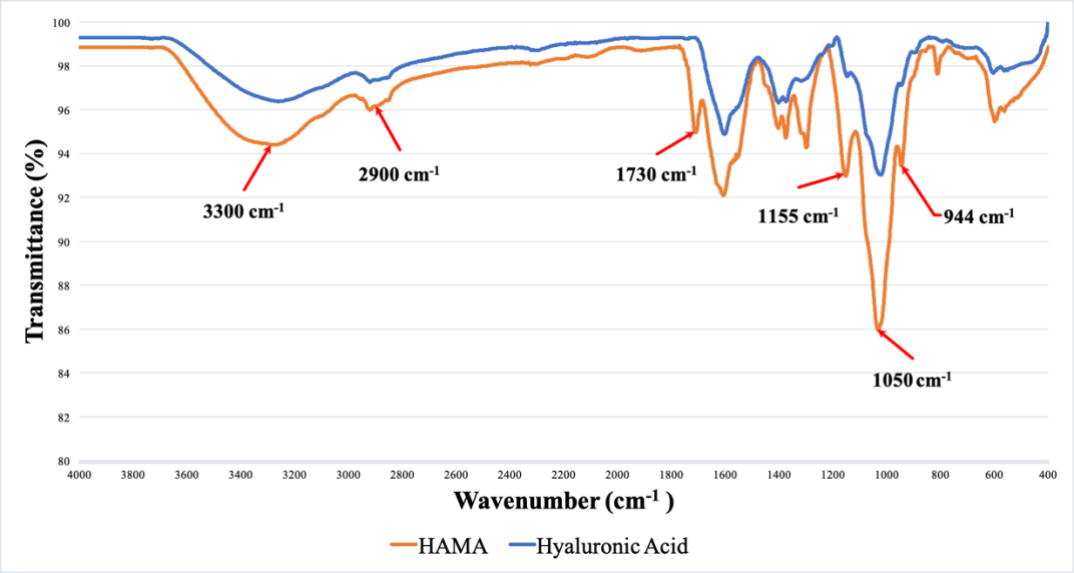

Figure 3.5. FTIR transmittance spectra of hyaluronic acid and HAMA. Featured specific bands are displayed in the HAMA spectrum.

3.2 Characterization of Photo-Crosslinked ColHA Hybrid Hydrogels

Before *in vitro* studies of the ColHA scaffolds, the physical properties of five different photo-crosslinked hydrogels were analyzed. 5 different compositions of ColHA scaffolds (given in Table 2.1) containing 0.5 mg/mL ColMA and different concentrations of HAMA (varying from 0.5 mg/mL to 5 mg/mL) as respect to Col:HA ratios of 1:1, 1:1.5, 1:2, 1:5 and 1:10 were designed.

3.2.1 Mechanical Characterization Tests

Mechanical characterization of the hydrogel scaffolds has significant importance in tissue engineering (Oyen, 2013). Since cells are mostly adapted to specific tissue properties, and response and sense the environment, the mechanical properties of engineered tissue scaffolds should be compatible with native tissue (Castilho et al., 2018). The mechanical properties of the scaffolds affect the proliferation, differentiation and orientation of the cells (Kelly et al., 2018).

For the mechanical characterization of ColHA hydrogels, compressing test was operated with five replicates of cylindrical shaped hydrogels with a height of 3.5 mm. For each gel, a stress-strain curve was generated (Figure 3.6), and Young's Modulus (E) was obtained from the slope of each curve with an equation, $E= \sigma/\varepsilon$, where σ is the stress (MPa) and ε the strain in the elastic region.

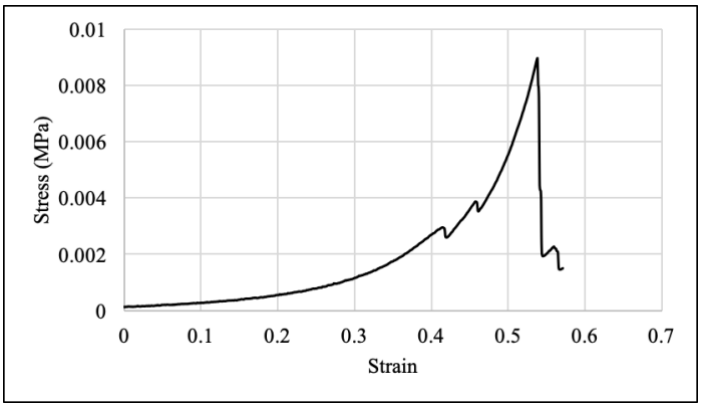

Figure 3.6. A representative typical compression stress-strain curve of ColMA:HAMA 1:10 sample.

In the mechanical test result (Figure 3.7), there was not a significant difference between different ratios except ColMA:HAMA 1:1 hydrogel. Young's modulus of 1:1 hydrogel was slightly lower than the cancerous prostate tissue, which has a Young's modulus 40.6 ± 15.9 kPa obtained with a Kelvin-Voigt Fractional Derivative (KVFD) viscoelastic model at 150 Hz (Hoyt et al., 2008). This result was expected since 1:1 design contains a low concentration of both ColMA and HAMA hydrogels and has the lowest stiffness among the designs. On the other hand, other compositions does not have a statistical significant difference upon each other. ColMA concentration was the same for all gel compositions while HAMA concentration was increased, there is a slight increase in Young modulus with the increment of HAMA composition. Mechanical test was applied to all six scaffold designs, further characterizations were conducted three chosen designs 1:2, 1:5, 1:10 and 1:1-high, which have close Young's modulus to cancerous prostate tissue.

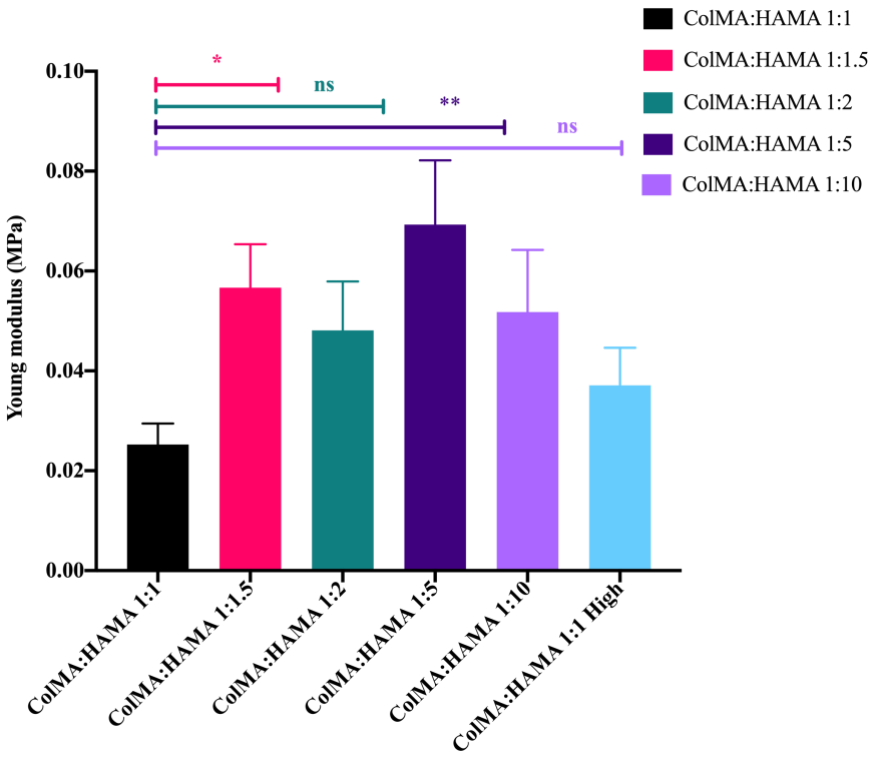

Figure 3.7. Compression test results of the hydrogel samples. Statistical significance was calculated using one-way ANOVA and Kruskal-Wallis multiple comparison test (*p<0.05, **p<0.01, ***p<0.005, ****p<0.001), n=5.

3.2.2 Swelling Tests

The swelling profile of the ColHA gels in the culture conditions was tested by the swelling test shown in Figure 3.8. Three photo-crosslinked samples of four different compositions of ColHA gels were freeze-dried and dry samples were incubated in PBS at 37 °C for two hours, and weights were recorded at seven time points. Four different compositions of ColHA hydrogels were subjected to this test did not show any significant difference in their swelling profile with each other; in other words, they have similar swelling profiles. The water content of the dried gels dramatically increased in the first 30 min of incubation in PBS. It was an expected result since hydrogels have very high swelling potential. After the initial peak in swelling rate, significant changes were not observed for dried hydrogel samples.

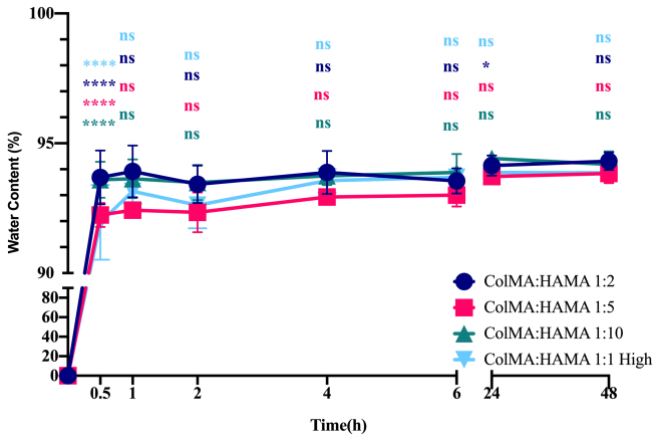

Figure 3.8. Swelling profiles of the photo crosslinked ColHA hydrogels incubated for two hours in PBS at, 37 °C. Statistical significance was calculated using two-way ANOVA and Tukey's multiple comparison test (*p<0.05, **p<0.01, ***p<0.005, ****p<0.001), n=3.

3.2.3 *In situ* Degradation Tests

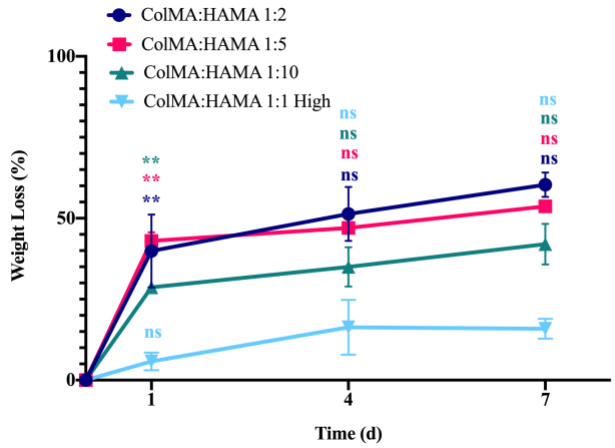

Figure 3.9. *In situ* degradation profiles of the photo crosslinked ColHA hydrogels incubated for a week in PBS at, 37 °C. Statistical significance was calculated using two-way ANOVA and Tukey's multiple comparison test (*p<0.05, **p<0.01, ***p<0.005, ****p<0.001), n=3.

Four compositions of ColHA hydrogels were chosen and subjected to *in situ* degradation test. The stability of the ColHA gels in the culturing conditions was tested by incubation in PBS at 37 °C for a week. The degradation results for photo crosslinked samples presented in Figure 3.9 showed a significant loss of sample weight about 40% first day, which was followed by a slight increase except ColMA:HAMA 1:1-high design. 1:1-high hydrogel has a lower degradation profile from other designs. After first day, a significant weight loss was not observed. However, 1:10 gel also had a slightly lower degradation rate than other samples. The reason of 1:10 gel had less degradation maybe its high HAMA concentration, since HAMA has a higher gelation capability than ColMA. It is known from the mechanical test, 1:2 gel has lower stiffness than other gels, and it had also a slightly higher degradation profile similar to 1:5 gel. Based on these results, ColMA:HAMA 1:10 gel, which contains 5 mg/mL HAMA and 0.5 mg/mL ColMA and ColMA:HAMA 1:1-high gel, which contains 5 mg/mL HAMA and 0.5 mg/mL ColMA, were chosen for this study.

3.3 *In Vitro* Studies

After mechanical characterizations of the hydrogels, ColMA:HAMA 1:10 hydrogel was selected to conduct the *in vitro* studies. This study aimed to design a hydrogel based prostate cancer model for the migration studies. Spheroids of widely used LNCaP and PC-3 prostate cancer cell lines were used to represent cancerous tissue in our ColHA hydrogel scaffold model. Also, human dermal fibroblast was involved in out 3D scaffold to study their contribution on the migration of the prostate cancer cells.

3.3.1 Confocal Laser Scanning Microscopy (CLSM) Studies

3.3.1.1 Live/Dead Assay of LNCaP & PC-3 Spheroids

Spheroids of LNCaP and PC-3 cell lines were prepared by hanging drop method for 5-7 days. The viability assay was performed for 1, 4 and 7 days of both LNCaP and PC-3 spheroids after their formation. The spheroids were transferred to a non-adhesive 24 well-plate and cultured at 37 °C with 5% CO_2 humidified atmosphere by renewing media every 2-3 days. Cytoskeleton and nucleus staining was performed for each sample. Figure 3.10 presents the viability and the structure of LNCaP spheroids. Live/Dead assay results show that spheroids have good viability. Phalloidin nucleus staining results are normal, there were no morphological changes in cell structure.

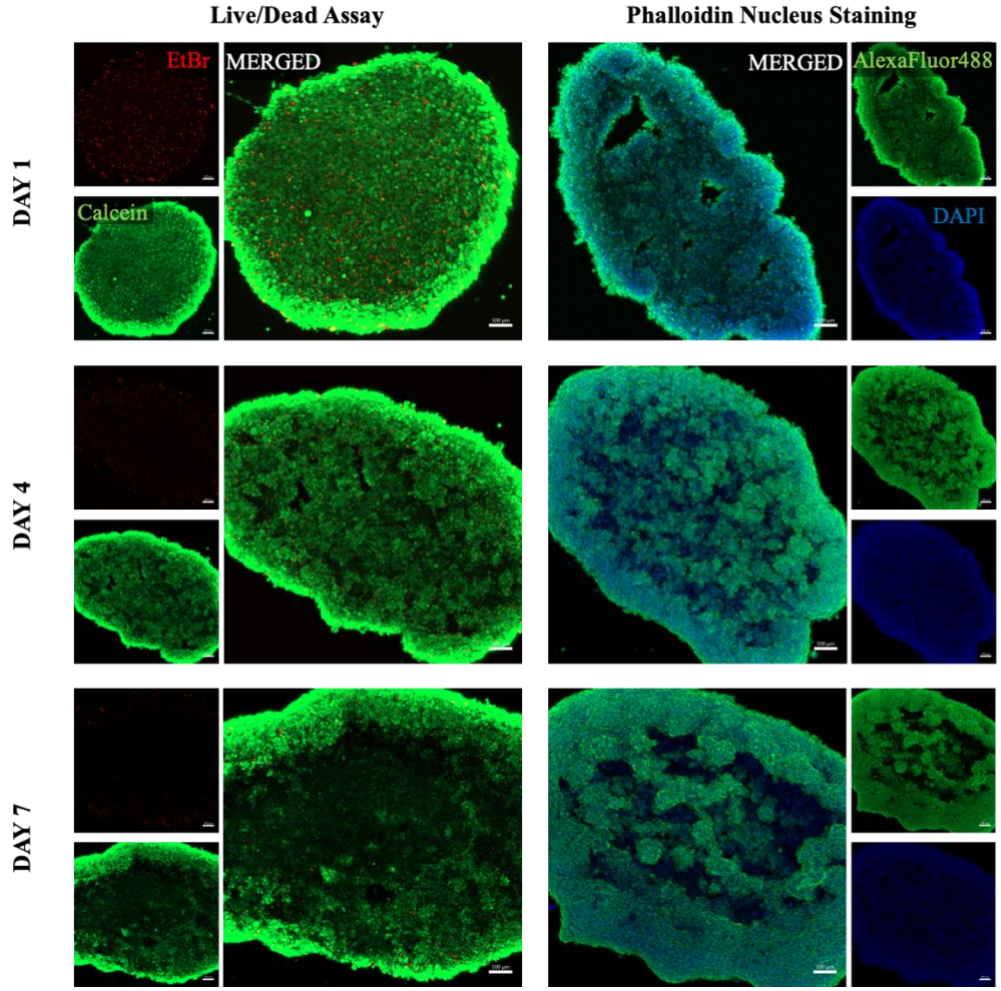

Figure 3.10. CLSM images of Live/Dead Assay (red:EtBr-dead, green:Calcein-live) and Phalloidin nucleus staining (green:cytoskeleton, blue:nucleus) of LNCaP spheroids at 1, 4 and 7 days after spheroid formation. Scale bars: 100 μm

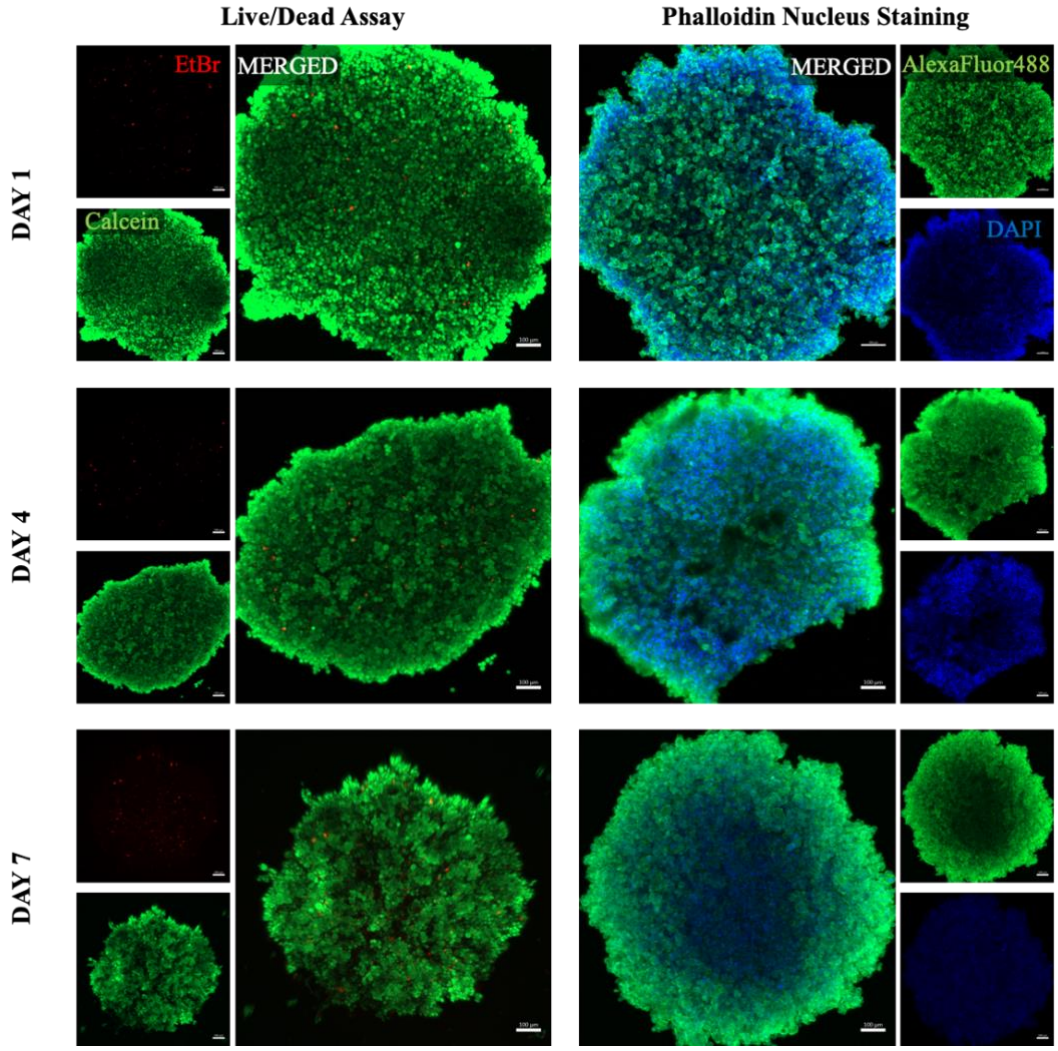

Figure 3.11. CLSM images of Live/Dead Assay (red:EtBr-dead, green:Calcein-live) and Phalloidin nucleus staining (green:cytoskeleton, blue:nucleus) of PC-3 spheroids at 1, 4 and 7 days after spheroid formation. Scale bars: 100 μm

PC-3 spheroids were also subjected to the same viability assay and stained, and CLSM images of spheroids are presented in Figure 3.11. Live/Dead assay of PC-3 spheroids shows that spheroids which were produced by the hanging drop method have good viability gave the similar results as LNCaP spheroids. Also, it was observed that the structures of the spheroids were changing for both cell lines; even though, they were produced by the same method due to hanging drop method rely on simultaneous action of surface tension and gravitational force, and, it is not

possible to interfere to their shapes. Phalloidin nucleus staining results are normal, there were no morphological changes in cell structure.

3.3.1.2 Characterization of Microtumor Models

3.3.1.2.1 Live/Dead Assay of LNCaP & PC-3 Spheroids in Hydrogel

ColHA hybrid hydrogels were photo-crosslinked via UV lamp to produce 3D hydrogel scaffold of microtumor models. The photo-crosslinking conditions of this study were determined as 365 nm, 1 W/cm^2 from 3 cm distance for 5 s. It is known that UV irradiation has harmful effects on cell viability, DNA structure, and DNA damage repair mechanisms, and causes cell damage. Exposure to a higher wavelength of UV is less harmful for cells due to lower energy. (Masuma, Kashima, Kurasaki & Okuno, 2013).

Viability assay was applied to cell-loaded 3D hydrogel models, since the photo-crosslinkage via UV was done after loading cells to hydrogels. Moreover, it was crucial to show that the hydrogel model was appropriate for cell viability. Live/Dead assay carried on for both LNCaP and PC-3 spheroids and HDFa cells encapsulated in the 3D hydrogels.

Figure 3.12 and Figure 3.13 present the viability assay of the LNCaP and PC-3 spheroids, respectively, in photo-crosslinked hydrogel. For both spheroid containing gels, a slightly higher number of dead cells were observed on the first day of the experiment in comparison with the day 4 and day 7. Although UV exposure conditions were kept very short and less harmful; it was expected to observe dead cell within the spheroids after UV exposure. However, it was shown that the dead cell population decreased as the gels were incubated in the culture conditions. It can be concluded that UV exposure of the gels was not harmful, and hydrogels were not cytotoxic to cells. Phalloidin nucleus staining results are normal, there were no morphological changes in cell structure.

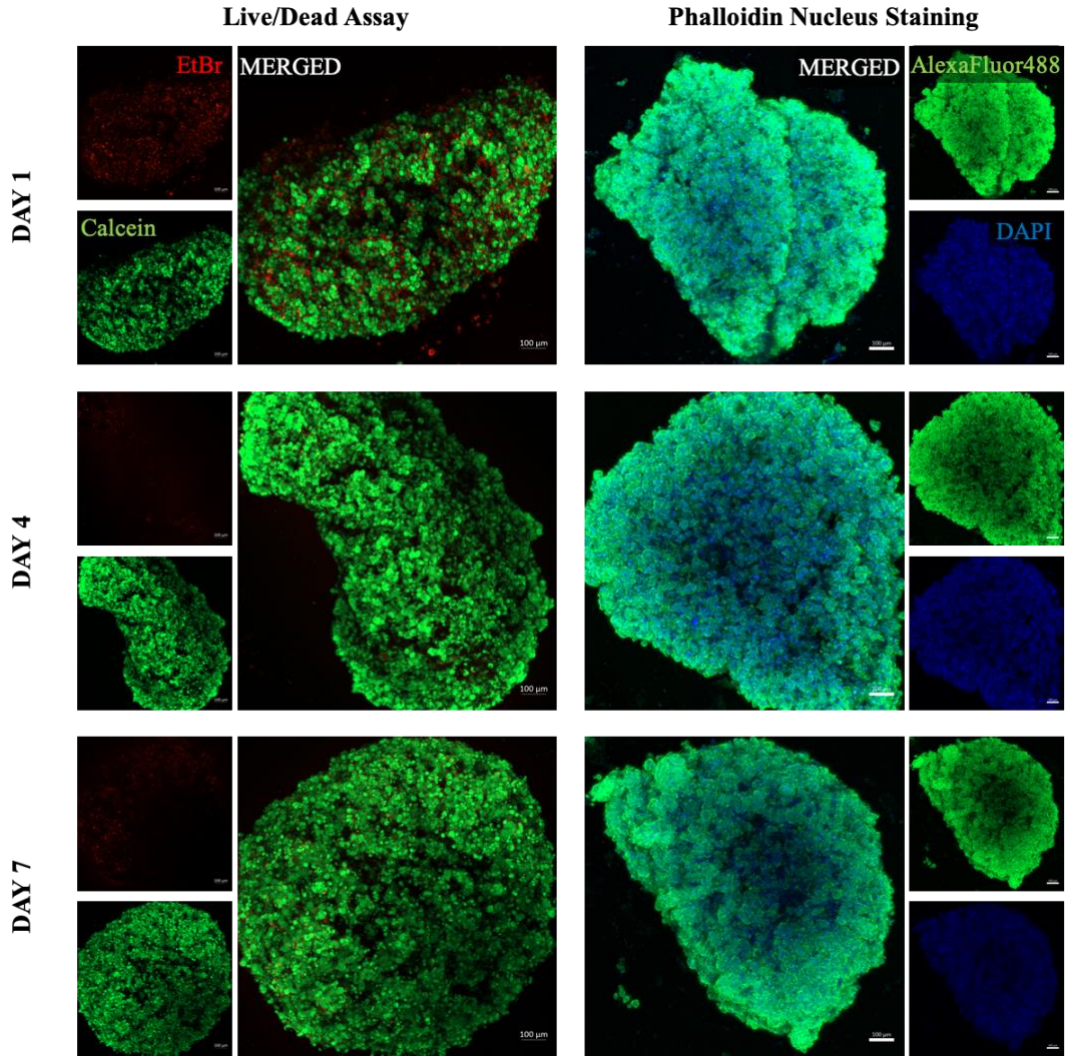

Figure 3.12. CLSM images of Live/Dead Assay (red:EtBr-dead, green:Calcein-live) and Phalloidin nucleus staining (green:cytoskeleton, blue:nucleus) of LNCaP spheroids at 1, 4 and 7 days after UV-crosslinking of the ColMA:HAMA 1:10 3D hydrogel tumor models containing 5 mg/mL HAMA and 0.5 mg/mL ColMA. Scale bars: 100 µm.

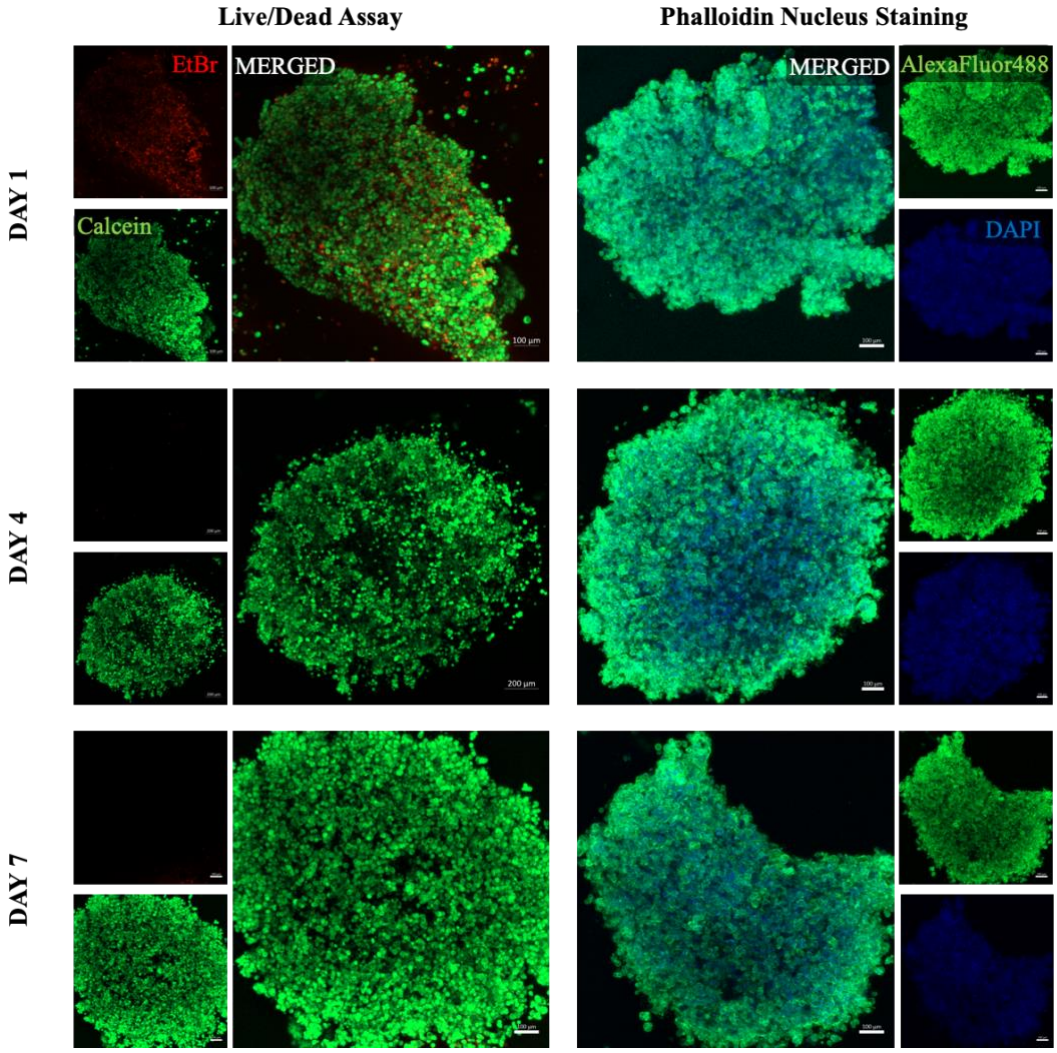

Figure 3.13. CLSM images of Live/Dead Assay (red:EtBr-dead, green:Calcein-live) and Phalloidin nucleus staining (green:cytoskeleton, blue:nucleus) of PC-3 spheroids at 1, 4 and 7 days after UV-crosslinking of the ColMA:HAMA 1:10 3D hydrogel tumor models containing 5 mg/mL HAMA and 0.5 mg/mL ColMA. Scale bars: 100 µm.

3.3.1.2.2 Live/Dead Assay of HDFa Cells in Hydrogel

Fibroblast cells loaded 3D hydrogel scaffolds were subjected to Live/Dead Assay, represented in Figure 3.14. It is observed that HDFa cells were alive after the UV

exposure of the gels, and after 1-week of incubation, they remained alive within the gel.

These viability assays show that the 3D hydrogel scaffold of microtumor model provides a sufficient environment for the cells (PC-3, LNCaP and HDFa) to live in.

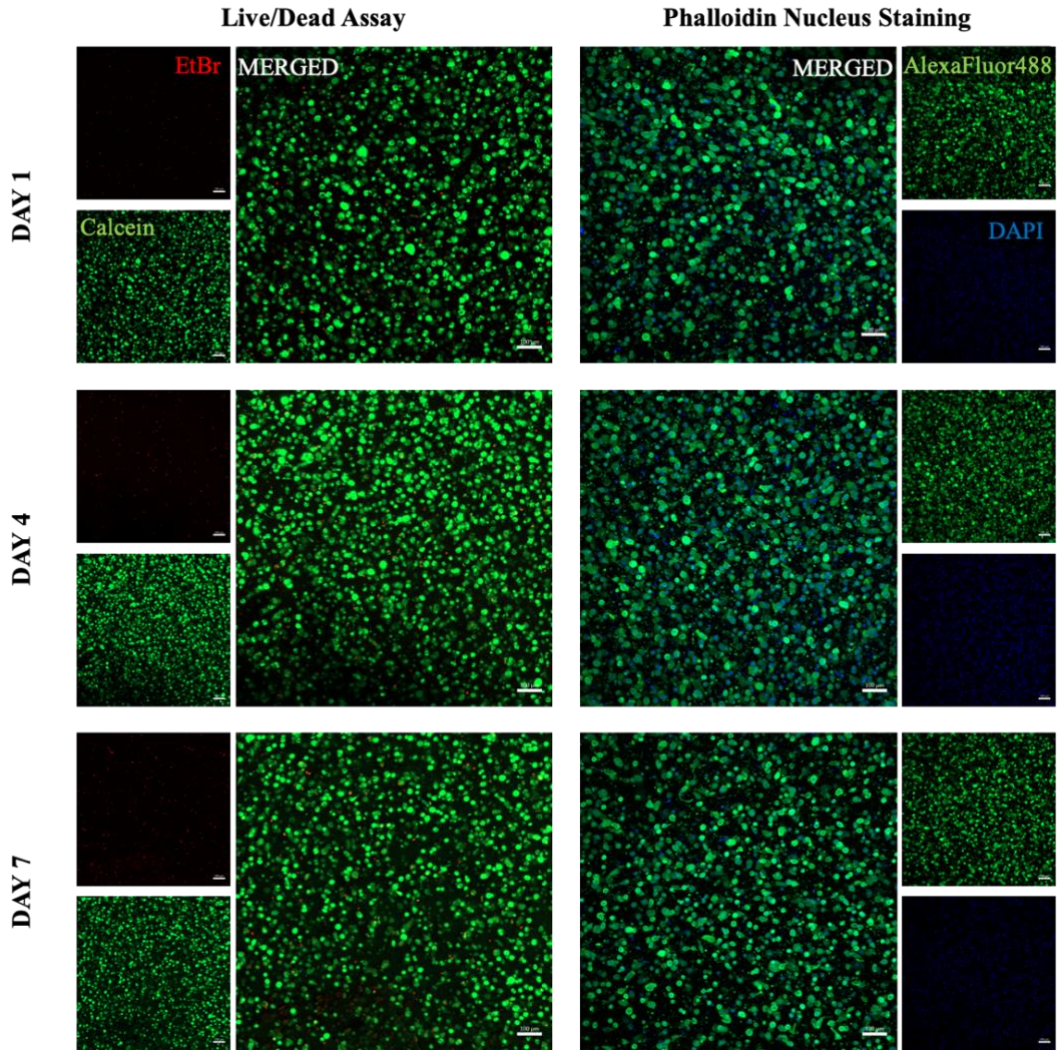

Figure 3.14. CLSM images of Live/Dead Assay (red:EtBr-dead, green:Calcein-live) and Phalloidin nucleus staining (green:cytoskeleton, blue:nucleus) of HDFa at 1, 4 and 7 days after UV-crosslinking of the ColMA:HAMA 1:10 3D hydrogel tumor models containing 5 mg/mL HAMA and 0.5 mg/mL ColMA. Scale bars: 100 µm.

3.3.1.3 Cell Migration Observations

3.3.1.3.1 ColMA:HAMA 1:10

ColMA:HAMA 1:10 gel was chosen as the final hydrogel composition due to its appropriate Young's modulus, non-cytotoxic feature, and easy-to-handle structure. For migration studies, spheroids were stained with Q-tracker 655 before being encapsulated into hydrogels to distinguish them from HDFa cells. After culturing the coculture of cancer spheroids and fibroblasts cells for 14 days, 3D cell-loaded hydrogels were stained with Alexa Fluor 488 for cytoskeleton and DAPI for nucleus and analyzed with CLSM as shown in Figure 3.15.

Spheroids preserved their location in the middle on the microtumor model, and the fibroblasts were scattered all around the microtumor model. Especially, on days 7 and 14, in the CLSM image of LNCaP microtumor model, it was observed that cancer cells moved out of the spheroid. However, in this microtumor model, elongated morphology of cancer cell was not observed. Tumor cells can be separated into three groups: elongated morphology, rounded morphology, and a mixture of both (Croft & Olson, 2008). They may switch between the elongated and rounded modes of morphology as an adaptive response to the microenvironment (Wolf et al., 2003). Thus, it was expected to observe cell elongations as an indicator of metastasis of prostate cancer. In Figure 3.15, ColMA:HAMA 1:10 gel was prepared with 5 mg/mL HAMA and 0.5 mg/mL ColMA concentration. To observe the elongated morphology of the cancer cells, the composition of the gel was altered. An increase of ColMA concentration to 5 mg/mL was planned since collagen is the major component of the tumor microenvironment. Also, it is known that collagen influences tumor cell behavior through integrins, and some signaling pathways. It was expected that the increase in the collagen concentration promotes cancer cell invasion and metastasis (Xu et al., 2019; Egeblad, Rasch & Weaver, 2010; Pickup, Mouw & Weaver, 2014).

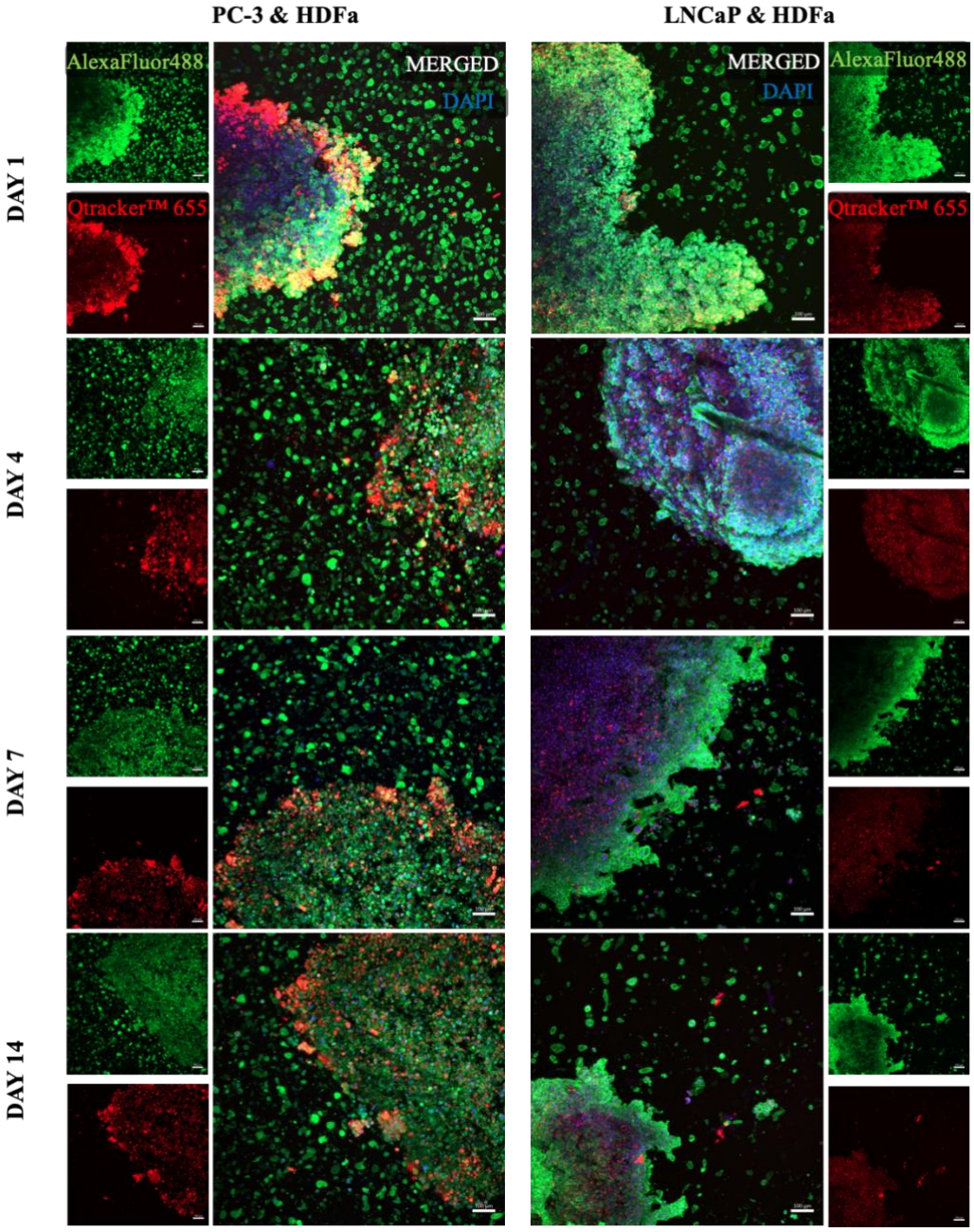

Figure 3.15. CLSM images of PC-3 and LNCaP spheroids and HDFa within the ColMA:HAMA 1:10 3D hydrogel tumor models containing 5mg/mL HAMA and 0.5 mg/mL ColMA at 1, 4, 7 and 14 days. Cells were stained for nucleus (DAPI, blue) and cytoskeleton (Alexa Fluor 488, green). Cancer cell spheroids were stained with Qtracker655 (red). Scale bars: 100 μm

3.3.1.3.2 High Concentration ColMA:HAMA 1:1

This design of 3D hydrogel scaffold contains an equal amount of ColMA and HAMA hydrogels; however, its composition is different from the CoLMA:HAMA 1:1 design which was used in the mechanical tests. This design contains both ColMA and HAMA in 5mg/mL concentration; thus, it was named as high concentration ColMA:HAMA 1:1. New 3D microtumor models were generated with this ratio, PC-3 and LNCaP spheroids, previously live-stained with CellTracker™ Green CMFDA Dye, which is used for monitoring the cell movement, transferred only to daughter cells not adjacent cells in the population and retained for several generations, were located in the middle of the hydrogel. Also, HDFa loaded microtumor models were prepared. Samples were stained with phalloidin and nucleus analzsed with CLSM for the elongation and migration of cancer cells at 1, 4, 7 and 14 days.

In Figure 3.16, CLSM micrographs of 3D microtumor models of LNCaP spheroids at different magnifications are shown. In Figure 3.17, CLSM micrographs of 3D microtumor models of LNCaP spheroids with and without HDFa cells are shown.

In Figure 3.12 and 3.15, representing the LNCaP spheroids encapsulated in ColMA:HAMA 1:10 3D hydrogel tumor model containing 5mg/mL HAMA and 0.5 mg/mL ColMA hydrogel without and with HDF cells, respectively, migration or elongation of cancer cells was not observed. In Figure 3.16, on days 7 and 14, the elongation of LNCaP cancer cells stained with green cell tracker was observed in the high concentration ColMA:HAMA 1:1 3D hydrogel tumor model, which is containing 5 mg/mL HAMA and 5 mg/mL ColMA in the presence of HDF cells at the concentration a million cells per mL. On the other hand, as shown in Figure 3.17, the migration of cancer cells was not observed in the absence of HDF cells in the high concentration ColMA:HAMA 1:1 hydrogel model.

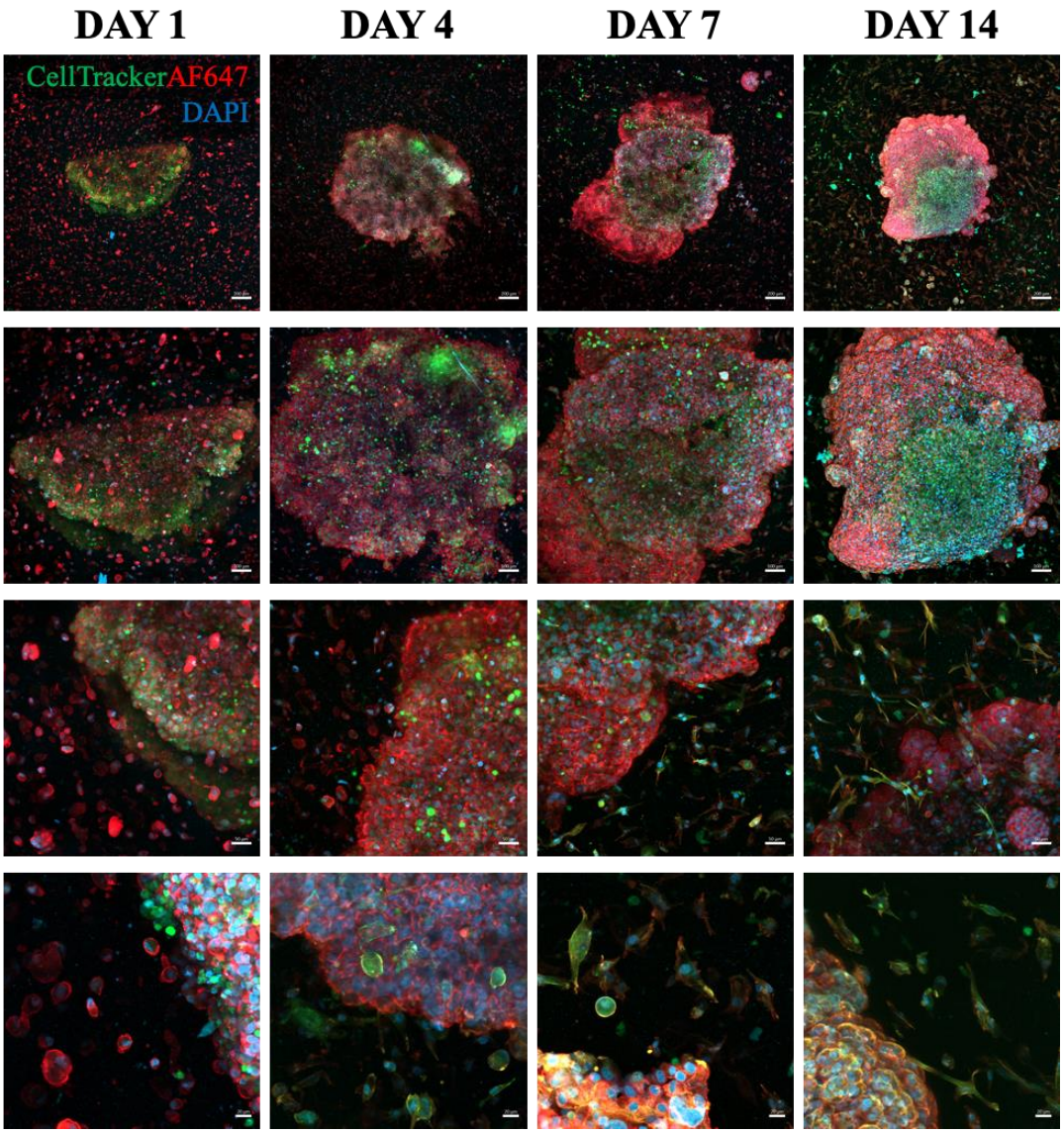

Figure 3.16. CLSM images of LNCaP spheroids and HDFa within the ColMA:HAMA 1:1-High 3D hydrogel tumor models containing 5mg/mL HAMA and 5 mg/mL ColMA at 1, 4, 7 and 14 days. Cells were stained for nucleus (DAPI, blue) and cytoskeleton (Alexa Fluor 647, red). Cancer cell spheroids were stained with CellTracker™ Green CMFDA Dye (green). Scale bars: 200 µm, 100 µm, 50 µm and 20 µm for each row from top to bottom.

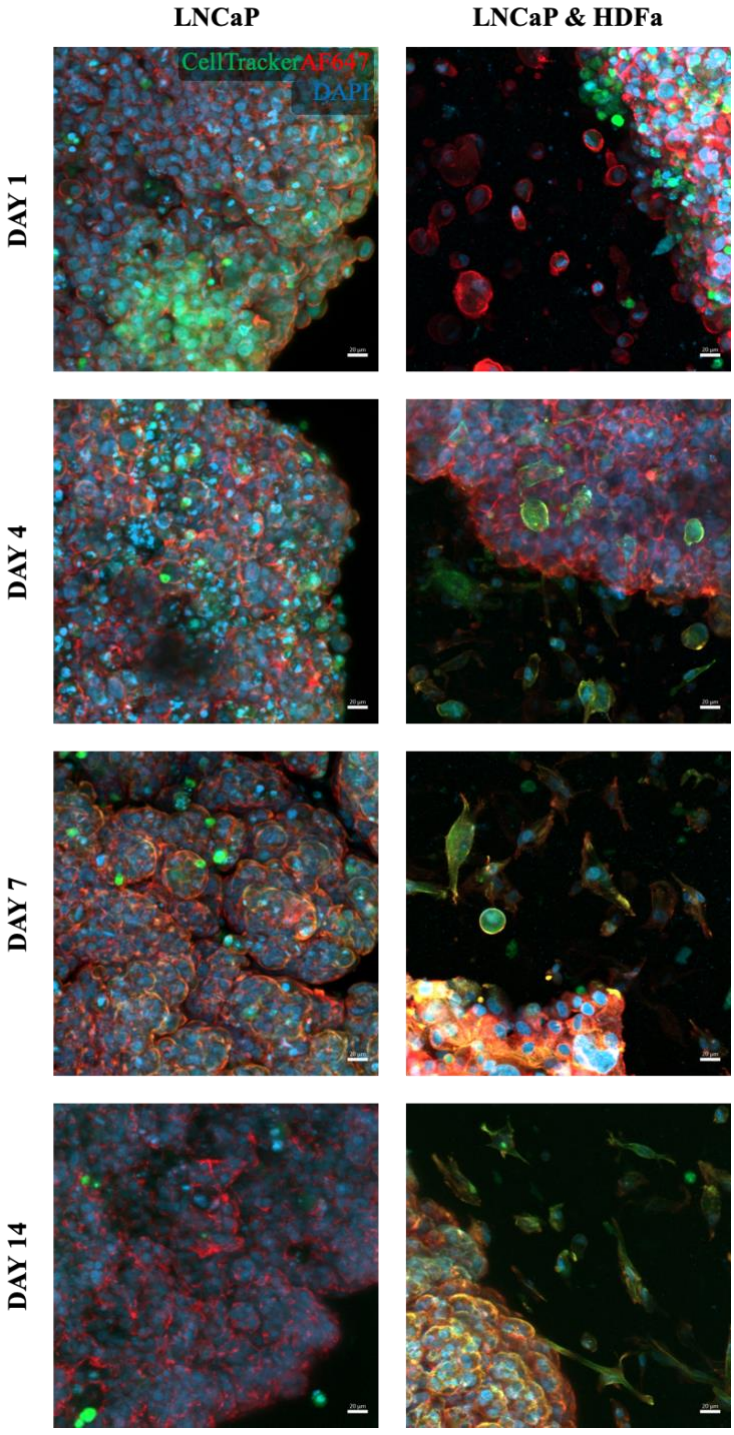

Figure 3.17. CLSM images of 3D microtumor models containing LNCAP spheroids with or without HDFa at 1, 4, 7 and 14 days. Cells were stained for nucleus (DAPI, blue) and cytoskeleton (Alexa Fluor 647, red). Cancer cell spheroids were stained with CellTracker™ Green CMFDA Dye (green). Scale bars: 20 µm.

In Figure 3.18, CLSM micrographs of 3D microtumor models of PC-3 spheroids at different magnifications are shown. In Figure 3.19, CLSM micrographs of 3D microtumor models of PC-3 spheroids with and without HDFa cells are shown.

In Figure 3.13 and 3.15, representing the PC-3 spheroids encapsulated in ColMA:HAMA 1:10 3D hydrogel tumor model containing 5mg/mL HAMA and 0.5 mg/mL ColMA hydrogel without and with HDF cells, respectively, migration or elongation of cancer cells was not observed. On the other hand, in Figure 3.19, the elongation of LNCaP cancer cells stained with green cell tracker was observed in the high concentration ColMA:HAMA 1:1-high 3D hydrogel tumor model containing 5mg/mL HAMA and 5 mg/mL ColMA hydrogel on days 7 and 14, in the presence of HDF cells at the concentration a million cells per mL. The same situation was observed for both LNCaP and PC-3 cells. Migration or elongation of the cells was not observed in the ColMA:HAMA 1:10 hydrogel, with and without HDF (Figure 3.13 & 3.15). After ColMA concentration was increased to 5 mg/mL from 0.5 mg/mL, the hydrogel with HDF cells provided a sufficient environment for migration of the cells.

These results show that the increase in the ColMA concentration in the composition of 3D hydrogel microtumor model and in the presence of HDF cells improve the microenvironment to become more suitable for metastatis of prostate cancer cell lines. It is known that the collagen found in the ECM is important for the cell adhesion and anchorage-independent growth of the prostate cancers (Banyard et al., 2007; Martins Cavaco, Dâmaso, Casimiro & Costa, 2020). It was expected that the increase in the collagen concentration promotes cancer cell invasion and metastasis (Xu et al., 2019; Pickup, Mouw & Weaver, 2014). Also, it was shown that collagen also promotes EMT by transforming growth factor-beta signaling (Shintani, Maeda, Chaika, Johnson & Wheelock, 2008; Smith & Bhowmick, 2016). It was known that the fibroblast population is high in the tumors, and they play an important role in cancer invasion and migration (Wang et al., 2021). It was shown that the fibroblasts around the metastatic prostate cancer cells secrete VEGF and increase metastases through EMT (Kaminski et al., 2006). The presence of human dermal fibroblasts in

the 3D model may promote prostate cancer cells undergoing EMT by secreting growth factors.

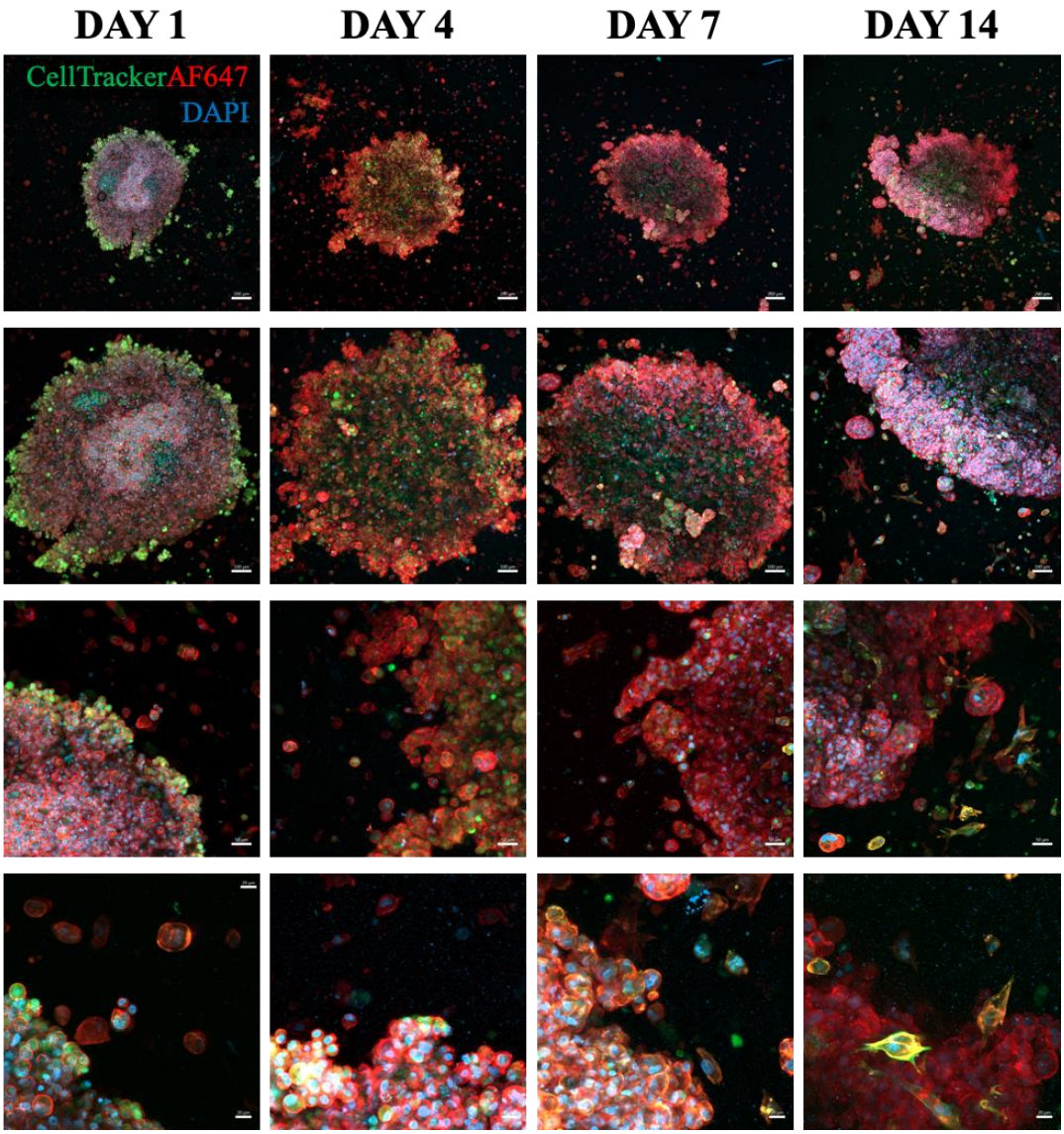

Figure 3.18. CLSM images of PC-3 spheroids and HDFa within the ColMA:HAMA 1:1-High 3D hydrogel tumor models containing 5mg/mL HAMA and 0.5 mg/mL ColMA at 1, 4, 7 and 14 days. Cells were stained for nucleus (DAPI, blue) and cytoskeleton (Alexa Fluor 647, red). Cancer cell spheroids were stained with CellTracker™ Green CMFDA Dye (green). Scale bars: 200 µm, 100 µm, 50 µm and 20 µm for each row from top to bottom.

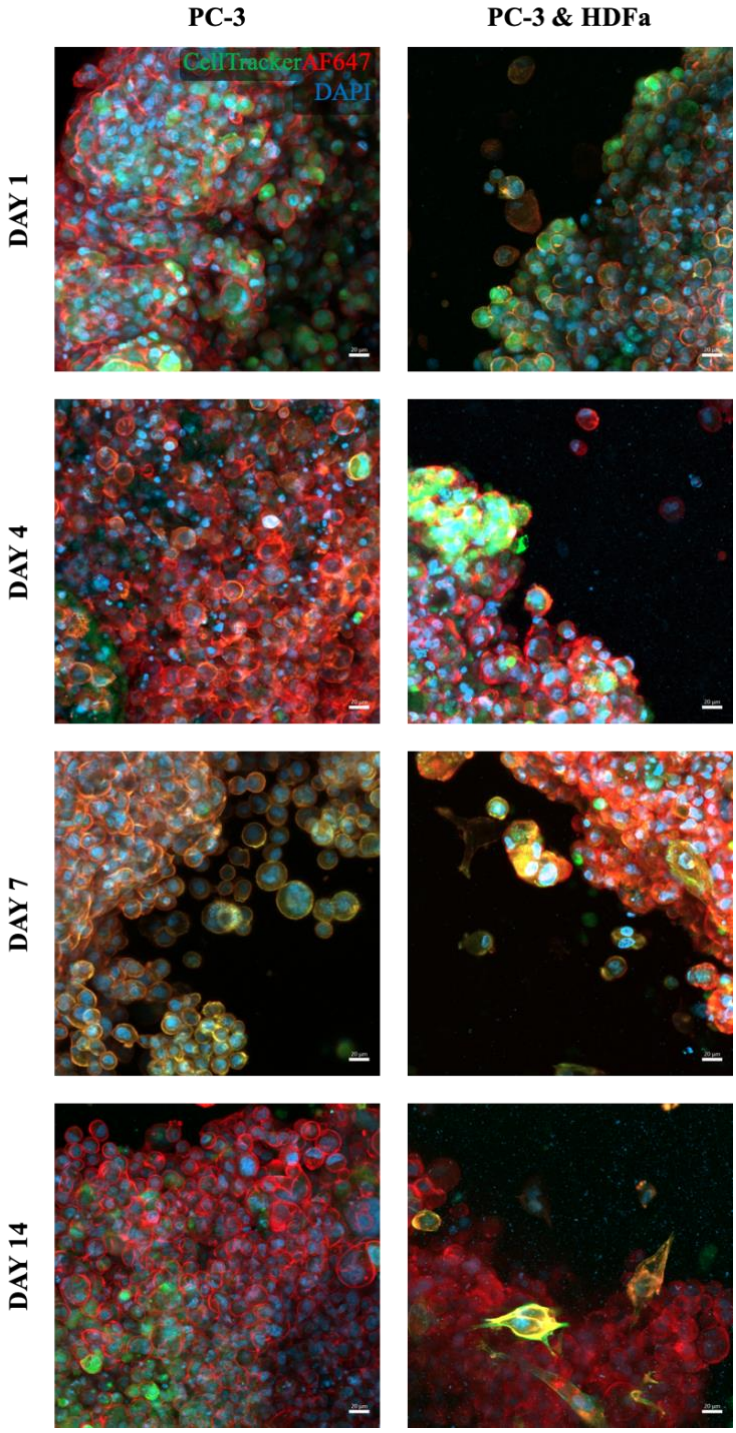

Figure 3.19. CLSM images of 3D microtumor models containing PC-3 spheroids with or without HDFa at 1, 4, 7 and 14 days. Cells were stained for nucleus (DAPI, blue) and cytoskeleton (Alexa Fluor 647, red). Cancer cell spheroids were stained with CellTracker™ Green CMFDA Dye (green). Scale bars: 20 μm.

3.4 Molecular Level Changes: Expression of E-cadherin and Vimentin Absence and Presence of HDFa

To show the presence of fibroblasts influences the movement of cancer cells as an indicator of the metastasis of prostate cancer, expression of E-cadherin and vimentin proteins, which are known as EMT markers were analyzed from immunostained samples of the 3D hydrogel microtumor models containing HDFa and not. E-cadherin is a cell-cell adhesion molecule and plays an important role in epithelial cell behavior (van Roy & Berx, 2008). On the other hand, vimentin is an intermediate filament protein expressed by mesenchymal cells (Satelli & Li, 2011). Therefore, the downregulation of E-cadherin and upregulation of vimentin are expected as a result of EMT. It was shown that the reduction or absence of E-cadherin provides cancer cell lines metastatic potential (Thakuri, Liu, Luker & Tavana, 2017); whereas, the gain of vimentin indicates the development of metastases in prostate cancer tumor biology (Singh et al., 2003). Also, LNCaP and PC-3 cells were cultured in TCP flasks with and without HDF cells.

Figure 3.20-24 represent CLSM micrographs of immunostained samples. E-cadherin signals were observed in the TCP flask cultures; however, the signals from E-cadherin cannot seen easily seen in hydrogel samples while vimentin signals were observed. It can be concluded that there was a downregulation of E-cadherin in hydrogel samples. Downregulation of E-cadherin leads cells to lose their cell-cell adhesion and gain motility; thus, the prostate cancer cells can go through EMT and invade the adjacent sites (Onder et al., 2008). On the other hand, vimentin gives cells the ability to move and sustain their structure during migration (Richardson et al., 2017).

Figure 3.20 presents the E-cadherin and vimentin expressions of LNCaP spheroids in ColMA:HAMA 1:1-high hydrogel in presence and absence of HDF. LNCaP spheroids entrapped with HDF in the hydrogel model have more vimentin signals on the edge of the spheroids for both day 7 and 14. It is showing that the cells found on the edge have more metastatic potential than the cells found inside the spheroid.

Figure 3.21 presents the E-cadherin and vimentin expression of LNCaP cells on TCP flasks with and without HDF as a control. The downregulation in the expression of E-cadherin was not observed. Figure 3.22 presents the E-cadherin and vimentin expressions of PC-3 spheroids in ColMA:HAMA 1:1-high hydrogel in the presence and absence of HDF. PC-3 spheroid entrapped without HDF has higher intensity of both vimentin and E-cadherin on one edge for day 7. Cancer cells that show both epithelial and mesenchymal characteristics have the ability to migrate as clusters. This phenomenon is called hybrid EMT. Hybrid EMT is more dangerous than partial EMT; thus, cluster migration promotes cancer cells more capability to survive than single-cell migration when they migrate (Sinha, Saha, Samanta & Bishayee, 2020). Figure 3.21 presents the E-cadherin and vimentin expression of PC-3 cells on TCP flasks with and without HDF as a control. EMT was not observed in the TCP flask cultures since the 2D cancer models are not relevant in mimicking the microtumor environment.

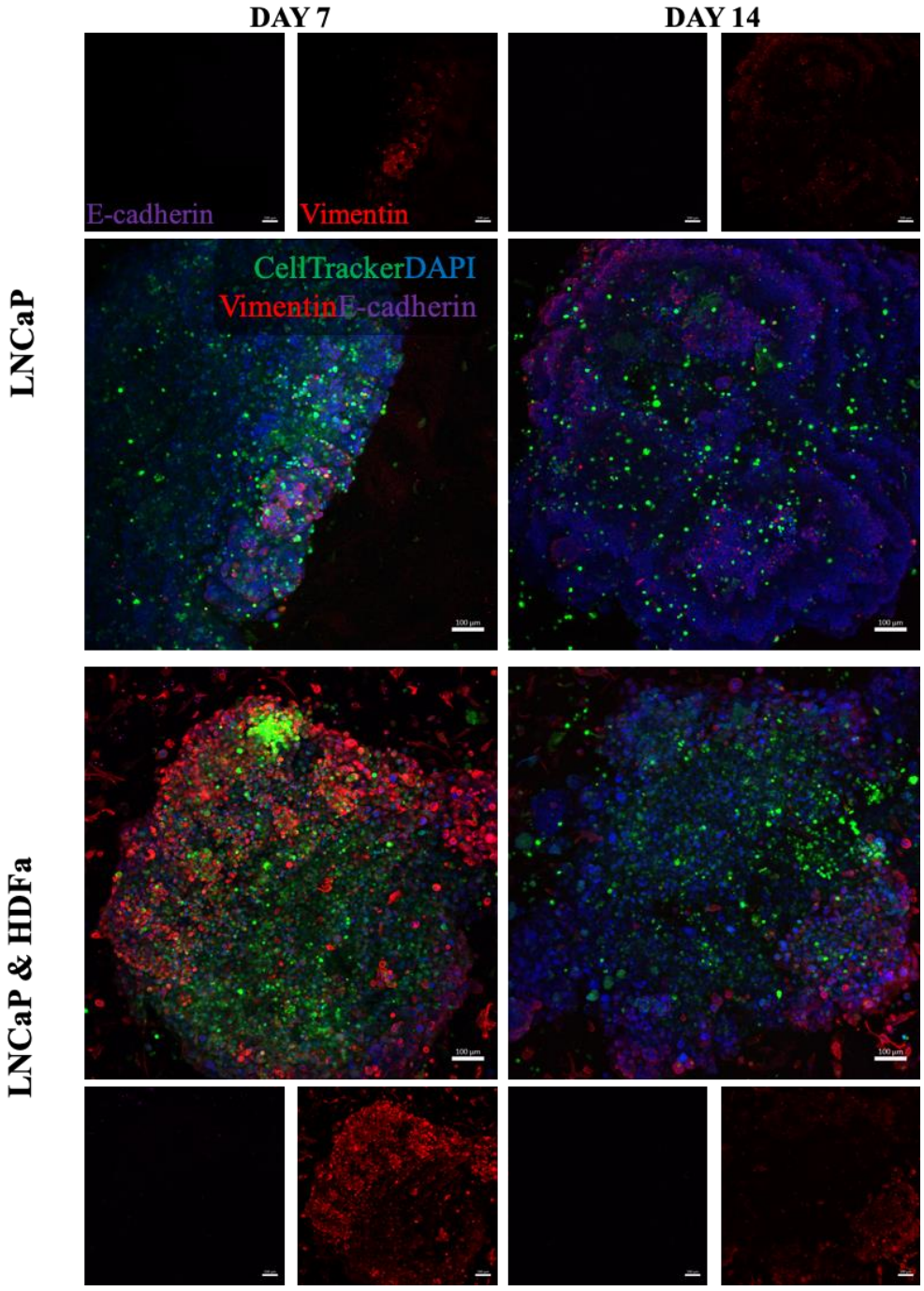

Figure 3.20. CLSM images of immunostained 3D microtumor models containing LNCaP spheroids with or without HDFa at 7 and 14 days. Cells were stained for nucleus (DAPI, blue), vimentin (Alexa Fluor 555, red) and E-cadherin (Alexa Fluor 647, violet). Cancer cell spheroids were stained with CellTracker™ Green CMFDA Dye (green). Scale bars: 100 µm.

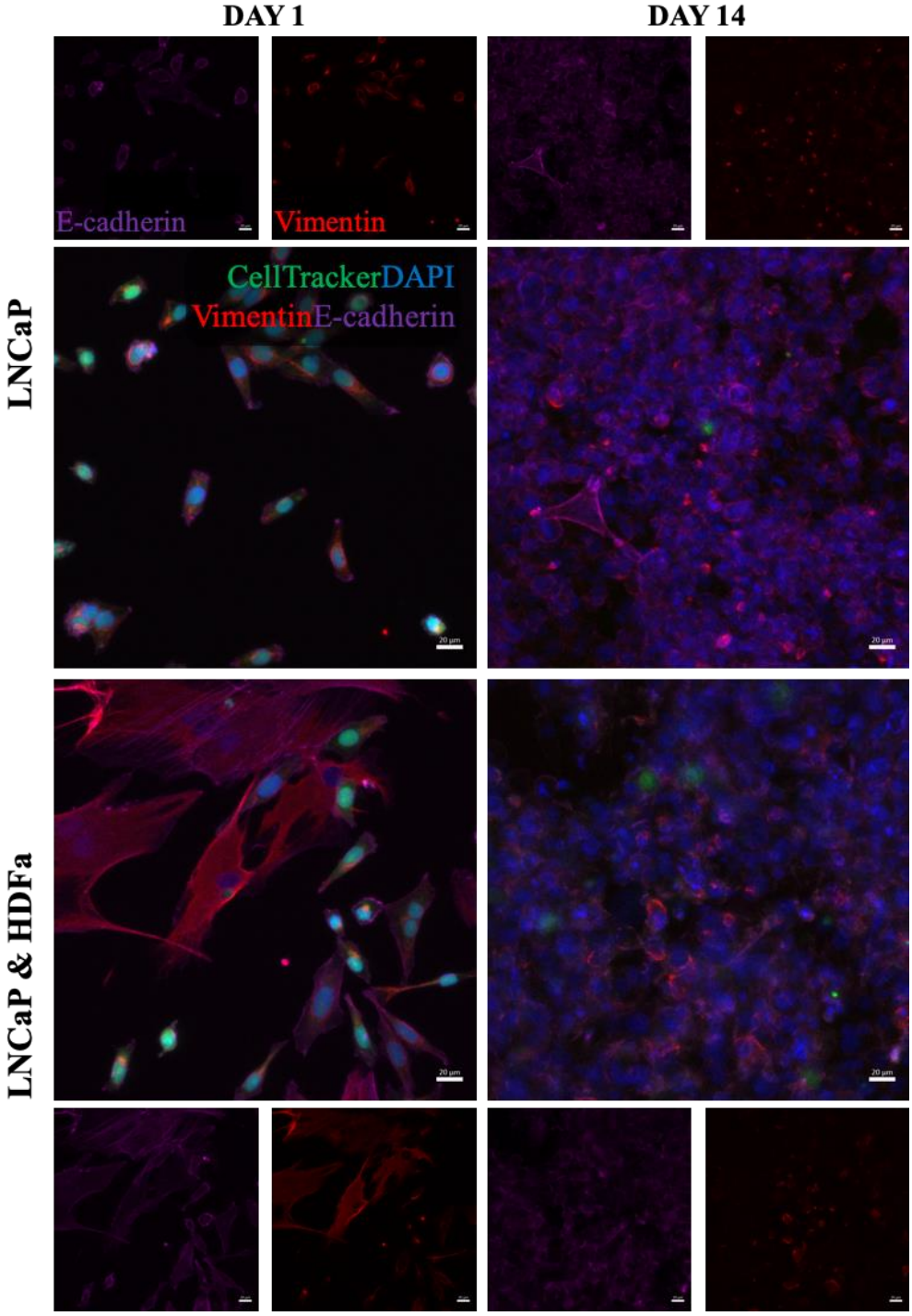

Figure 3.21. CLSM images of immunostained LNCaP cells with or without HDFa on TCPs at 1 and 14 days. Cells were stained for nucleus (DAPI, blue), vimentin (Alexa Fluor 555, red) and E-cadherin (Alexa Fluor 647, violet). Cancer cells were stained with CellTracker™ Green CMFDA Dye (green). Scale bars: 20 μm.

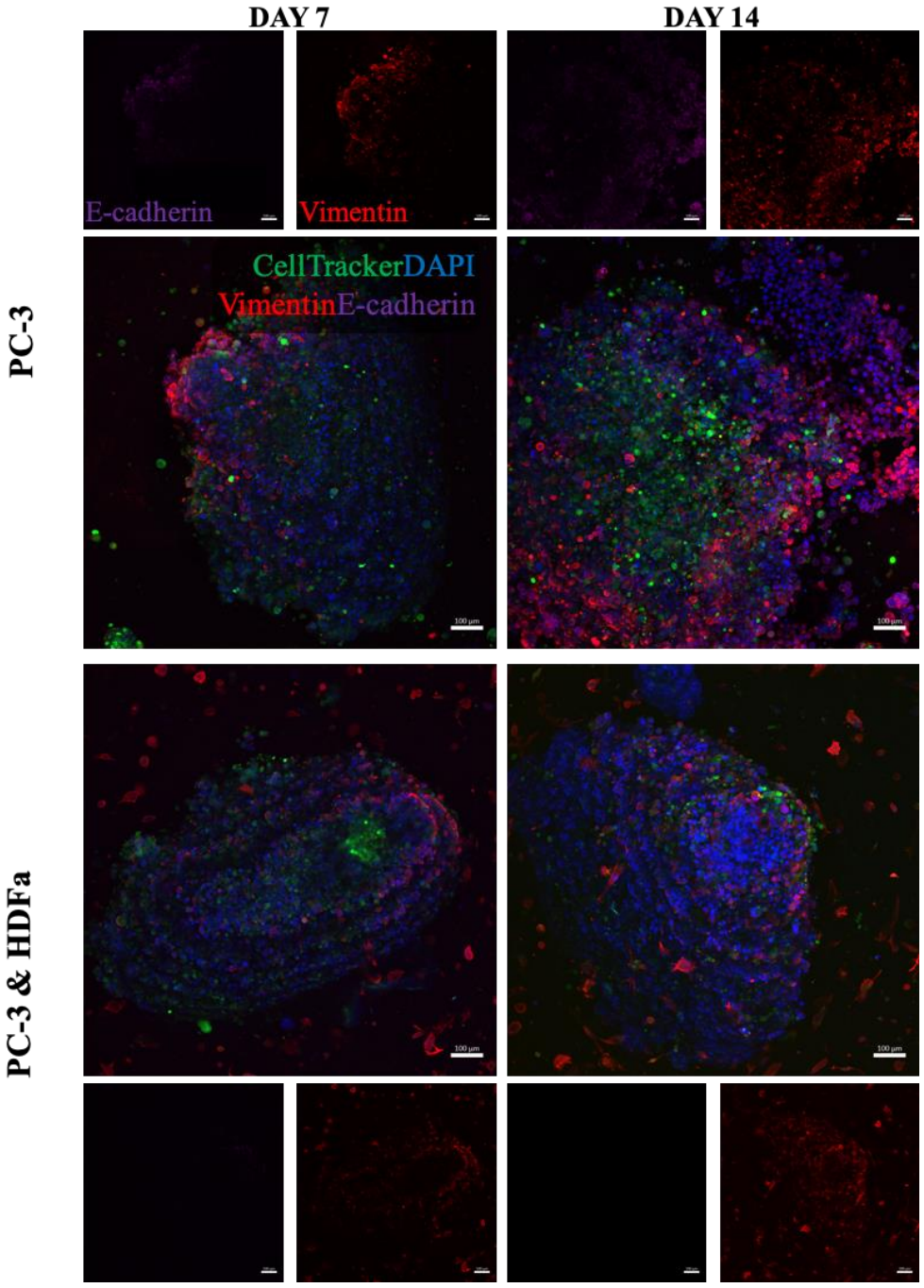

Figure 3.22. CLSM images of immunostained 3D microtumor models containing PC-3 spheroids with or without HDFa at 7 and 14 days. Cells were stained for nucleus (DAPI, blue), vimentin (Alexa Fluor 555, red) and E-cadherin (Alexa Fluor 647, violet). Cancer cell spheroids were stained with CellTracker™ Green CMFDA Dye (green). Scale bars: 100 µm.

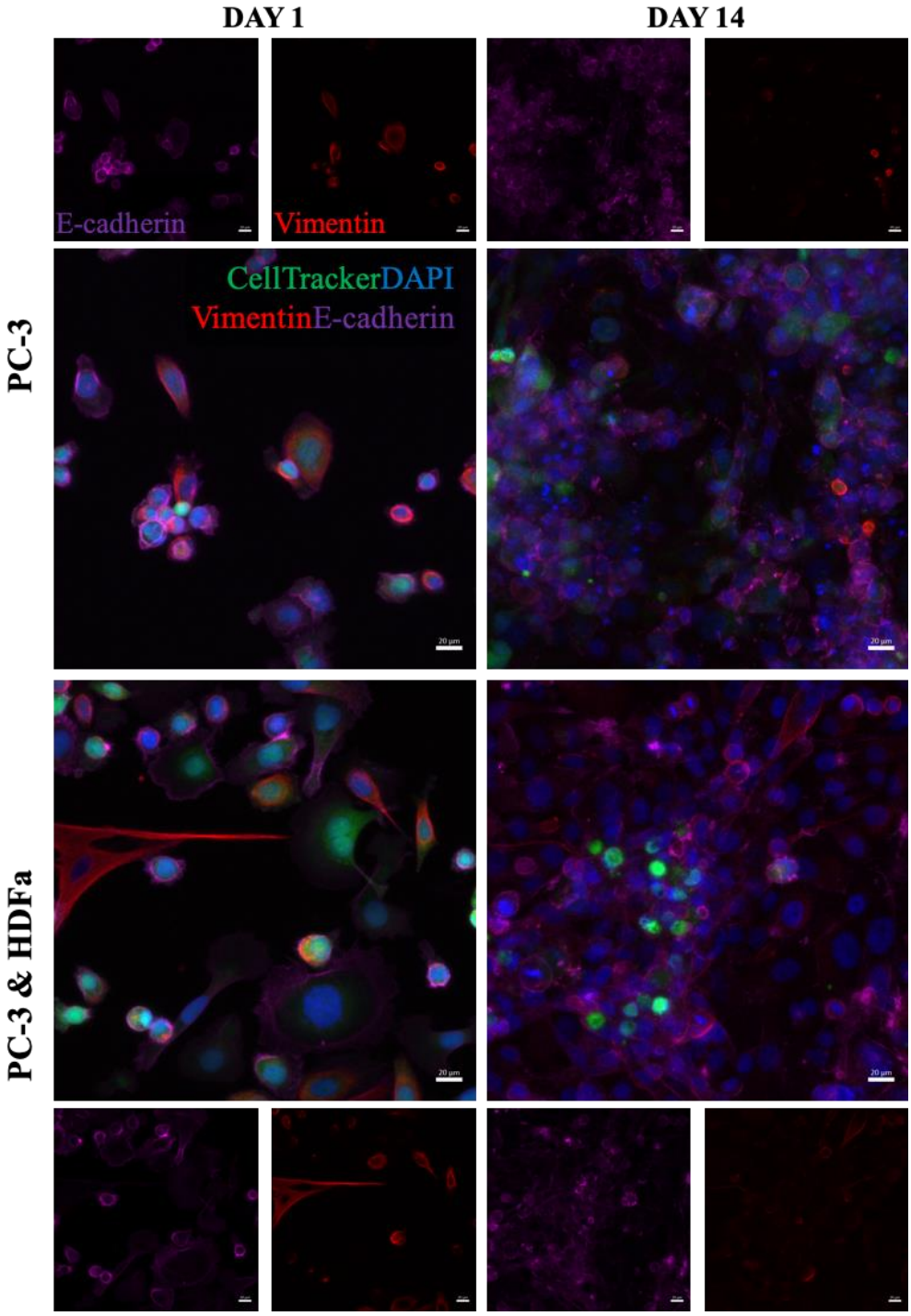

Figure 3.23. CLSM images of immunostained PC-3 cells with or without HDFa on TCPs at 1 and 14 days. Cells were stained for nucleus (DAPI, blue), vimentin (Alexa Fluor 555, red) and E-cadherin (Alexa Fluor 647, violet). Cancer cells were stained with CellTracker™ Green CMFDA Dye (green). Scale bars: 20 μm

The intensity of signals was measured with FiJi software and the expression levels of E-cadherin and vimentin were shown in Figures 3.25 and 26. The intensity of signals between hydrogel and TCP flask cannot be compared, since different laser powers were used due to material differences. When E-cadherin and vimentin expression levels are compared in TCP flask, E-cadherin has a higher expression level than vimentin in 2D monolayer culture. It was not expected the metastasis marker changes in the TCP flask, even the presence of HDF, because 2D cell cultures are lacking in mimicking the appropriate tumor microenvironment for metastasis. In Figure 3.25, the expression level of EMT markers in hydrogels is shown. When the E-cadherin and vimentin are compared, vimentin has relatively higher expression than E-cadherin in contrast to TCP flask as expected. Results show that all vimentin expressions were upregulated from day 7 to day 14. Also, the presence of the HDF upregulates the vimentin expression for four conditions. On the other hand, the expression of E-cadherin downregulated in the presence of HDF in both PC-3 LNCaP hydrogels on day 14. In PC-3 hydrogels with HDF has a high E-cadherin expression level on day 7 but it was downregulated on day 14. It can be concluded that hydrogel design and the presence of HDF provide a sufficient environment for EMT.

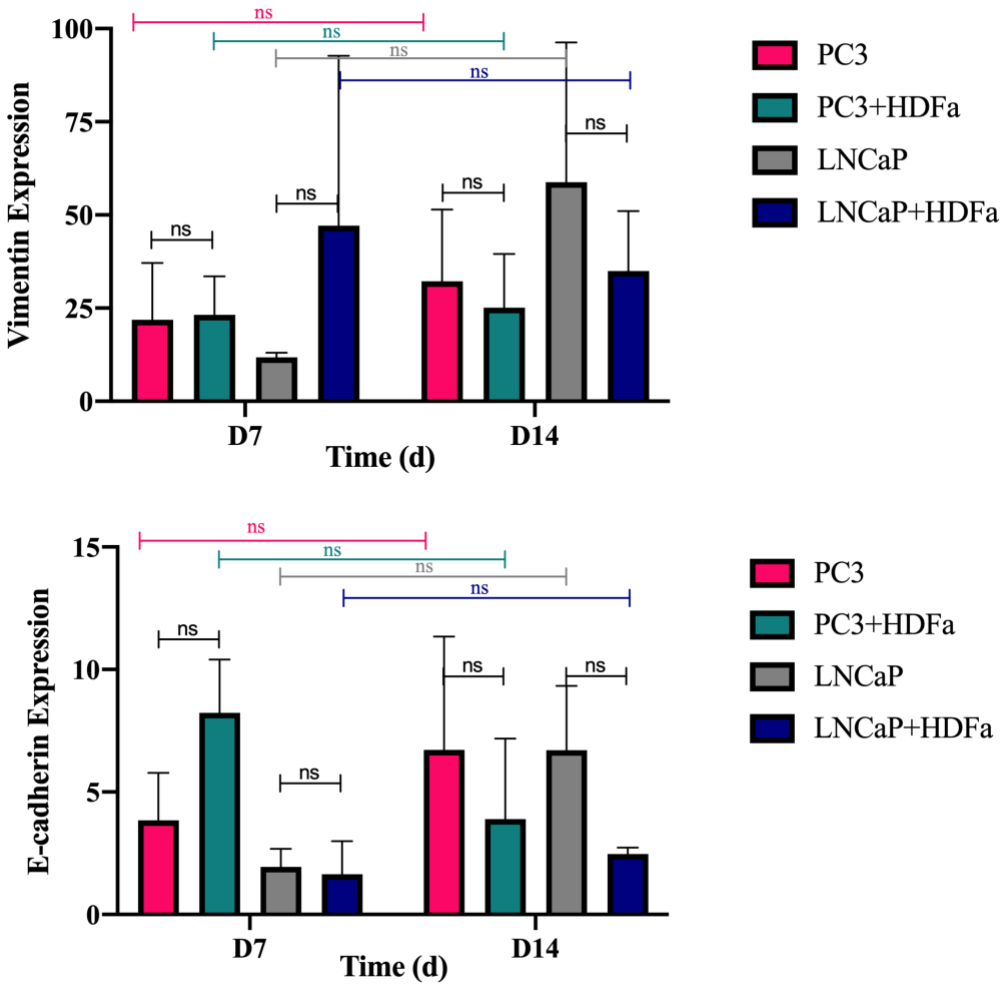

Figure 3.24. Vimentin and E-cadherin expression levels of hydrogel encapsulated PC3 and LNCaP spheroids cells with and without HDF as determined from their fluorescence intensities. Fluorescence intensities were calculated using FiJi software. Results were given as optimized to the cell number by dividing signal intensities by the number of cells counted from the same surface. (Two-way ANOVA, Tukey test for pairwise comparison, n=3)

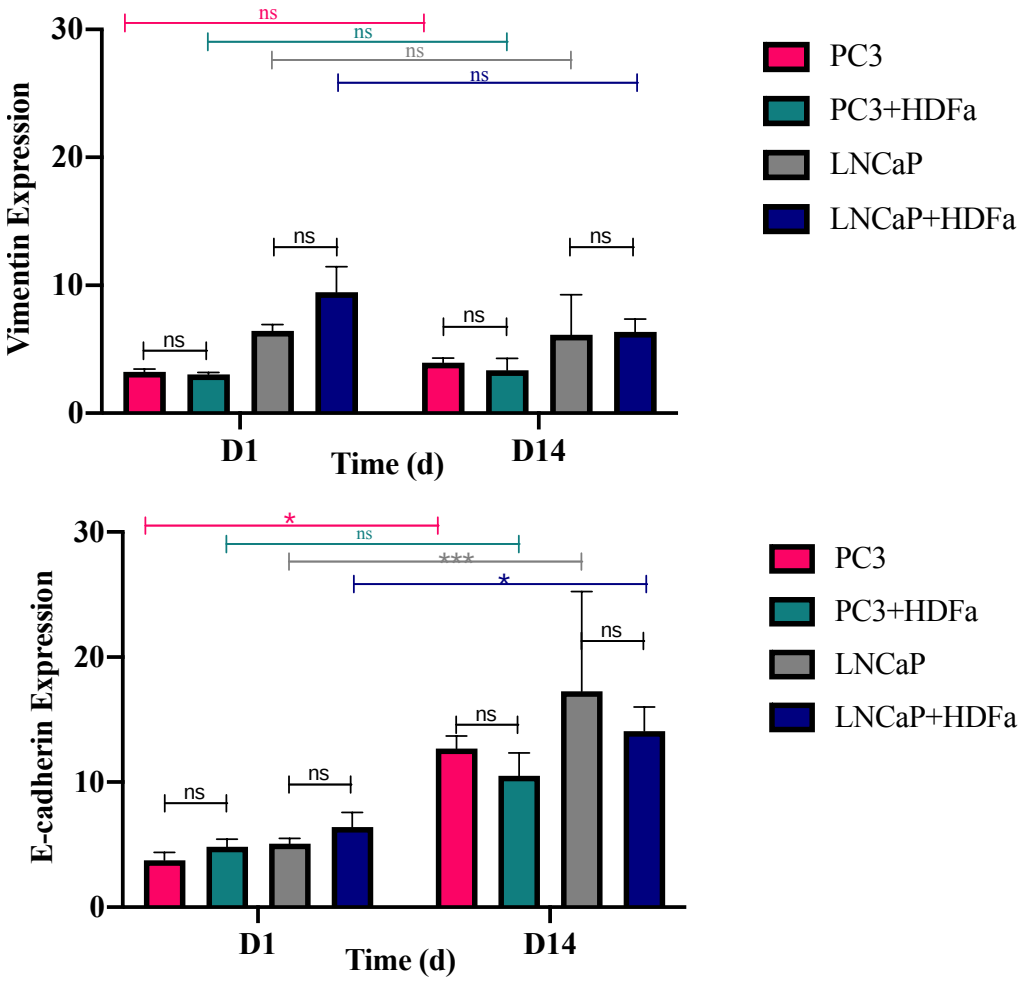

Figure 3.25. Vimentin and E-cadherin expression levels of TCP culture of PC3 and LNCaP cells with and without HDF as determined from their fluorescence intensities. Fluorescence intensities were calculated using FiJi software. Results were given as optimized to the cell number by dividing signal intensities by the number of cells counted from the same surface. (Two-way ANOVA, Tukey test for pairwise comparison, n=3)

CHAPTER 4

CONCLUSION

Prostate cancer is the second most prevalent cancer that causes a large number of deaths in men in the world. There is an increase in the studies of prostate cancer metastasis. This situation leads to a need for the microtumor model that mimics the prostate cancer microenvironment rather than 2D tumor models.

In this study, a 3D hydrogel-based prostate cancer microtumor model was designed for cancer migration studies. For this purpose, natural hydrogels such as methacrylated collagen and hyaluronic acid were used to develop the microenvironment of the prostate cancer tissue. Furthermore, the model contained human dermal fibroblast cells, which are known as a promoter of metastasis in the tissue. Spheroids of LNCaP and PC-3 prostate cancer cell lines were located in the photo-crosslinked hydrogel to represent the cancerous tumor. Different compositions of gels were designed and it was shown that the higher ColMA concentration in the 3D tumor model provides a better microenvironment for the formation of elongated morphology and the movement of the prostate cancer cells. Also, the effect of the HDF cells on the migration of prostate cancer cells was shown with the immunocytochemistry analysis with CLSM micrographs of the prostate cancer cells through the EMT marker proteins; vimentin and e-cadherin.

In the future, this 3D hydrogel-based prostate cancer microtumor model has the potential for other cancer types thanks to its tunable nature. Also, this testing platform may be applied in the drug screening studies and evaluation of treatments in patient-specific microtumor models.

REFERENCES

Abate-Shen, C., & Shen, M. (2000). Molecular genetics of prostate cancer. *Genes & Development*, *14*(19), 2410-2434. doi: 10.1101/gad.819500

Ahangar, P., Akoury, E., Ramirez Garcia Luna, A., Nour, A., Weber, M., & Rosenzweig, D. (2018). Nanoporous 3D-Printed Scaffolds for Local Doxorubicin Delivery in Bone Metastases Secondary to Prostate Cancer. *Materials*, *11*(9), 1485. doi: 10.3390/ma11091485

Antunes, J., Gaspar, V. M., Ferreira, L., Monteiro, M., Henrique, R., Jerónimo, C., & Mano, J. F. (2019). In-air production of 3D co-culture tumor spheroid hydrogels for expedited drug screening. *Acta Biomaterialia*, *94*, 392–409. https://doi.org/10.1016/j.actbio.2019.06.012

Balazs, E., & Laurent, T. (1998). *The chemistry, biology and medical applications of hyaluronan and its derivatives*. London: Portland Press.

Banerjee, P. P., Banerjee, S., Brown, T. R., & Zirkin, B. R. (2018). Androgen action in prostate function and disease. *American journal of clinical and experimental urology*, *6*(2), 62.

Banyard, J., Bao, L., Hofer, M. D., Zurakowski, D., Spivey, K. A., Feldman, A. S., et al. (2007). Collagen XXIII expression is asso- ciated with prostate cancer recurrence and distant metastases. Clinical Cancer Research: An Official Journal of the American Association for Cancer Research, 13(9), 2634–2642. https://doi. org/10.1158/1078-0432.CCR-06-2163.

Barron, D., & Rowley, D. (2012). The reactive stroma microenvironment and prostate cancer progression. *Endocrine-Related Cancer*, *19*(6), R187-R204. doi: 10.1530/erc-12-0085

Barry, M. (2001). Prostate-Specific–Antigen Testing for Early Diagnosis of Prostate Cancer. *New England Journal Of Medicine*, *344*(18), 1373-1377. doi: 10.1056/nejm200105033441806

Benien, P., & Swami, A. (2014). 3D tumor models: history, advances and future perspectives. *Future Oncology*, *10*(7), 1311-1327. doi: 10.2217/fon.13.274

Billiet, T., Gevaert, E., De Schryver, T., Cornelissen, M., & Dubruel, P. (2014). The 3D printing of gelatin methacrylamide cell-laden tissue-engineered constructs with high cell viability. *Biomaterials*, *35*(1), 49-62. doi: 10.1016/j.biomaterials.2013.09.078

Bissell, M., Hall, H., & Parry, G. (1982). How does the extracellular matrix direct gene expression?. *Journal Of Theoretical Biology*, *99*(1), 31-68. doi: 10.1016/0022-5193(82)90388-5

Blanco-Fernandez, B., Gaspar, V., Engel, E., & Mano, J. (2021). Proteinaceous Hydrogels for Bioengineering Advanced 3D Tumor Models. *Advanced Science*, *8*(4), 2003129. doi: 10.1002/advs.202003129

Boucherit, N., Gorvel, L., & Olive, D. (2020). 3D Tumor Models and Their Use for the Testing of Immunotherapies. *Frontiers In Immunology*, *11*. doi: 10.3389/fimmu.2020.603640

Bray, F., Ferlay, J., Soerjomataram, I., Siegel, R. L., Torre, L. A., & Jemal, A. (2018). Global cancer statistics 2018: GLOBOCAN estimates of incidence and mortality worldwide for 36 cancers in 185 countries. *CA: A Cancer Journal for Clinicians*, *68*(6), 394–424. https://doi.org/10.3322/caac.21492

Brett, A., Pandey, S. & Fraizer, G. (2013). The Wilms' tumor gene (WT1) regulates E-cadherin expression and migration of prostate cancer cells. *Mol Cancer* **12,** 3. https://doi.org/10.1186/1476-4598-12-3

Brinkman, W., Nagapudi, K., Thomas, B., & Chaikof, E. (2003). Photo-Cross-Linking of Type I Collagen Gels in the Presence of Smooth Muscle Cells: Mechanical Properties, Cell Viability, and Function. *Biomacromolecules*, *4*(4), 890-895. doi: 10.1021/bm0257412

Burdick, J., Chung, C., Jia, X., Randolph, M., & Langer, R. (2004). Controlled Degradation and Mechanical Behavior of Photopolymerized Hyaluronic Acid Networks. *Biomacromolecules*, *6*(1), 386-391. doi: 10.1021/bm049508a

Campbell, M., Wein, A., & Kavoussi, L. (2007). *Campbell-Walsh Urology*. Philadelphia, PA: W.B. Saunders.

Caballero, D., Reis, R., & Kundu, S. (2020). Trends in biomaterials for three-dimensional cancer modeling. *Biomaterials For 3D Tumor Modeling*, 3-41. doi: 10.1016/b978-0-12-818128-7.00001-0

Castilho, M., Hochleitner, G., Wilson, W., van Rietbergen, B., Dalton, P., & Groll, J. et al. (2018). Mechanical behavior of a soft hydrogel reinforced with three-dimensional printed microfibre scaffolds. *Scientific Reports*, *8*(1). doi: 10.1038/s41598-018-19502-y

Catoira, M., Fusaro, L., Di Francesco, D., Ramella, M., & Boccafoschi, F. (2019). Overview of natural hydrogels for regenerative medicine applications. *Journal Of Materials Science: Materials In Medicine*, *30*(10). doi: 10.1007/s10856-019-6318-7

Chandrasekharan, A., Seong, K., Yim, S., Kim, S., Seo, S., Yoon, J., & Yang, S. (2018). In situ photocrosslinkable hyaluronic acid-based surgical glue with tunable mechanical properties and high adhesive strength. *Journal Of Polymer Science Part A: Polymer Chemistry*, *57*(4), 522-530. doi: 10.1002/pola.29290

Chen, H., Qin, J., & Hu, Y. (2019). Efficient Degradation of High-Molecular-Weight Hyaluronic Acid by a Combination of Ultrasound, Hydrogen Peroxide, and Copper Ion. *Molecules*, *24*(3), 617. doi: 10.3390/molecules24030617

Chiarugi, P., Paoli, P., & Cirri, P. (2014). Tumor Microenvironment and Metabolism in Prostate Cancer. *Seminars In Oncology*, *41*(2), 267-280. doi: 10.1053/j.seminoncol.2014.03.004

Coakley, F., & Hricak, H. (2000). RADIOLOGIC ANATOMY OF THE PROSTATE GLAND: A CLINICAL APPROACH. *Radiologic Clinics Of North America*, *38*(1), 15-30. doi: 10.1016/s0033-8389(05)70147-0

Croft, D., & Olson, M. (2008). Regulating the Conversion between Rounded and Elongated Modes of Cancer Cell Movement. *Cancer Cell*, *14*(5), 349-351. doi: 10.1016/j.ccr.2008.10.009

Egeblad, M., Rasch, M., & Weaver, V. (2010). Dynamic interplay between the collagen scaffold and tumor evolution. *Current Opinion In Cell Biology*, *22*(5), 697-706. doi: 10.1016/j.ceb.2010.08.015

Ellem, S. J., De-Juan-Pardo, E. M., & Risbridger, G. P. (2014). In vitro modeling of the prostate cancer microenvironment. *Advanced Drug Delivery Reviews*, *79*, 214–221. https://doi.org/10.1016/j.addr.2014.04.008

Elshafae, S., Dirksen, W., Alasonyalilar-Demirer, A., Breitbach, J., Yuan, S., & Kantake, N. et al. (2020). Canine prostatic cancer cell line (LuMa) with osteoblastic bone metastasis. *The Prostate*, *80*(9), 698-714. doi: 10.1002/pros.23983

Estermann, S., Pahr, D., & Reisinger, A. (2020). Quantifying tactile properties of liver tissue, silicone elastomers, and a 3D printed polymer for manufacturing realistic organ models. *Journal Of The Mechanical Behavior Of Biomedical Materials*, *104*, 103630. doi: 10.1016/j.jmbbm.2020.103630

Ferlay, J., Colombet, M., Soerjomataram, I., Mathers, C., Parkin, D. M., Piñeros, M., Znaor, A., & Bray, F. (2019). Estimating the global cancer incidence and mortality in 2018: GLOBOCAN sources and methods. *International Journal of Cancer*, *144*(8), 1941–1953. https://doi.org/10.1002/ijc.31937

Ferlay J EM, Lam F, Colombet M, Mery L, Pineros M, Znaor A, Soerjomataram I, et al. Global cancer observato- ry: cancer tomorrow. Lyon, France: International Agency for Research on Cancer. Available from: https://gco.iarc. fr/tomorrow, Accessed 06 July 2020. [Internet]

Fontana, F., Raimondi, M., Marzagalli, M., Sommariva, M., Gagliano, N., & Limonta, P. (2020). Three-Dimensional Cell Cultures as an In Vitro Tool for Prostate Cancer Modeling and Drug Discovery. *International Journal Of Molecular Sciences*, *21*(18), 6806. doi: 10.3390/ijms21186806

Giannoni, E., Bianchini, F., Masieri, L., Serni, S., Torre, E., Calorini, L., & Chiarugi, P. (2010). Reciprocal Activation of Prostate Cancer Cells and Cancer-Associated Fibroblasts Stimulates Epithelial-Mesenchymal Transition and Cancer Stemness. *Cancer Research*, *70*(17), 6945-6956. doi: 10.1158/0008-5472.can-10-0785

Globocan Observatory, W. (2020). Cancer Today - World. *International Agency for Research on Cancer*, *876*, 2019-2020. https://gco.iarc.fr/today/data/factsheets/populations/900-world-fact-sheets.pdf

Han, Y., Liu, C., Zhang, D., Men, H., Huo, L., & Geng, Q. et al. (2019). Mechanosensitive ion channel Piezo1 promotes prostate cancer development through the activation of the Akt/mTOR pathway and acceleration of cell cycle. *International Journal Of Oncology*. doi: 10.3892/ijo.2019.4839

Haffner, M., Zwart, W., Roudier, M., True, L., Nelson, W., & Epstein, J. et al. (2020). Genomic and phenotypic heterogeneity in prostate cancer. *Nature Reviews Urology*, *18*(2), 79-92. doi: 10.1038/s41585-020-00400-w

Hassanpour, S., & Dehghani, M. (2017). Review of cancer from perspective of molecular. *Journal Of Cancer Research And Practice*, *4*(4), 127-129. doi: 10.1016/j.jcrpr.2017.07.001

Hill, C., Saad, S., Britton, R., Gescher, A., Sale, S., Brown, K., & Howells, L. (2015). Inhibition of prostate cancer cell growth by 3′,4′,5′-trimethoxyflavonol (TMFol). *Cancer Chemotherapy And Pharmacology*, *76*(1), 179-185. doi: 10.1007/s00280-015-2771-2

Horning, A., Wang, Y., Lin, C., Louie, A., Jadhav, R., & Hung, C. et al. (2017). Single-Cell RNA-seq Reveals a Subpopulation of Prostate Cancer Cells with Enhanced Cell-Cycle–Related Transcription and Attenuated Androgen Response. *Cancer Research*, *78*(4), 853-864. doi: 10.1158/0008-5472.can-17-1924

Horoszewicz, J. S., Leong, S. S., Kawinski, E., Karr, J. P., Rosenthal, H., Chu, T. M., Mirand, E. A., & Murphy, G. P. (1983). LNCaP model of human prostatic carcinoma. *Cancer research*, *43*(4), 1809–1818.

Hoyt, K., Castaneda, B., Zhang, M., Nigwekar, P., di Sant'Agnese, P., & Joseph, J. et al. (2008). Tissue elasticity properties as biomarkers for prostate cancer. *Cancer Biomarkers*, *4*(4-5), 213-225. doi: 10.3233/cbm-2008-44-505

Huang, B., & Gao, J. (2018). Application of 3D cultured multicellular spheroid tumor models in tumor-targeted drug delivery system research. *Journal Of Controlled Release*, *270*, 246-259. doi: 10.1016/j.jconrel.2017.12.005

Huang, Y., Tong, L., Yi, L., Zhang, C., Hai, L., & Li, T. et al. (2017). Three-dimensional hydrogel is suitable for targeted investigation of amoeboid migration of glioma cells. *Molecular Medicine Reports*. doi: 10.3892/mmr.2017.7888

Huang, Q., Whitington, T., Gao, P., Lindberg, J., Yang, Y., & Sun, J. et al. (2014). A prostate cancer susceptibility allele at 6q22 increases RFX6 expression by modulating HOXB13 chromatin binding. *Nature Genetics*, *46*(2), 126-135. doi: 10.1038/ng.2862

Hutmacher, D., Loessner, D., Rizzi, S., Kaplan, D., Mooney, D., & Clements, J. (2010). Can tissue engineering concepts advance tumor biology research?. *Trends In Biotechnology*, *28*(3), 125-133. doi: 10.1016/j.tibtech.2009.12.001

Isaacs, W. B., Bova, G. S., Morton, R. A., Bussemakers, M. J., Brooks, J. D., & Ewing, C. M. (1994). Molecular biology of prostate cancer. *Seminars in oncology*, *21*(5), 514–521.

Jia, J., Zhang, H., Shi, Q., Yang, C., Ma, J., & Jin, B. et al. (2019). KLF5 downregulation desensitizes castration-resistant prostate cancer cells to docetaxel by increasing BECN1 expression and inducing cell autophagy. *Theranostics*, *9*(19), 5464-5477. doi: 10.7150/thno.33282

Júnior, Z., Botta, S., Ana, P., França, C., Fernandes, K., & Mesquita-Ferrari, R. et al. (2015). Effect of papain-based gel on type I collagen - spectroscopy applied for microstructural analysis. *Scientific Reports*, *5*(1). doi: 10.1038/srep11448

Kaighn ME, Narayan KS, Ohnuki Y, Lechner JF, Jones LW (July 1979). Establishment and characterization of a human prostatic carcinoma cell line (PC-3). *Investigative Urology*. **17** (1): 16–23. PMID 447482

Kaminski, A., Hahne, J. C., Haddouti, E. L. M., Florin, A., Wellmann, A., & Wernert, N. (2006). Tumour-stroma interactions between metastatic prostate cancer cells and fibroblasts. *International Journal of Molecular Medicine*, *18*(5), 941–950. https://doi.org/10.3892/ijmm.18.5.941

Kapałczyńska, M., Kolenda, T., Przybyła, W., Zajączkowska, M., Teresiak, A., & Filas, V. et al. (2016). 2D and 3D cell cultures – a comparison of different types of cancer cell cultures. *Archives Of Medical Science*. doi: 10.5114/aoms.2016.63743

Katt, M., Placone, A., Wong, A., Xu, Z., & Searson, P. (2016). In Vitro Tumor Models: Advantages, Disadvantages, Variables, and Selecting the Right Platform. *Frontiers In Bioengineering And Biotechnology*, *4*. doi: 10.3389/fbioe.2016.00012

Kelly, N., Flood, H., Hoey, D., Kiely, P., Giri, S., Coffey, J., & Walsh, M. (2018). Direct mechanical characterization of prostate tissue—a systematic review. The Prostate, 79(2), 115-125. doi: 10.1002/pros.23718

Khan, M., Hamid, A., Adhami, V., Lall, R., & Mukhtar, H. (2015). Role of Epithelial Mesenchymal Transition in Prostate Tumorigenesis. *Current Pharmaceutical Design*, *21*(10), 1240-1248. doi: 10.2174/1381612821666141211120326

Kort-Mascort, J., Bao, G., Elkashty, O., Flores-Torres, S., Munguia-Lopez, J., & Jiang, T. et al. (2021). Decellularized Extracellular Matrix Composite Hydrogel Bioinks for the Development of 3D Bioprinted Head and Neck in Vitro Tumor Models. *ACS Biomaterials Science & Engineering*, *7*(11), 5288-5300. doi: 10.1021/acsbiomaterials.1c00812

Kundu, B., Bastos, A., Brancato, V., Cerqueira, M., Oliveira, J., & Correlo, V. et al. (2019). Mechanical Property of Hydrogels and the Presence of Adipose Stem Cells in Tumor Stroma Affect Spheroid Formation in the 3D Osteosarcoma Model. *ACS Applied Materials & Interfaces*, *11*(16), 14548-14559. doi: 10.1021/acsami.8b22724

Kundu, B., Reis, R., & Kundu, S. (2020). Metastasis in three-dimensional biomaterials. *Biomaterials For 3D Tumor Modeling*, 191-216. doi: 10.1016/b978-0-12-818128-7.00009-5

Kwa, M. Q., Herum, K. M., & Brakebusch, C. (2019). Cancer-associated fibroblasts: how do they contribute to metastasis? *Clinical and Experimental Metastasis*, *36*(2), 71–86. https://doi.org/10.1007/s10585-019-09959-0

Lange EM. 2010. Identification of genetic risk factors for prostate cancer: analytic approaches using hereditary prostate cancer families. In Male reproductive cancers: epidemiology, pathol- ogy and genetics (ed. Foulkes WD, Cooney KA), pp. 203–228. Springer, New York.

Lawrence, M. G., Taylor, R. A., Toivanen, R., Pedersen, J., Norden, S., Pook, D. W., Frydenberg, M.,Papargiris, M. M., Niranjan, B., Richards, M. G., Wang, H., Collins, A. T., Maitland, N. J., & Risbridger, G. P. (2013). A preclinical xenograft model of prostate cancer using human tumors. *Nature Protocols*, *8*(5), 836–848. https://doi.org/10.1038/nprot.2013.043

Lee, N., Erisken, C., Iskratsch, T., Sheetz, M., Levine, W., & Lu, H. (2021). Polymer fiber-based models of connective tissue repair and healing. Retrieved 30 December 2021, from

Li, Z., Zhou, Y., Yao, H., Wang, J., Wang, D., & Liu, Q. (2015). Greener synthesis of electrospun collagen/hydroxyapatite composite fibers with an excellent microstructure for bone tissue engineering. *International Journal Of Nanomedicine*, 3203. doi: 10.2147/ijn.s79241

Lichtenstein, P., Holm, N., Verkasalo, P., Iliadou, A., Kaprio, J., & Koskenvuo, M. et al. (2000). Environmental and Heritable Factors in the Causation of Cancer — Analyses of Cohorts of Twins from Sweden, Denmark, and Finland. *New England Journal Of Medicine*, *343*(2), 78-85. doi: 10.1056/nejm200007133430201

Litwin, M., & Tan, H. (2017). The Diagnosis and Treatment of Prostate Cancer. *JAMA*, *317*(24), 2532. doi: 10.1001/jama.2017.7248

Liu, C., Lewin Mejia, D., Chiang, B., Luker, K., & Luker, G. (2018). Hybrid collagen alginate hydrogel as a platform for 3D tumor spheroid invasion. *Acta Biomaterialia*, *75*, 213-225. doi: 10.1016/j.actbio.2018.06.003

Madduma-Bandarage, U., & Madihally, S. (2020). Synthetic hydrogels: Synthesis, novel trends, and applications. *Journal Of Applied Polymer Science*, *138*(19), 50376. doi: 10.1002/app.50376

Martins Cavaco, A., Dâmaso, S., Casimiro, S., & Costa, L. (2020). Collagen biology making inroads into prognosis and treatment of cancer progression and metastasis. *Cancer And Metastasis Reviews*, *39*(3), 603-623. doi: 10.1007/s10555-020-09888-5

Meacham, C., & Morrison, S. (2013). Tumour heterogeneity and cancer cell plasticity. *Nature*, *501*(7467), 328-337. doi: 10.1038/nature12624

Michaelson, M., Cotter, S., Gargollo, P., Zietman, A., Dahl, D., & Smith, M. (2008). Management of Complications of Prostate Cancer Treatment. *CA: A Cancer Journal For Clinicians*, *58*(4), 196-213. doi: 10.3322/ca.2008.0002

Molla, M., Katti, D., & Katti, K. (2017). In vitro design of mesenchymal to epithelial transition of prostate cancer metastasis using 3D nanoclay bone-mimetic scaffolds. *Journal Of Tissue Engineering And Regenerative Medicine*, *12*(3), 727-737. doi: 10.1002/term.2492

Monteiro, M., Gaspar, V., Ferreira, L., & Mano, J. (2020). Hydrogel 3D in vitro tumor models for screening cell aggregation mediated drug response. *Biomaterials Science*, *8*(7), 1855-1864. doi: 10.1039/c9bm02075f

Morgan, M., Saba, S., & Gower, W. (2000). Fibronectin influences cellular proliferation and apoptosis similarly in LNCaP and PC-3 prostate cancer cell lines. *Urologic Oncology: Seminars And Original Investigations*, *5*(4), 155-159. doi: 10.1016/s1078-1439(99)00058-7

Mosaad, E., Chambers, K., Futrega, K., Clements, J., & Doran, M. (2018). Using high throughput microtissue culture to study the difference in prostate cancer cell behavior and drug response in 2D and 3D co-cultures. *BMC Cancer*, *18*(1). doi: 10.1186/s12885-018-4473-8

Muguruma, M., Teraoka, S., Miyahara, K., Ueda, A., Asaoka, M., & Okazaki, M. et al. (2020). Differences in drug sensitivity between two-dimensional and

three-dimensional culture systems in triple-negative breast cancer cell lines. *Biochemical And Biophysical Research Communications*, *533*(3), 268-274. doi: 10.1016/j.bbrc.2020.08.075

Neuwirt, H., Bouchal, J., Kharaishvili, G., Ploner, C., Jöhrer, K., & Pitterl, F. et al. (2020). Cancer-associated fibroblasts promote prostate tumor growth and progression through upregulation of cholesterol and steroid biosynthesis. *Cell Communication And Signaling*, *18*(1). doi: 10.1186/s12964-019-0505-5

Nieberler, M., Reuning, U., Reichart, F., Notni, J., Wester, H., & Schwaiger, M. et al. (2017). Exploring the Role of RGD-Recognizing Integrins in Cancer. *Cancers*, *9*(12), 116. doi: 10.3390/cancers9090116

Onder, T., Gupta, P., Mani, S., Yang, J., Lander, E., & Weinberg, R. (2008). Loss of E-Cadherin Promotes Metastasis via Multiple Downstream Transcriptional Pathways. Cancer Research, 68(10), 3645-3654. doi: 10.1158/0008-5472.can-07-2938

Oyen, M. (2013). Mechanical characterisation of hydrogel materials. *International Materials Reviews*, *59*(1), 44-59. doi: 10.1179/1743280413y.0000000022

Oudshoorn, M. H., Rissmann, R., Bouwstra, J. A., & Hennink, W. E. (2007). Synthesis of methacrylated hyaluronic acid with tailored degree of substitution. Polymer, 48(7), 1915-1920.

Packer, J., & Maitland, N. (2016). The molecular and cellular origin of human prostate cancer. *Biochimica Et Biophysica Acta (BBA) - Molecular Cell Research*, *1863*(6), 1238-1260. doi: 10.1016/j.bbamcr.2016.02.016

Patrawala, L., Calhoun, T., Schneider-Broussard, R., Li, H., Bhatia, B., & Tang, S. et al. (2006). Highly purified CD44+ prostate cancer cells from xenograft human tumors are enriched in tumorigenic and metastatic progenitor cells. *Oncogene*, *25*(12), 1696-1708. doi: 10.1038/sj.onc.1209327

Pogoda, K., Pięta, E., Roman, M., Piergies, N., Liberda, D., & Wróbel, T. et al. (2021). In search of the correlation between nanomechanical and biomolecular properties of prostate cancer cells with different metastatic potential. *Archives Of Biochemistry And Biophysics*, *697*, 108718. doi: 10.1016/j.abb.2020.108718

Pickup, M., Mouw, J., & Weaver, V. (2014). The extracellular matrix modulates the hallmarks of cancer. *EMBO Reports*, *15*(12), 1243-1253. doi: 10.15252/embr.201439246

Prystupa, D., & Donald, A. (1996). Infrared study of gelatin conformations in the gel and sol states. *Polymer Gels And Networks*, *4*(2), 87-110. doi: 10.1016/0966-7822(96)00003-2

Qiao, H., & Tang, T. (2018). Engineering 3D approaches to model the dynamic microenvironments of cancer bone metastasis. *Bone Research*, *6*(1). doi: 10.1038/s41413-018-0008-9

Rae, C., & Mairs, R. (2016). Evaluation of the radiosensitizing potency of chemotherapeutic agents in prostate cancer cells. *International Journal Of Radiation Biology*, *93*(2), 194-203. doi: 10.1080/09553002.2017.1231946

Ravichandran, R., Islam, M., Alarcon, E., Samanta, A., Wang, S., & Lundström, P. et al. (2016). Functionalised type-I collagen as a hydrogel building block for bio-orthogonal tissue engineering applications. *Journal Of Materials Chemistry B*, *4*(2), 318-326. doi: 10.1039/c5tb02035b

Rawla, P. (2019). Epidemiology of Prostate Cancer. *World Journal Of Oncology*, *10*(2), 63-89. doi: 10.14740/wjon1191

Redmond, J., McCarthy, H., Buchanan, P., Levingstone, T., & Dunne, N. (2021). Advances in biofabrication techniques for collagen-based 3D in vitro culture models for breast cancer research. *Materials Science And Engineering: C*, *122*, 111944. doi: 10.1016/j.msec.2021.111944

Reiter, R., Tan, D., Manchester, L., Korkmaz, A., Fuentes-Broto, L., & Hardman, W. et al. (2013). A Walnut-Enriched Diet Reduces the Growth of LNCaP Human Prostate Cancer Xenografts in Nude Mice. *Cancer Investigation*, *31*(6), 365-373. doi: 10.3109/07357907.2013.800095

Rich, J. (2016). Cancer stem cells. *Medicine*, *95*(1S), S2-S7. doi: 10.1097/md.0000000000004764

Richardson, A., Havel, L., Koyen, A., Konen, J., Shupe, J., & Wiles, W. et al. (2017). Vimentin Is Required for Lung Adenocarcinoma Metastasis via Heterotypic Tumor Cell–Cancer-Associated Fibroblast Interactions during Collective Invasion. Clinical Cancer Research, 24(2), 420-432. doi: 10.1158/1078-0432.ccr-17-1776

Russell, P., & Kingsley, E. (2003). Human Prostate Cancer Cell Lines. *Prostate Cancer Methods And Protocols*, 21-40. doi: 10.1385/1-59259-372-0:21

Saltzman, W. M. (2004). *Tissue engineering: engineering principles for the design of replacement organs and tissues*. Oxford university press.

Sartor, O., & de Bono, J. S. (2018). Metastatic prostate cancer. *New England Journal of Medicine*, *378*(7), 645–657. https://doi.org/10.1056/NEJMra1701695

Satelli, A., & Li, S. (2011). Vimentin in cancer and its potential as a molecular target for cancer therapy. *Cellular And Molecular Life Sciences*, *68*(18), 3033-3046. doi: 10.1007/s00018-011-0735-1

Scardino, P., & Kelman, J. (2010). Dr. Peter Scardino's prostate book. New York: Avery.

Senbanjo, L., & Chellaiah, M. (2017). CD44: A Multifunctional Cell Surface Adhesion Receptor Is a Regulator of Progression and Metastasis of Cancer Cells. *Frontiers In Cell And Developmental Biology*, *5*. doi: 10.3389/fcell.2017.00018

Shao, H., Moller, M., Wang, D., Ting, A., Boulina, M., & Liu, Z. (2020). A Novel Stromal Fibroblast-Modulated 3D Tumor Spheroid Model for Studying Tumor-Stroma Interaction and Drug Discovery. *Journal Of Visualized Experiments*, (156). doi: 10.3791/60660

Shintani, Y., Maeda, M., Chaika, N., Johnson, K., & Wheelock, M. (2008). Collagen I Promotes Epithelial-to-Mesenchymal Transition in Lung Cancer Cells via Transforming Growth Factor–β Signaling. American Journal Of Respiratory Cell And Molecular Biology, 38(1), 95-104. doi: 10.1165/rcmb.2007-0071oc

Sing, S., Tey, C., Tan, J., Huang, S., & Yeong, W. (2020). 3D printing of metals in rapid prototyping of biomaterials: Techniques in additive manufacturing. *Rapid Prototyping Of Biomaterials*, 17-40. doi: 10.1016/b978-0-08-102663-2.00002-2

Singh, S., Sadacharan, S., Su, S., Belldegrun, A., Persad, S., & Singh, G. (2003). Overexpression of vimentin: role in the invasive phenotype in an androgen-independent model of prostate cancer. *Cancer research*, *63*(9), 2306–2311.

Sinha, D., Saha, P., Samanta, A., & Bishayee, A. (2020). Emerging Concepts of Hybrid Epithelial-to-Mesenchymal Transition in Cancer Progression. Biomolecules, 10(11), 1561. doi: 10.3390/biom10111561

Sioud, M., Juzenas, P., Zhang, Q., Kleinauskas, A., & Peng, Q. (2021). Evaluation of In Vitro Phototoxicity of a Minibody-IR700 Conjugate Using Cell Monolayer and Multicellular Tumor Spheroid Models. *Cancers*, *13*(13), 3356. doi: 10.3390/cancers13133356

Sleeman, J., & Thiele, W. (2009). Tumor metastasis and the lymphatic vasculature. *International Journal Of Cancer*, *125*(12), 2747-2756. doi: 10.1002/ijc.24702

Smith, B., & Bhowmick, N. (2016). Role of EMT in Metastasis and Therapy Resistance. Journal Of Clinical Medicine, 5(2), 17. doi: 10.3390/jcm5020017

Song, H. H. G., Park, K. M., & Gerecht, S. (2014). Hydrogels to model 3D in vitro microenvironment of tumor vascularization. *Advanced Drug Delivery Reviews*, *79*, 19–29. https://doi.org/10.1016/j.addr.2014.06.002

Stock, K., Estrada, M., Vidic, S., Gjerde, K., Rudisch, A., & Santo, V. et al. (2016). Capturing tumor complexity in vitro: Comparative analysis of 2D and 3D tumor models for drug discovery. *Scientific Reports*, *6*(1). doi: 10.1038/srep28951

Sung, H., Ferlay, J., Siegel, R., Laversanne, M., Soerjomataram, I., Jemal, A., & Bray, F. (2021). Global Cancer Statistics 2020: GLOBOCAN Estimates of Incidence and Mortality Worldwide for 36 Cancers in 185 Countries. *CA: A Cancer Journal For Clinicians*, *71*(3), 209-249. doi: 10.3322/caac.21660

Tang, Y., Huang, B., Dong, Y., Wang, W., Zheng, X., Zhou, W., Zhang, K., & Du, Z. (2017). Three-dimensional prostate tumor model based on a hyaluronic acid-alginate hydrogel for evaluation of anti-cancer drug efficacy. *Journal of Biomaterials Science, Polymer Edition*, *28*(14), 1603–1616. https://doi.org/10.1080/09205063.2017.1338502

Temples, M., Adjei, I., Nimocks, P., Djeu, J., & Sharma, B. (2020). Engineered Three-Dimensional Tumor Models to Study Natural Killer Cell Suppression. *ACS Biomaterials Science & Engineering*, *6*(7), 4179-4199. doi: 10.1021/acsbiomaterials.0c00259

Thakuri, P., Liu, C., Luker, G., & Tavana, H. (2017). Biomaterials-Based Approaches to Tumor Spheroid and Organoid Modeling. *Advanced Healthcare Materials*, *7*(6), 1700980. doi: 10.1002/adhm.201700980

Tikkinen, K., Dahm, P., Lytvyn, L., Heen, A., Vernooij, R., & Siemieniuk, R. et al. (2018). Prostate cancer screening with prostate-specific antigen (PSA) test: a clinical practice guideline. *BMJ*, k3581. doi: 10.1136/bmj.k3581

Turley, E., Noble, P., & Bourguignon, L. (2002). Signaling Properties of Hyaluronan Receptors. *Journal Of Biological Chemistry*, *277*(7), 4589-4592. doi: 10.1074/jbc.r100038200

Tuxhorn, J. A., Ayala, G. E., Smith, M. J., Smith, V. C., Dang, T. D., & Rowley, D. R. (2002). Reactive stroma in human prostate cancer: Induction of myofibroblast phenotype and extracellular matrix remodeling. *Clinical Cancer Research*, *8*(9), 2912–2923.

van Bokhoven, A., Varella-Garcia, M., Korch, C., Johannes, W., Smith, E., & Miller, H. et al. (2003). Molecular characterization of human prostate carcinoma cell lines. *The Prostate*, *57*(3), 205-225. doi: 10.1002/pros.10290

Van Hemelryk, A., & van Weerden, W. (2020). Novel patient-derived 3D culture models to guide clinical decision-making in prostate cancer. *Current Opinion In Endocrine And Metabolic Research*, *10*, 7-15. doi: 10.1016/j.coemr.2020.02.005

Varnosfaderani, Z., Emamzadeh, R., Nazari, M., & Zarean, M. (2019). Detection of a prostate cancer cell line using a bioluminescent affiprobe: An attempt to develop a new molecular probe for ex vivo studies. *International Journal Of Biological Macromolecules*, *138*, 755-763. doi: 10.1016/j.ijbiomac.2019.07.085

Villers, A., & Grosclaude, P. (2008). Épidémiologie du cancer de la prostate. Article de revue. *Medecine Nucleaire*, *32*(1), 2–4. https://doi.org/10.1016/j.mednuc.2007.11.003

van Roy, F., & Berx, G. (2008). The cell-cell adhesion molecule E-cadherin. *Cellular And Molecular Life Sciences*, *65*(23), 3756-3788. doi: 10.1007/s00018-008-8281-1

Wang, D., Narula, N., Azzopardi, S., Smith, R., Nasar, A., & Altorki, N. et al. (2016). Expression of the receptor for hyaluronic acid mediated motility (RHAMM) is associated with poor prognosis and metastasis in non-small cell lung carcinoma. *Oncotarget*, *7*(26), 39957-39969. doi: 10.18632/oncotarget.9554

Wang, G., Zhao, D., Spring, D., & DePinho, R. (2018). Genetics and biology of prostate cancer. *Genes & Development*, *32*(17-18), 1105-1140. doi: 10.1101/gad.315739.118

Wang, Y., Mirza, S., Wu, S., Zeng, J., Shi, W., & Band, H. et al. (2018). 3D hydrogel breast cancer models for studying the effects of hypoxia on epithelial to mesenchymal transition. *Oncotarget*, *9*(63), 32191-32203. doi: 10.18632/oncotarget.25891

Wang, Z., Liu, J., Huang, H., Ye, M., Li, X., & Wu, R. et al. (2021). Metastasis-associated fibroblasts: an emerging target for metastatic cancer. *Biomarker Research*, *9*(1). doi: 10.1186/s40364-021-00305-9

Wei, C., Pan, Y., Huang, H., & Li, Y. P. (2018). Estramustine phosphate induces prostate cancer cell line PC3 apoptosis by down-regulating miR-31 levels. *European review for medical and pharmacological sciences*, *22*(1), 40–45. https://doi.org/10.26355/eurrev_201801_14098

Windus, L. C. E., Kiss, D. L., Glover, T., & Avery, V. M. (2012). In vivo biomarker expression patterns are preserved in 3D cultures of Prostate Cancer. *Experimental Cell Research*, *318*(19), 2507–2519. https://doi.org/10.1016/j.yexcr.2012.07.013

Wolf, K., Mazo, I., Leung, H., Engelke, K., von Andrian, U., & Deryugina, E. et al. (2003). Compensation mechanism in tumor cell migration. *Journal Of Cell Biology*, *160*(2), 267-277. doi: 10.1083/jcb.200209006

Xia, C., Chen, P., Mei, S., Ning, L., Lei, C., & Wang, J. et al. (2016). Photo-crosslinked HAMA hydrogel with cordycepin encapsulated chitosan microspheres for osteoarthritis treatment. *Oncotarget*, *8*(2), 2835-2849. doi: 10.18632/oncotarget.13748

Xu, K., Ganapathy, K., Andl, T., Wang, Z., Copland, J. A., Chakrabarti, R., & Florczyk, S. J. (2019). 3D porous chitosan-alginate scaffold stiffness promotes differential responses in prostate cancer cell lines. *Biomaterials*, *217*(June). https://doi.org/10.1016/j.biomaterials.2019.119311

Xu, S., Xu, H., Wang, W., Li, S., Li, H., & Li, T. et al. (2019). The role of collagen in cancer: from bench to bedside. *Journal Of Translational Medicine*, *17*(1). doi: 10.1186/s12967-019-2058-1

Xue, Y., Yu, B., Liu, Y., Guo, R., Li, J., & Zhang, L. et al. (2019). Zinc promotes prostate cancer cell chemosensitivity to paclitaxel by inhibiting epithelial-mesenchymal transition and inducing apoptosis. *The Prostate*, *79*(6), 647-656. doi: 10.1002/pros.23772

Yang, K., Sun, J., Wei, D., Yuan, L., Yang, J., & Guo, L. et al. (2017). Photo-crosslinked mono-component type II collagen hydrogel as a matrix to induce chondrogenic differentiation of bone marrow mesenchymal stem cells. *Journal Of Materials Chemistry B*, *5*(44), 8707-8718. doi: 10.1039/c7tb02348k

Zafar, M., Zhu, D., & Zhang, Z. (2019). 3D Printing of Bioceramics for Bone Tissue Engineering. *Materials*, *12*(20), 3361. doi: 10.3390/ma12203361

Zanoni, M., Pignatta, S., Arienti, C., Bonafè, M., & Tesei, A. (2019). Anticancer drug discovery using multicellular tumor spheroid models. *Expert Opinion On Drug Discovery*, *14*(3), 289-301. doi: 10.1080/17460441.2019.1570129

Zhang, B., Lai, B., Xie, R., Davenport Huyer, L., Montgomery, M., & Radisic, M. (2018). Microfabrication of AngioChip, a biodegradable polymer scaffold with microfluidic vasculature. *Nature Protocols*, *13*(8), 1793-1813. doi: 10.1038/s41596-018-0015-8

Zhang, T., Chen, H., Zhang, Y., Zan, Y., Ni, T., Liu, M., & Pei, R. (2019). Photo-crosslinkable, bone marrow-derived mesenchymal stem cells-encapsulating hydrogel based on collagen for osteogenic differentiation. *Colloids and Surfaces B: Biointerfaces*, *174*(June 2018), 528–535. https://doi.org/10.1016/j.colsurfb.2018.11.050

Zhao, H., Nolley, R., Chen, Z., & Peehl, D. M. (2010). Tissue slice grafts: An in vivo model of human prostate androgen signaling. *American Journal of Pathology*, *177*(1), 229–239. https://doi.org/10.2353/ajpath.2010.090821